

# **Molecular and Cellular Investigations of Fracture Healing in a Mouse Model**

Inaugural Dissertation

Submitted to the

Faculty of Medicine

in partial fulfillment of the requirements

for the PhD-Degree

of the Faculties of Veterinary Medicine and Medicine

of the Justus-Liebig-University Giessen

by

Malhan, Deeksha

Giessen

January 16, 2019

From the Experimental Trauma Surgery, Faculty of Medicine

Director: Univ.-Prof. Dr. med. Dr. h.c. Christian Heiß

Of the Faculty of Medicine of the Justus-Liebig-University Giessen

First Supervisor and Committee Member: Univ.-Prof. Dr. med. Dr. h.c. Christian Heiß

Second Supervisor and Committee Member: Prof. Dr. med. vet. Sabine Wenisch

Committee Chair: Prof. Dr. Norbert Weißmann

## **ABSTRACT**

The success of fracture healing relies on coordinated overlapping cellular and molecular events. 10-15% of cases worldwide result in delayed healing, non-union or pseudarthrosis. Therefore, analysis of molecular and cellular healing events is important to discover new therapeutic attempts in clinical research. Besides, engineering a blueprint of differential regulation throughout physiological healing is essential to specify phase-specific markers. Such undercarriage will pinpoint irregular gene expression, whether chronological, temporal or functional. This study analyzed the healing progression of standard closed femoral fracture in C57BL/6N (age = 8 weeks) wild type male mice model. Fracture callus was assessed at days 3, 7, 10, 14, 21, and 28 post fracture by microarray and histological analysis. Results revealed increased bone mineralization with healing progression and bony bridging was seen by day 28. In-depth analysis of bone matrix mineralization showed changes in collagen orientation and osteocytes morphology with healing progression. Differential expression analysis followed by gene ontology associated genes with angiogenesis, ossification, extracellular matrix regulation, immune response, mitochondrial, and ribosomal activity. However, the overlapping genes between consecutive time points were not addressed before. This thesis compared consecutive time points to study the overlapping genes in correlation to healing events. In accordance to previous reports, this thesis showed the importance of angiogenesis, ossification, immune response, and extracellular matrix regulation leading to successful healing. However, the individual role of mitochondrial and ribosomal genes in bone regeneration remain unknown. Differential analysis in this study showed drastic downregulation among the mitochondrial and ribosomal genes during the early phase of healing. Further, histological evaluation of mitochondrial marker (GPX1) and ribosomal marker (UBB) showed patches of positive stain in osteocytes and blood vessels vicinity during the course of healing. In summary, this study shows the importance of mitochondrial and ribosomal genes besides angiogenesis, ossification, extracellular matrix, and immune response to reach the successful bony consolidation. Moreover, this mouse fracture model can be used as a template to identify specific molecular mechanism of fracture healing.

## ZUSAMMENFASSUNG

Eine erfolgreiche Frakturheilung ist das Ergebnis ineinandergreifender zellulärer und molekularer Ereignisse. Weltweit zeigen 10-15% aller Frakturen eine verzögerte Heilung, „Non-Union“ oder Pseudarthrose. Das detaillierte Verständnis der Frakturheilung ist essentiell für die Wahl der Behandlungsmethode. Daher ist die Analyse der molekularen und zellulären Heilungsprozesse wichtig, um neue therapeutische und klinisch relevante Ansätze zu entdecken. Anhand eines Modells zur physiologischen Knochenheilung können für die Heilungsphasen spezifische Marker identifiziert werden und chronologische oder funktionelle Abweichungen bei pathologischer Knochenheilung präzise aufgezeigt werden. In dieser Studie wurde der Heilungsprozess an einer geschlossenen Femurfraktur in einem C57BL/6N männlichem Wildtyp Mausmodell (Alter = 8 Wochen) untersucht. Hierbei wurde der Frakturkallus an den Tagen 3, 7, 10, 14, 21 und 28 mittels Mikroarray und histologischer Analysen untersucht. Hierbei zeigte sich an Tag 28 eine gesteigerte Knochenmineralisation mit fortschreitender Heilung und Verknöcherung des Kallus. Im Verlauf des Heilungsprozesses zeigten sich Veränderungen in der Kollagenfaserorientierung der Knochenmatrix und der Osteozytenmorphologie. Durch differentielle Genexpressionsanalysen konnten aktive Gene der Angiogenese, Ossifikation, extrazellulären Matrix, des Immunsystems sowie der mitochondrialen und ribosomalen Aktivität identifiziert und den Heilungsphasen zugeordnet werden. Eine derartige Studie mit aufeinander folgenden Zeitpunkten ist bisher einzigartig und zeigt zwischen den Zeitpunkten überlappende Genaktivitäten in den einzelnen Phasen der Frakturheilung. In Übereinstimmung mit vorangegangenen Studien zeigte sich hier die Bedeutung der Angiogenese, Ossifikation, extrazellulären Matrix und des Immunsystems für eine erfolgreiche Frakturheilung. Dennoch ist die Rolle der mitochondrialen und ribosomalen Gene bei der Frakturheilung bisher ungeklärt. In dieser Studie zeigte sich in der frühen Phase der Frakturheilung eine deutliche Herabregulation der mitochondrialen und ribosomalen Genaktivität. Zusätzlich zeigten sich bei den histologischen Analysen in den Osteozyten und den Blutgefäßen positive Areale für den mitochondrialen Marker (GPX1) sowie den ribosomalen Marker (UBB). Diese Studie belegt die Bedeutung von mitochondrialen und ribosomalen Genen zusätzlich zu der Angiogenese, Ossifikation, extrazellulären Matrix und dem Immunsystem an der erfolgreichen, knöchernen Konsolidierung bei der Frakturheilung. Darüber hinaus kann dieses Fraktur-/Mausmodell als Vorlage für die Identifizierung molekularer Mechanismen der Frakturheilung dienen.

*Dedicated to my parents*

# TABLE OF CONTENTS

<b>ABSTRACT</b>	<b>I</b>
<b>ZUSAMMENFASSUNG</b>	<b>II</b>
<b>TABLE OF CONTENTS</b>	<b>IV</b>
<b>1. INTRODUCTION</b>	<b>1</b>
1.1 Structure of Bone	2
1.2 Cellular Components of Bone	3
1.2.1 Osteoblasts	4
1.2.2 Osteocytes	5
1.2.3 Osteoclasts	5
1.2.4 Bone lining cells	6
1.3 Fracture Healing	7
1.3.1 Inflammatory phase	7
1.3.2 Reparative phase	7
1.3.3 Remodeling phase	8
<b>2. OBJECTIVES OF THIS STUDY</b>	<b>10</b>
<b>3. MATERIALS AND METHODS</b>	<b>11</b>
3.1 Experimental Design	11
3.2 Animal Ethical Declaration	12
3.3 Sample Preparation for Histological Evaluation	12
3.4 Histological Staining	12
3.4.1 Sirius Red Stain	12
3.4.2 Trichrome Masson Goldner Stain	13
3.4.3 Silver Nitrate Stain	13
3.5 Immunohistochemical Staining	13

3.5.1 Alpha Smooth Muscle Actin (ASMA) -----	13
3.5.2 Matrix Extracellular Phosphoglycoprotein (MEPE) -----	13
3.5.3 Extracellular Signal Regulated Kinase (ERK) -----	13
3.5.4 Glutathione Peroxidase 1 (GPX1)-----	14
3.5.5 Ubiquitin (UBB)-----	14
3.6 Image Acquisition and Histomorphometry -----	14
3.7 Quantification of Collagen Fibers-----	15
3.8 Statistical Analysis -----	15
3.9 RNA Preparation and Microarray Hybridization -----	16
3.10 Data Normalization and Filtering Criteria-----	16
3.11 Clustering of Differentially Expressed Genes -----	17
3.12 Functional Annotation of Differentially Expressed Genes-----	17
<b>4. RESULTS-----</b>	<b>18</b>
4.1 Comparison of FC cut-offs resulted in no variation in DEG pattern-----	18
4.2 Overlapping genes between two consecutive time points: hallmark either by mitochondrial activity or by ECM regulation-----	20
4.3 Hierarchical clustering of genes based on expression pattern across time points generated ten distinct clusters -----	23
4.4 D3 and D7 marked the active phase of differentially expressed angiogenesis genes----	26
4.5 Evaluation of ASMA activity during fracture healing showed higher positive signal at D7 -----	28
4.6 D10 and D14 marked the active time points with differentially expressed ossification genes -----	29
4.7 Trichrome Masson Goldner depicted changes in bone mineralization with progression of fracture healing process -----	32
4.8 D10 marked the active time point related to differentially expressed ECM genes -----	34
4.9 Changes in collagen fibers arrangement with progression of healing -----	37
4.10 Quantitative evaluation of osteocytes using silver nitrate stain showed lower count at D28-----	40

4.11 Evaluation of MEPE and ERK during fracture healing showed negative correlation across time points -----	42
4.12 High number of differentially expressed genes related to mitochondrial activity were present only at D3 and D7-----	44
4.13 Evaluation of GPX1 immunohistochemistry showed higher positive signal at D28---	48
4.14 High number of differentially expressed genes related to ribosomal activity were present only at D3 and D7 -----	50
4.15 Evaluation of UBB immunohistochemistry showed higher positive signal at D7-----	53
4.16 High number of differentially expressed genes related to immune response were present only at D10 -----	55
<b>5. DISCUSSION-----</b>	<b>58</b>
5.1 Fold change cut-off and data interpretation-----	59
5.2 Fracture healing: series of overlapping events -----	60
5.3 Hierarchical clustering method -----	61
5.4 Angiogenesis -----	62
5.5 Ossification -----	65
5.6 Extracellular matrix -----	66
5.6.1 Osteocytes and ECM markers -----	68
5.7 Mitochondrial activity -----	69
5.8 Ribosomal activity-----	71
5.9 Immune response -----	72
<b>6. CONCLUSION-----</b>	<b>75</b>
<b>7. IMPLICATIONS AND FUTURE DIRECTION-----</b>	<b>76</b>
<b>APPENDICES-----</b>	<b>77</b>
Preparation of samples for paraffin embedding -----	77
Sirius Red Staining-----	78
Trichrome Masson Goldner Stain -----	79
Silver Nitrate Staining-----	80

Immunohistochemical Staining -----	81
Histomorphometry using ImageJ (version 1.51) -----	84
RNA isolation and Quality Control-----	85
Quality assessment of Beadchip array using R -----	86
Hierarchical clustering of DEG using R -----	87
Functional annotation using NCBI-DAVID (version 6.7) -----	88
<b>ABBREVIATIONS LIST -----</b>	<b>91</b>
<b>ACKNOWLEDGMENTS -----</b>	<b>95</b>
<b>THESIS DECLARATION -----</b>	<b>96</b>
<b>REFERENCES-----</b>	<b>97</b>

# 1. INTRODUCTION

Fracture healing is a well-orchestrated series of biological events involving cellular recruitment, growth, and differentiation [1]. Fracture healing involves overlapping phases that begins with inflammation, advances to endochondral ossification, and ends with a remodeling phase. The interdependent healing events requires an interplay between different cell types and regulatory factors. Any dysregulation at cellular or molecular level during fracture healing results in delayed healing or non-union [2]. Developing new strategies to heal bone fractures continues to evolve with increasing knowledge of underlying molecular mechanism. Further, interdisciplinary research in recent years enabled to identify multiple signaling molecules involved in fracture healing.

Transcriptomics is one of the most used technique to examine the underlying molecular mechanism of diseases. Microarray technology was previously used to exploit the temporal and spatial changes during fracture healing in a mouse model [3-5]. Nakzawa T et al. 2004 reported that differentially expressed genes present in the early phase of healing are important for periosteal callus formation [3]. Khan SN et al. 2008 reported the importance of leptin and its receptor in bone mineralization [4]. Bais M et al. 2009 showed the presence of common genes and signaling pathways shared between fracture healing and embryonic stem cells [5]. The information gained so far with transcriptomics has advanced the understanding of fracture healing. However, a deep understanding of overlapping healing events in successful fracture healing is still required. Therefore, fracture healing studies in wild type animal models are important for understanding the underlying cellular and molecular interactions.

This experimental study hypothesized that differentially expressed genes overlapping between two successive time points can elucidate temporal alteration in molecular regulation during the healing. The study also hypothesized that ribosomal and mitochondrial genes are upregulated in the early phase of healing rather than the late phase. To test these hypothesis, a closed femoral fracture model of an eight-week-old wild type male mice was used. The animals were sacrificed at 3, 7, 10, 14, 21, and 28 days post-fracture and 0-day served as control. Whole genome transcriptomics and histological analysis were carried out to infer molecular and cellular changes. The study aims to examine the differentially expressed genes involved in angiogenesis, ossification, extracellular matrix regulation, immune response, mitochondrial, and ribosomal activity.

This study inferred multifunctional role of candidate genes in progressing fracture healing. Further, this thesis provided the first evidence -to my knowledge- of overlapping genes across consecutive time points of healing. Differential gene expression followed by gene ontology revealed significant downregulation of mitochondrial and ribosomal genes during successful healing. Immunohistochemical finding suggests a cross talk between ERK and MEPE, which reflected on regulatory role of extracellular matrix in healing. Further, morphological changes of osteocytes and collagen fiber arrangement with healing progression seen in this study reflected on bone mineralization and bone quality. The collective data from microarray analysis and histology provides a better understanding of fracture healing.

### **1.1 *Structure of Bone***

The skeletal system forms a solid framework that supports and protects the body's organs and anchors the skeletal muscle. Bone is a dynamic connective tissue whose structure and composition reflects a balance between mechanical integrity and homeostasis [6].

The mechanical properties of bone relies on its complex hierarchical structure [7]. Bone is divided into cortical (or compact) and trabecular (or cancellous) bone at macroscopic level [8]. Bone consists of dense outer layer of cortical bone with a porous interior of trabecular bone (Figure 1). The microstructure of cortical bone is composed of regular and cylindrical shaped lamellae. In contrast, the microstructure of trabecular bone is comprised of irregular and sinuous convolutions of lamellae [8].

A long bone typically remains in the process of ossification for many years. The ossification of long bone goes through three parts distinctly: the epiphysis, metaphysis, and diaphysis [6]. The epiphysis refers to the either end of long bone separated from the rest of bone by a layer of growth plate cartilage. The metaphysis refers to the regions of transition from wider epiphysis to slender diaphysis (Figure 1). The ossification of diaphysis takes place before epiphysis by means of primary and secondary ossification centers [9].

Inner and outer membrane surface of bone plays important role in bone modeling & remodeling, and fracture healing [10]. The outermost layer of bone composes of periosteum (Figure 1), which is responsible for appositional bone growth, partial blood supply to bone, and bone healing. Periosteum consists of an outer fibrous layer that

provides structural support and an inner cambium layer which is rich with osteoprogenitor cells (Figure 1). The inner layer of bone comprises of endosteum which arises from periosteum. Endosteum composes of a thin membrane and bone cells like osteoblasts and osteoclasts are present in endosteum [11].

Bone is mainly made of the extracellular matrix (ECM), which consists of vast variety of organic and inorganic constituents. The organic phase is composed of collagenous and inorganic phase is composed of non-collagenous proteins. ECM molecules control cell behavior and provides template for cell attachment and survival [12].

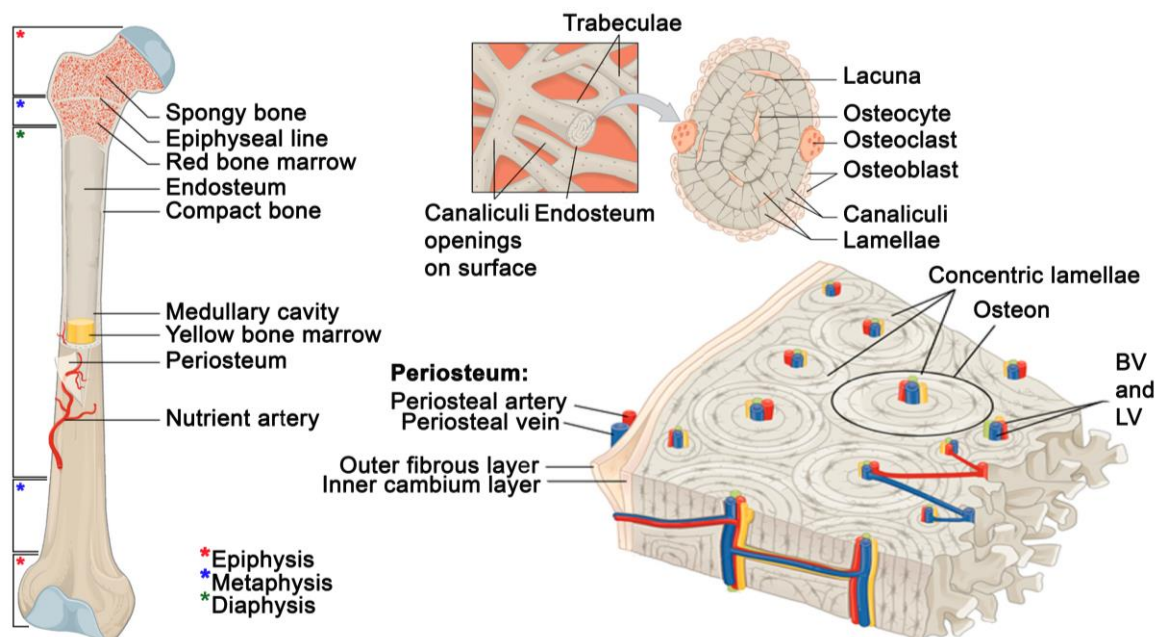


**Figure 1: An outline of the anatomical structure of bone.** Cortical bone makes up to 80% of bones weight and trabecular bone makes up to 20% of bones weight. The periosteum forms the outer layer of bone and the endosteum lines the medullary cavity. (Modified from [13], BV: Blood vessels, LV: Lymphatic vessels).

Type I collagen is the most rich collagenous protein present in bone tissue. Besides, collagen affects the structural characteristics and controls the distribution of apatite [14]. The main components of non-collagenous protein in ECM are Bone sialoproteins (BSP), osteopontin (OPN), osteonectin (ONC), and osteocalcin (OCN).

## 1.2 Cellular Components of Bone

Bone homeostasis is maintained by chemical, biological, and mechanical signaling molecules [15]. Three main cell types associated with bone homeostasis are osteoblasts, osteoclasts, and osteocytes. These cells are ordered into two lineages: the osteoblasts

lineage which represents the bone formation and the osteoclast lineage which represents bone resorption. Osteoblast lineage consists of chondrocytes, pre-osteoblasts, osteocytes, and bone lining cells that originate from mesenchymal stem cells [16]. Osteoclast lineage consists of macrophages, osteoclasts, and other multinucleated cells that originate from hematopoietic stem cells [17]. The balance between bone formation and bone resorption is important to preserve integrity of bone (Figure 2). Imbalanced bone formation and resorption result in systemic skeletal diseases like osteomalacia and osteoporosis [18]. Bone remodeling occurs with the coordinated activity of osteoblasts, osteoclasts, osteocytes, and bone lining cells that form the basic multicellular unit (BMU) [19, 20].

### **1.2.1 Osteoblasts**

Osteoblasts preserve skeletal architecture by deposition of bone matrix and osteoclasts regulation [21]. Osteoblasts migrate from bone marrow to bone surface where bone matrix deposition takes place in bone formation (Figure 2). Proliferation and differentiation of osteoblasts is carried out by cross talk of different signaling pathways. Transforming growth factor – beta (TGF- $\beta$ ) promotes osteoblast differentiation through Extracellular signal-regulated kinases (ERK), Wnt, and Bone Morphogenetic Protein (BMP) signaling [22]. ERK is a part of Mitogen Activated Protein Kinases (MAPK) signaling that also promotes osteoblasts adhesion to the bone matrix proteins like type I collagen beside osteoblast proliferation [23]. Disruption among signaling molecules leads to multiple diseases like tumor metastasis, osteoarthritis, neurodegenerative diseases, osteoporosis [24-28].

Cell growth and proliferation needs the fundamental mitochondrial biogenesis for energy production and ribosomal biogenesis for protein production. Mitochondrial biogenesis is orchestrated by the transcriptional regulatory circuits between mitochondrial DNA and genes encoded by nucleus [29]. Wnt signaling increases mitochondrial biogenesis, which in turn, contributes to increased osteoblast differentiation [30]. Cellular metabolism results in reactive oxygen species (ROS) production, which contribute to cellular damage and apoptosis [31]. In such situations, antioxidant enzyme like Glutathione peroxidase 1 (Gpx1) provides protection against oxidative stress to cells by keeping homeostasis [32]. Ribosome biogenesis controls growth, cell division rate, and cell survival [33]. Ubiquitin proteasome complex is one of the major part of ribosome biogenesis [34]. Runt related transcription factor 2 (Runx2) is the first transcription factor required to control osteoblast

lineage [35]. The main regulator of osteoblast differentiation i.e. Runx2 suppress ribosomal RNA (rRNA) gene transcription [36]. The inverse relation between rRNA and Runx2 provides a strong mechanistic link between ribosome biogenesis and osteogenesis [37]. Further, ubiquitin mediated protein degradation negatively regulate osteoblast migration and differentiation [38].

### **1.2.2 Osteocytes**

Osteocytes compose 90-95% of total bone cells and are the most abundant & long-lived cells [39]. Osteocytes communicate with each other by a meshwork of cell processes that run through canaliculi set in bone matrix [40] (Figure 2). Further, osteocytes act as an orchestrator of bone remodeling through regulation of both osteoclasts and osteoblasts [41]. Osteocytes express selective markers like Dentin Matrix Protein 1 (DMP1), Matrix Extracellular Phosphoglycoprotein (MEPE), and Sclerostin (SOST) with an important role in bone formation, homeostasis, and pathology [42]. Dysregulation in osteocyte specific markers like MEPE or SOST results in severity like multiple myeloma [43] and dentin structural diseases [44].

### **1.2.3 Osteoclasts**

Osteoclasts are multinucleated cells formed by the fusion of mononuclear progenitors of the monocyte/macrophage family [45]. Osteoclast activity involves cell polarization to form resorptive machinery characterized by attaching bone matrix and forming ruffled border [46].

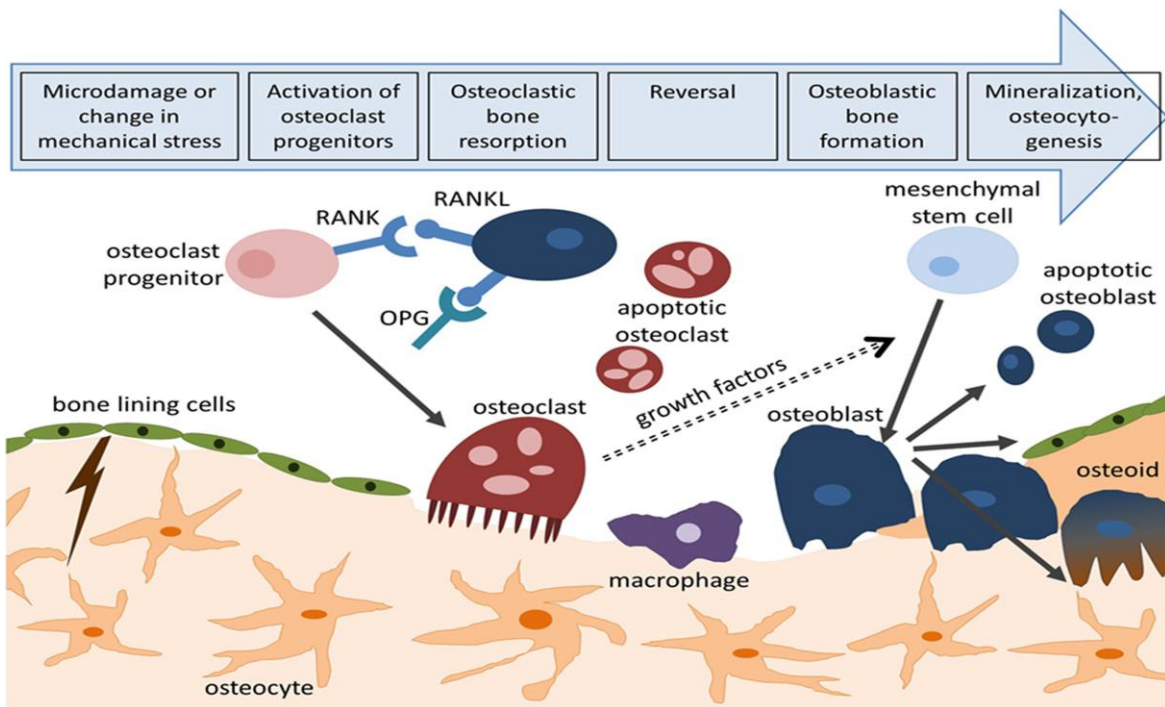


**Figure 2: Overview of cellular events in basic multicellular unit.** Bone homeostasis is preserved by a balanced osteoblast and osteoclast activity. Osteocytes acts as mechanosensors and provide support under stress condition. Bone lining cells are the old osteoblasts that make passage for mineral exchange (Adapted from [47]).

The ruffled border transport enzymes and minerals into resorption cavity to degrade bone matrix proteins. The presence of ruffled border points to the active sites of osteoclasts mediated resorption. Differentiation of osteoclasts is regulated by Macrophage colony-stimulating factor (M-CSF), Receptor Activator of Nuclear Factor Kappa B Ligand (RANKL), and Osteoprotegerin (OPG) [45]. RANKL is also expressed in abundance by T-lymphocytes. RANKL promotes osteoclastogenesis while OPG inhibits osteoclastogenesis (Figure 2). The balance between RANKL and OPG governs the quantity of bone resorbed [48]. Dysregulation in osteoclast activity leads to autoimmune disease like rheumatoid arthritis [49] and systemic skeletal disease like osteoporosis [50].

#### **1.2.4 Bone lining cells**

Bone lining cells cover inactive bone surfaces where neither bone resorption nor bone formation can take place [51]. Bone lining cells enter the lacuna and clean the leftover collagen fibers with the help of Matrix Metalloproteinases (MMPs) after withdrawing osteoclasts from resorption pit [52]. Therefore, bone lining cells are important for balanced bone remodeling (Figure 2).

### **1.3 Fracture Healing**

Fracture repair is a complex process involving timed cellular recruitment, gene expression, and synthesis of compounds that regenerate native tissue to restore the mechanical integrity [53]. Many factors like fracture location, degree of stability, infection, patient's characteristics, and premedication are associated with the success of fracture healing [2]. 10-15% of cases result in delayed or non-union that need higher treatment costs [2]. Understanding fracture healing in a physiological condition is important step in developing therapeutics.

Fracture healing is represented by a series of overlapping healing events that recapitulate stages of embryonic development [54]. The fracture healing has five main healing events, which are discussed below (Figure 3).

#### **1.3.1 Inflammatory phase**

Injury disrupts the blood vessels and surrounding soft tissue along with bone matrix. This leads to bleeding, hypoxic condition, and hematoma formation which triggers the early inflammatory response [55]. The onset of inflammation triggers migrating cytokines and growth factors at the site of injury to set up vascularization and preserve bone homeostasis [56]. T-lymphocytes and macrophage/monocytes act as initiating cell types in healing [57]. Pro-inflammatory cytokines like Interleukin 1 (IL-1), IL-6, tumor necrosis factor (TNF) are among the early released cells during inflammatory phase [58] (Figure 3). Lymphocytes migrate into the fracture callus after macrophage recruitment and begin the cell differentiation with adaptive immune response [59]. The timely termination of inflammation and early onset of revascularization process are independent and essential for a regenerative healing process [60]. However, systemic inflammation seen in patients with rheumatoid arthritis, diabetes mellitus, multiple trauma can increase fracture healing time or cause non-union [61].

#### **1.3.2 Reparative phase**

Reparative phase overlaps with the inflammatory phase and contribute in blood vessel development. The hematoma formed during injury recruits mesenchymal stem cells that differentiate into chondrocytes to induce callus formation (Figure 3). Soft callus formation gives stability to fracture [62]. The peak of soft callus formation occurs 7-9 days post-

trauma [2]. Chondrocytes multiply to become hypertrophic and calcify the ECM. The soft callus becomes mechanically rigid as the hard callus formation progresses and calcified cartilage get replaced by woven bone [63]. Fracture heals by two different mechanism: direct and indirect healing. Indirect healing occurs without stable condition while direct healing takes place in the presence of rigidly stable condition [64]. Direct healing involves intramembranous ossification. While, indirect healing involves endochondral and intramembranous ossification [63]:

1. Endochondral ossification is characterized by the differentiation of mesenchymal stem cells into chondrocytes, which forms cartilaginous matrix and later get replaced by bone (Figure 3). Soft callus formation gives a stability to fracture. As the cartilage mineralizes, blood vessels invasion mediates an influx of osteoprogenitor cells that produce a central hard callus on top of mineralized cartilage matrixes and an influx of osteoclasts that resorb the calcified cartilage. As a result, the bony callus matures and undergoes remodeling with time, finally allowing bone to regain its original architecture and role [65] (Figure 3). While occasionally, problem in transition of cartilage to bone occurs and results in severe condition of osteoarthritis [66].

2. Intramembranous ossification is characterized by direct differentiation of mesenchymal stem cells into osteoblasts. Intramembranous ossification occurs near to proximal and distal end to form hard callus [67]. While sometimes, progressive osseous heteroplasia occurs because of predominance of intramembranous ossification [68]. Further, skeletal dysplasia in osteogenesis imperfecta type II patients occur because of disorder in intramembranous and endochondral ossification [69].

### **1.3.3 Remodeling phase**

The woven bone transforms to lamellar bone during remodeling phase of healing. Bone remodeling is tightly regulated by osteoclast and osteoblast (Figure 3). The process of remodeling advances in tunnels with osteoclast forming “cutting cones” that remove the old and make way for osteoblasts to form new bone [70]. The balanced activity of osteoclasts and osteoblasts results in gradual increase of bone density and improved weight bearing quality [71]. While, imbalanced osteoclast and osteoblast activity results in systemic skeletal disease like osteoporosis [72].

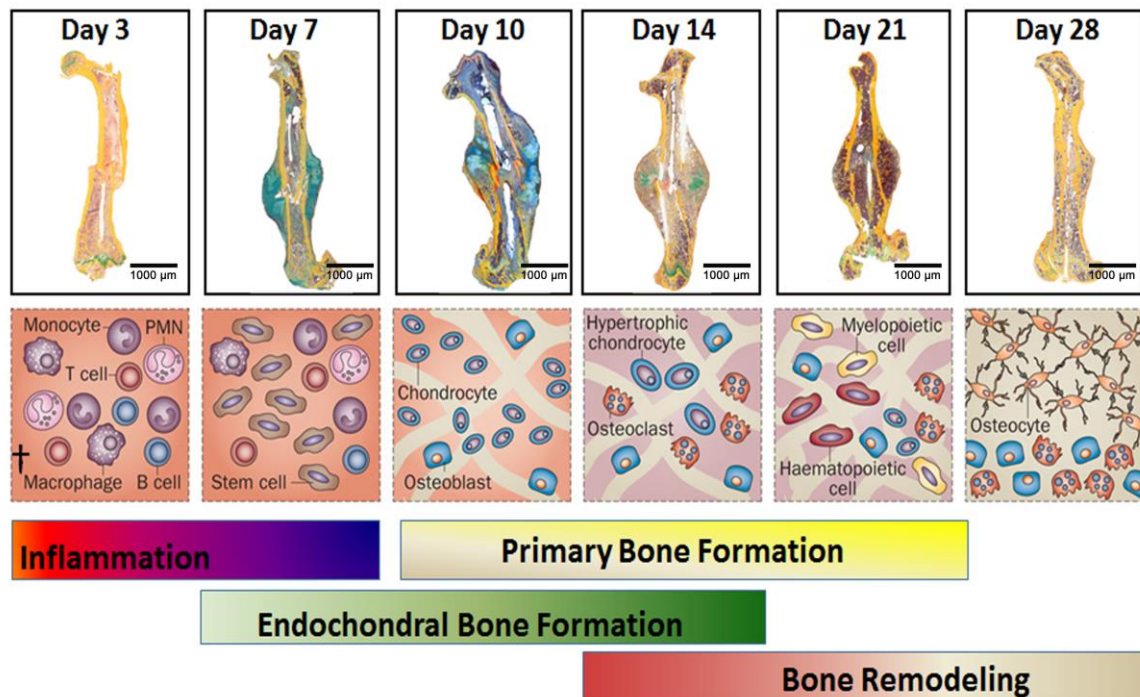


**Figure 3: Interdependent stages of fracture healing in a wild type mouse model.** Inflammatory response is initiated upon fracture through hematoma by (day=D) D3, leading to cartilaginous callus formation within D7, which serve basis for the new bone formation. The cartilage shows chondrocytes hypertrophy by D10 marking the initiation of ossification and continues until D14. A bony bridged callus is formed at D21 and later remodeling is initiated in which cortical bone reshape to its original status by D28 († adapted from [73]).

## **2. OBJECTIVES OF THIS STUDY**

Many cellular and molecular events like inflammation, ossification are important for the positive regulation of fracture healing. Several different animal models were generated and implemented in fracture healing study. This study aims at exploring the progression of bone healing using a standardized closed femoral fracture mice model. Different milestone of this study are:

1. Analysis of underlying molecular mechanism behind fracture healing through the application of high-throughput sequencing data.
2. Explain the role of mitochondrial and ribosomal genes in fracture healing.
3. Role of angiogenesis, ossification, ECM regulation, and immune response in successful bone healing.
4. Examine the role of differentially expressed genes present at each healing event.
5. Inferring the importance of overlapping genes present between consecutive time points.
6. Evaluation of collagen fibers orientation during progression of healing.
7. Examine the osteocytes morphological changes in correspondence to bone healing.
8. Histological evaluation of bone mineralization and extracellular matrix biomarkers.
9. Explore GPX1 and UBB signal localization and distribution around fractured callus and in osteocyte vicinity.

### 3. MATERIALS AND METHODS

This work was performed on historical samples, whereas mice housing and operation, sample collection, embedding of histological samples as well as RNA extraction, hybridization and microarray sequencing were all carried out by members of the Biology of Bone Healing team of the Julius Wolff Institute, at the Charité - Universitätsmedizin Berlin, Berlin, Germany.

#### 3.1 *Experimental Design*

A standard mid diaphyseal closed fracture was generated in the left femora of eight-week-old male wild type mice (C57BL/6N; Charles River Laboratories, Wilmington, MA, USA) using the method developed by Bonnarens and Einhorn [74]. Animals received 2.5% isoflurane mixed with oxygen inhalation and subcutaneous injection of 1 mg Buprenorphin (Reckitt Benckiser, Ludwigschafen am Rhein, Germany) per kilogram body weight for anesthesia before surgery. Under anesthesia, the animals were prepared for surgical procedure by shaving and cleaning (Braunoderm®, B. Braun Melsungen AG, Hesse, Germany) the left hind limb. The left knee was bent and an incision was made through the skin to the middle of patella. The patella was then dislocated laterally to expose the femoral condyles. A 0.55 mm sterile hollow needle (BD Microlance™, Becton Dickinson Life Sciences, Heidelberg, Germany) was used to create a passage for the intramedullary pin through the distal end. Later, the needle was removed to insert an intramedullary pin (Thermo spinal needle 17, 0.5 × 0.9 mm, Thermo Europe N. V., Leuven, Belgium) into the bone marrow cavity. The cutter was used to adapt the pin length according to the mice femur. After the pin alignment, the patella was repositioned and the limb was sutured successfully.

Animals were euthanized at (D = Days, N = 67) D3, D7, D10, D14, D21, and D28 post-fracture. D0 served as the control for the study of differential gene expression. D7, D10, D14, D21, and D28 were used for histological evaluation. Mice were anesthetized and euthanized by Carbon dioxide (CO<sub>2</sub>) inhalation as certified by the regional ethical committee. Furthermore, mice were euthanized by cervical dislocation for differential gene expression analysis. After euthanasia, the left femurs were cleaned and collected.

The animal experiments and sample collection were carried out by members of the Biology of Bone Healing team of the Julius Wolff Institute, at the Charité - Universitätsmedizin Berlin, Berlin, Germany.

### ***3.2 Animal Ethical Declaration***

The study was performed in full compliance with the institutional laws and the German animal protection laws. Animal experiments were approved by the Animal Ethics Committee in the state of Berlin, Germany (“Landesamt für Gesundheit und Soziales, Berlin”, Permit number: G0206/08).

### ***3.3 Sample Preparation for Histological Evaluation***

After euthanasia, samples were collected and fixed in 4% Paraformaldehyde solution (PFA) for 48 hours to perform decalcified histology. Samples collection, infiltration and paraffin embedding were carried by members of the Julius Wolff Institute, at the Charité - Universitätsmedizin Berlin, Berlin, Germany. The detailed embedding protocol is present in Appendix 1. The solidified blocks were stored at 4°C for 24 hours before sectioning. A motorized rotary microtome (Thermo / Microm HM 355 S, Thermo Scientific GmbH, Karlsruhe, Germany) was used to cut 5 µm thick sections. Sections were immediately placed in a warm water bath (40°C) to allow stretching. Then, the sections were mounted on a glass slide (SuperFrost Plus®, R.Langenbrinck GmbH, Labor- und Medizintechnik, Emmendingen, Germany) and dried in an incubator for 24 hours at 37°C. The sectioning and subsequent staining were carried out at the Experimental Trauma Surgery of the Justus-Liebig-University, Giessen, Germany to fulfill the requirement of this thesis.

### ***3.4 Histological Staining***

Different histological stains provide visualization and analysis of cellular changes, bone mineralization, and extracellular matrix organization. The paraffin embedded sections were used to perform the following staining:

**3.4.1 Sirius Red Stain** differentiates type I, type II, and type III collagen within a sample under polarized light [75]. Type I collagen appears as yellow-red, type II collagen appears as blue-light yellow, and type III collagen appears as green. The stain was used to investigate the organization and heterogeneity of collagen fibers orientation during callus maturation in fracture healing. The detailed staining protocol is present in Appendix 2.

**3.4.2 Trichrome Masson Goldner Stain** differentiates the mineralized and non-mineralized bone matrix within a sample [76]. Mineralized bone matrix appears as green and non-mineralized bone matrix appears as red. The stain was performed to qualitatively analyze the changes in bone mineralization with progression of fracture healing process. The detailed staining protocol is present in Appendix 3.

**3.4.3 Silver Nitrate Stain** differentiates osteocytes and their canaliculi network by staining acidic protein present in the bone matrix within a sample.[72]. The stain was used to analyze the morphological changes in osteocytes during fracture healing. Active osteocytes appears as spindle shaped with canaliculi, intermediated osteocytes appears as spherical shaped, and inactive osteocytes appears as empty lacunae. The detailed staining protocol is present in Appendix 4. All the histological stains were carried out in Experimental Trauma Surgery, at the Justus-Liebig-University Giessen, Giessen, Germany.

### **3.5 *Immunohistochemical Staining***

Immunohistochemical (IHC) stains help in analyzing protein signal activity to describe cellular regulation within a sample based on antibody-antigen reactions. Antigens were retrieved by pretreating paraffin sections with citrate buffer at 60°C for 1 hour. Following IHC stains were performed as indicated in the general protocol present in Appendix 5:

**3.5.1 Alpha Smooth Muscle Actin (ASMA)** serve as a biological marker to visualize blood vessel formation [77]. The stain was performed to investigate blood vessel formation during fracture healing. ASMA labeling was performed using a rabbit polyclonal primary antibody dilution in 1:100 ratio and visualized with vector red Alkaline phosphatase (AP)-kit (AK 5200, Vectastain ABC kit, Vector Laboratories, Inc., Burlingame, CA, USA). The sections were then counter-stained with Methyl Green.

**3.5.2 Matrix Extracellular Phosphoglycoprotein (MEPE)** serve as a biological marker of ECM formation and bone mineralization [78]. The stain was performed to investigate the changes within ECM during fracture healing. MEPE labeling was performed using a rabbit polyclonal primary antibody diluted in 1:100 ratio and visualized using vector red AP-kit. The sections were then counter-stained with Toluidine Blue.

**3.5.3 Extracellular Signal Regulated Kinase (ERK)** serve as a biological marker of cell migration and adhesion on ECM [23]. The stain was performed to investigate the changes

within ECM during fracture healing. ERK labeling was performed using a rabbit polyclonal primary antibody diluted in 1:100 ratio and visualized using vector red AP-kit. The sections were then counter-stained with Toluidine Blue.

**3.5.4 Glutathione Peroxidase 1 (GPX1)** serve as a biological marker of oxidative stress in cardiovascular diseases [79]. GPX1 is a part of mitochondrion. The stain was performed to investigate changes in mitochondrial activity during fracture healing. GPX1 labeling was performed using a rabbit polyclonal primary antibody diluted in 1:325 ratio and visualized using vector red AP-kit. Two different set of samples were stained using similar protocol. One set of sections were then counter-stained with Toluidine Blue to perform quantitative evaluation of GPX1 activity in the callus region. The other set of sections were counter-stained with Silver Nitrate to investigate the activity of GPX1 in osteocyte vicinity.

**3.5.5 Ubiquitin (UBB)** serve as a biological marker for proteasome dysfunction in neurodegeneration [80]. UBB is a conserved protein involved in ribosome activity. The stain was performed to investigate the changes in ribosomal activity during fracture healing. UBB labeling was performed using a rabbit polyclonal primary antibody diluted in 1:150 ratio and visualized using vector red AP-kit. One set of sections were then counter-stained with Toluidine Blue to perform quantitative evaluation of UBB activity in the callus region. The other set of sections were counter-stained with Silver Nitrate to investigate the activity of UBB in osteocyte vicinity.

### ***3.6 Image Acquisition and Histomorphometry***

All images were acquired using a Leica microscope (Leica DM5500 photomicroscope equipped with DFC7000 camera, LASX software version 3.0; Leica Microsystem Ltd., Wetzlar, Germany). All histological stained were imaged using 10X and 40X magnification. The sections of GPX1 and UBB counter-stained with Silver Nitrate were visualized using Texas-Red filter (Leica Microsystem Ltd., Wetzlar, Germany) at > 560 nm emission and imaged at oil emersion (100X) magnification. The excitation wavelength range was set between 365 to 560 nm for the fluorescent red substrate.

Sirius red sections were visualized using Leica microscope equipped with additional polarized analyzer (11555079, Analyzer 180, Rotatable; Leica Microsystem Ltd., Wetzlar, Germany) and lambda filter (11513908, Lambda plate in holder; Leica Microsystem Ltd.,

Wetzlar, Germany). Analyzer was kept at 150° and lambda plate was kept at 75° for all samples. Monochrome and colored images were taken using 10X, 20X, 40X, and oil emersion (100X) magnification.

Histomorphometry was performed using ImageJ software (version 1.51n, National Institute of Health, Bethesda, MD, USA). Trainable Weka Segmentation (version 3.2.13) [81] plugin was used to calculate tissue area after IHC stains. Cell Counter plugins was used to count osteocytes after Silver Nitrate staining. The complete protocol is present in Appendix 6. Image capturing and analysis were carried out in the Experimental Trauma Surgery, at the Justus-Liebig-University, Giessen, Germany.

### ***3.7 Quantification of Collagen Fibers***

An automated standalone CT-FIRE (version 2.0 Beta) package from MATLAB (version R2017b, MathWorks, Natick, MA, USA) was used to computationally segment collagen fibers from Sirius red stained monochrome pictures (Figure 4).. CT-FIRE was used before to quantify fibril structure taken from transmission electron microscopy or fluorescence microscopy [82, 83].

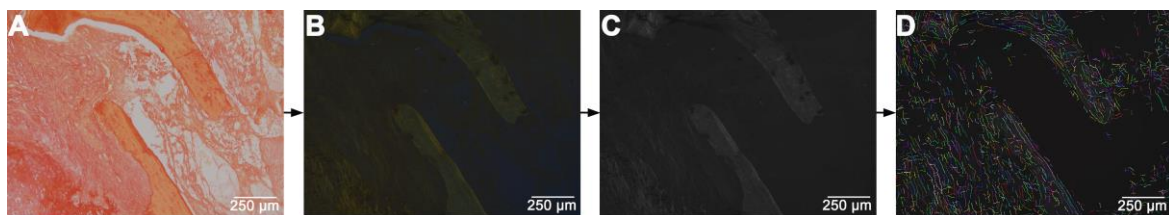


***Figure 4: Application of Sirius red stained images to quantitative evaluate collagen fiber orientation using CT-FIRE. This study established the methodology to perform quantification of collagen fibers from Sirius red stained images under polarized light.***

### ***3.8 Statistical Analysis***

Descriptive statistics were carried out to test normality of data sets. Data were analyzed using IBM SPSS Statistical Package 24.0 (IBM Corporation, Armonk, NY, USA). One-way analysis of variance (ANOVA) test with Bonferroni correction was used for parametric distribution (Fiber width, straightness, and angle). Significance analysis for non-parametric distribution was performed using Mann Whitney U-test (Fiber length, histomorphometry). Bar graphs were presented as Mean  $\pm$  Standard Error of Mean (SEM).

### ***3.9 RNA Preparation and Microarray Hybridization***

After euthanasia, samples were collected for RNA isolation. Collected tissues were circumscribed by 1 mm on either side of the fracture callus. Tissues were flash frozen in liquid nitrogen and stored at -80°C until used for RNA extraction. During sample preparation, tissues were pulverized using pestle and mortar under continuous cooling with liquid nitrogen and then homogenized in TRIZOL using T10, Ultraturrax while placed on ice. Following homogenization, total RNA was isolated from samples using TRIZOL as per the manufacturer's protocol (Invitrogen Life Technologies, Berlin, Germany) including DNase I (Invitrogen Life Technologies, Berlin, Germany) digestion. 150 ng of each RNA samples per group were taken and mixed in a given pooled and RNA mix was distributed into three vials (200 ng each) for microarray analysis.

Transcriptome profiling was performed using Illumina's MouseRef-8 v2.0 Expression Bead Chips (Illumina, Ambion, TX, USA). RNA processing for cRNA synthesis and labeling was done according to standard protocols as described in the user manual of Illumina TotalPrep RNA amplification kit (Illumina, Ambion, TX, USA). Hybridization of the labeled and fragmented cRNA to the microarray and subsequent staining, washing and scanning of the arrays were done as instructed in the Illumina Whole-Genome Gene Expression direct Hybridization Assay guide.

RNA isolation and microarray hybridization were carried out by the members of the Biology of Bone Healing team of the Julius Wolff Institute, at the Charité - Universitätsmedizin Berlin, Berlin, Germany. The detailed RNA isolation protocol is present in Appendix 7.

### ***3.10 Data Normalization and Filtering Criteria***

The raw data was analyzed using the R project for Statistical Computing (version 3.0.3). Different packages provided by Bioconductor (version 3.5) were used to process and normalize the array files. Illumina whole genome sequencing generated IDAT files that store the intensity values of each probe. Illuminaio package [84] was used to read the IDAT files. Bead array package [85] was used to read the intensity data and perform background corrections and normalization. Limma package [86] was used to analyze differential expression in microarray data. Quintiles were normalized between array using above mentioned packages. Quality assessment of array data was carried out by

calculating Pearson's correlation coefficient between arrays. Fold Change (FC) was calculated as the differences between each post-fracture day (D3, D7, D10, D14, D21, and D28) and D0. The significance level (P-value) was calculated using a two-tailed student t-test. The script used for quality assessment is present in Appendix 8. The microarray data analysis was carried out in the Experimental Trauma Surgery, at the Justus-Liebig-University, Giessen, Germany as a part of this thesis.

### ***3.11 Clustering of Differentially Expressed Genes***

Clustering of genes based on the expression pattern identifies co-regulated and functionally related genes. Hierarchical clustering method using R (version 3.0.3) and Bioconductor packages was implemented to obtain set of DEG with similar expression profile. The script used for hierarchical clustering is present in Appendix 9.

### ***3.12 Functional Annotation of Differentially Expressed Genes***

Functional annotation of genes provides an insight to the molecular function, cellular component, and biological process. An online server; Database for Annotation, Visualization and Integrated Discovery (DAVID) bioinformatics database (version 6.7, <https://david.ncifcrf.gov/>) [87] provides an integrated and updated information about the involved molecular function, cellular component, and biological processes for gene of interest. Furthermore, DAVID provides an option of functional annotation clustering to cluster functionally similar terms associated with gene list. DAVID analysis was performed to investigate the role of DEG during fracture healing. The set of genes obtained after hierarchical clustering were functionally clustered using DAVID with enrichment score  $\geq 1.5$ . Enrichment score is a method to identify the over-represented functional annotation terms for gene clusters. The detailed protocol used is present in Appendix 10.

## 4. RESULTS

### 4.1 Comparison of FC cut-offs resulted in no variation in DEG pattern

FC and P-value are the standard cut-offs criteria to analyze DEG in microarray data. However, a P-value of 0.01 is favorable over a 0.05 value. Therefore, discrepancies in data can result from the implemented FC. Although literature reports FC cut-offs of |1|, |1.5|, and |2| as acceptable, but the resulting pattern variation was not addressed. Therefore, differences in pattern change with FC cut-offs were investigated. The obtained DEG from each FC were functionally annotated and six highly represented biological processes were: angiogenesis, ossification, ECM, immune response, mitochondrial, and ribosomal activity. The percentage distribution of biological processes was plotted in pie charts separately for upregulated and downregulated genes (Figure 5).

Expectedly the number of DEGs negatively correlated with FC value. FC cut-off of |1|, |1.5|, and |2| resulted in 2949, 1235, and 379 DEG respectively. Nonetheless, overlapping genes were observed between upregulated and downregulated panel at all FC cut-offs (Table 1).

**Table 1: Number of differentially expressed genes and overlapping genes at each FC cut-off**

FC cut-offs	No. of DEG	No. of upregulated genes	No. of downregulated genes	No. of overlapping genes
1	2650	1138	1314	198
1.5	1106	374	699	33
2	438	122	309	7

Among the upregulated panel, 18% of angiogenesis genes were present at  $FC \geq |1|$ , the percentage declined to 8% at  $FC \geq |1.5|$ , and then further to 7% at  $FC \geq |2|$  (Figure 5 A, C, E). Furthermore, 14% of ossification genes were present at  $FC \geq |1|$ , whereas the percentage increased to 21% at  $FC \geq |1.5|$ , and then further increased to 27% at  $FC \geq |2|$ . ECM genes occupied 17% at  $FC \geq |1|$ , 24% at  $FC \geq |1.5|$ , and 27% at  $FC \geq |2|$  (Figure 5 A, C, E).

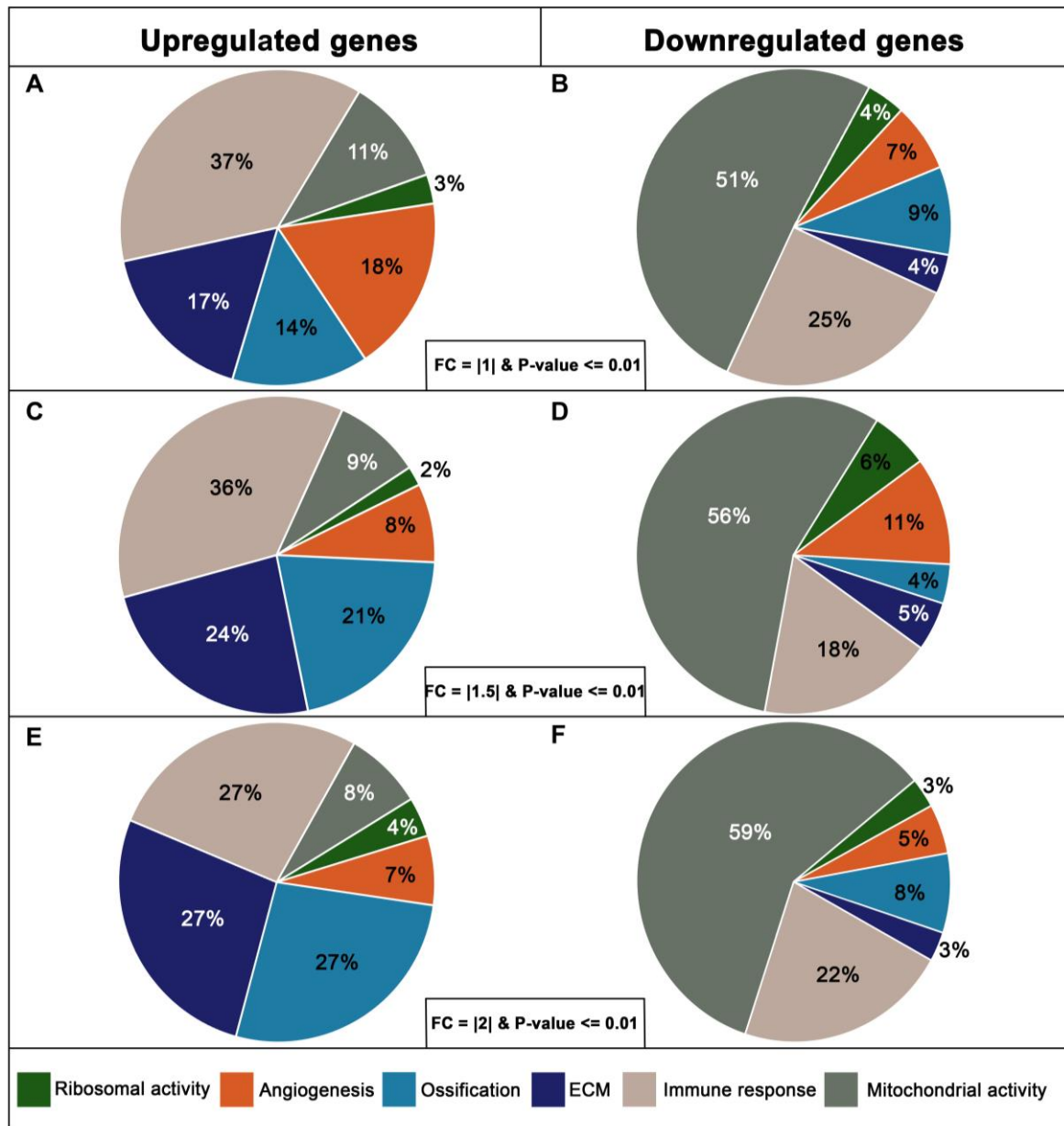


**Figure 5: Higher cut-off reduce the number of genes without affecting gene ontology prediction.** FC cut-offs of  $|1|$ ,  $|1.5|$ , and  $|2|$  along with  $P\text{-value} \leq 0.01$  were investigated to address pattern variation.  $FC \geq |1|$  and  $FC \geq |1.5|$ , (A, B) showed higher percentage of immune response genes in upregulated panel, and (D, E) higher percentage of mitochondrial genes in downregulated panel. At  $FC \geq |2|$ , (C) 27% of each of immune response, ECM, and ossification genes were present in upregulated panel, (F) highest percentage of mitochondrial genes were present in the downregulated panel. (FC: fold change).

Interestingly, immune response genes showed higher percentage of 37% and 36% at  $FC \geq |1|$  and  $FC \geq |1.5|$ , respectively (Figure 5A). While, the percentage of immune response genes declined to 27% at  $FC \geq |2|$ . Furthermore, 11% of mitochondrial genes were present

at  $FC \geq |1|$ , the percentage decreased to 9% at  $FC \geq |1.5|$ , and then to 8% at  $FC \geq |2|$  (Figure 5 A, C, E). Ribosomal genes showed lower percentage at all FC cut-off in upregulated panel. 3% of ribosomal activity related genes were present at  $FC \geq |1|$ , the percentage declined to 2% at  $FC \geq |1.5|$ , and then further increased to 4% at  $FC \geq |2|$ .

Among the downregulated panel, 7% of angiogenesis genes were present at  $FC \leq |1|$ , the percentage increased to 11% at  $FC \leq |1.5|$ , and then declined to 5% at  $FC \leq |2|$  (Figure 5 B, D, F). Furthermore, 4% of ossification genes were present at  $FC \leq |1|$  and  $FC \leq |1.5|$ , and then the percentage increased to 8% at  $FC \leq |2|$ . ECM genes showed 4% at  $FC \leq |1|$ , percentage increased to 5% at  $FC \leq |1.5|$ , and then decreased to 3% at  $FC \leq |2|$  (Figure 5 B, D, F). Immune response genes were 25% at  $FC \leq |1|$ , 18% at  $FC \leq |1.5|$ , and 22% at  $FC \leq |2|$ . Interestingly, mitochondrial genes showed higher percentage at all FC cut-off in the downregulated panel (Figure 5 B, D, F). Mitochondrial genes were 51%, 56%, and 59% at  $FC \leq |1|$ ,  $FC \leq |1.5|$ , and  $FC \leq |2|$  respectively (Figure 5 B, D, F). Furthermore, 4% of ribosomal genes were present at  $FC \leq |1|$ , the percentage increased to 6% at  $FC \leq |1.5|$ , and then decreased to 3% at  $FC \leq |2|$ .

Despite the decline in number of DEG, the biological processes with highest representation remained the same in upregulated and downregulated panels. Immune response genes occupied higher percentage at  $FC \geq |1|$  and  $FC \geq |1.5|$  in the upregulated panel when compared to other processes (Figure 5). Whereas at  $FC \geq |2|$ , immune response, ECM, and ossification genes showed equal percentage of 27%. Mitochondrial genes showed more than 50% at all FC cut-offs in the downregulated panel (Figure 5 B, D, F). Choice of higher FC cut-off provided with list of highly affected genes. Therefore, further analysis was performed using  $FC \geq |2|$  and P-value  $\leq 0.01$  cut-off.

#### ***4.2 Overlapping genes between two consecutive time points: hallmark either by mitochondrial activity or by ECM regulation***

Fracture healing process represents a series of overlapping cellular events. Genes present in two consecutive time points, regardless if up- or down-regulated, were taken as overlapping gene list. Investigating overlapping genes aimed to understand overlapping of healing phases. Obtained overlapping gene lists were functionally annotated and highly representative biological processes obtained were: angiogenesis, ossification, ECM, immune response, mitochondrial, and ribosomal activity. Furthermore, the percentage

distribution of biological processes in the consecutive time points were presented in pie-charts (Figure 6).

201 and 212 genes were differentially expressed at D3 and D7, respectively. 181 common (overlapping) genes were expressed at D3 as well as D7 (Figure 6A). Functional annotation of overlapping genes showed higher percentage (40%) of mitochondrial genes (Figure 6B). 20% of ECM and 16% of immune response genes were present in overlap of D3 & D7. Ossification, angiogenesis, and ribosomal genes were present in equal percentage (8%) in overlap of D3 & D7 (Figure 6B).

212 and 146 genes were differentially expressed at D7 and D10, respectively. 22 overlapping genes were present at D7 and D10 (Figure 6A). Overlapping genes between D7 and D10 showed higher percentage (44%) of ECM genes (Figure 6B). 25% of ossification genes and 19% of mitochondrial genes were present between D7 & D10. 12% of immune response genes were present in overlap of D7 & D10. No genes involved in angiogenesis or ribosomal activity were present in overlap of D7 and D10 (Figure 6B).

146 and 132 genes were differentially expressed at D10 and D14, respectively. 91 genes overlapped between D10 and D14 (Figure 6A). Functional annotation of overlapping genes showed higher percentage (44%) of ECM genes (Figure 6B). 20% of immune response genes and 17% of ossification genes were present between D10 & D14. Furthermore, 13% of mitochondrial genes were present between D10 & D14 overlap. 4% of ribosomal genes and 2% of angiogenesis genes were present in the overlap of D10 & D14 (Figure 6B).

132 and 34 genes were differentially expressed at D14 and D21, respectively. 16 genes overlapped between D14 and D21 (Figure 6A). Overlapping genes between D14 and D21 showed higher percentage (41%) of ECM genes (Figure 6B). 29% of ossification genes and 18% of immune response genes were present between D14 & D21. 12% of mitochondrial genes were present between D14 & D21 overlap (Figure 6B).

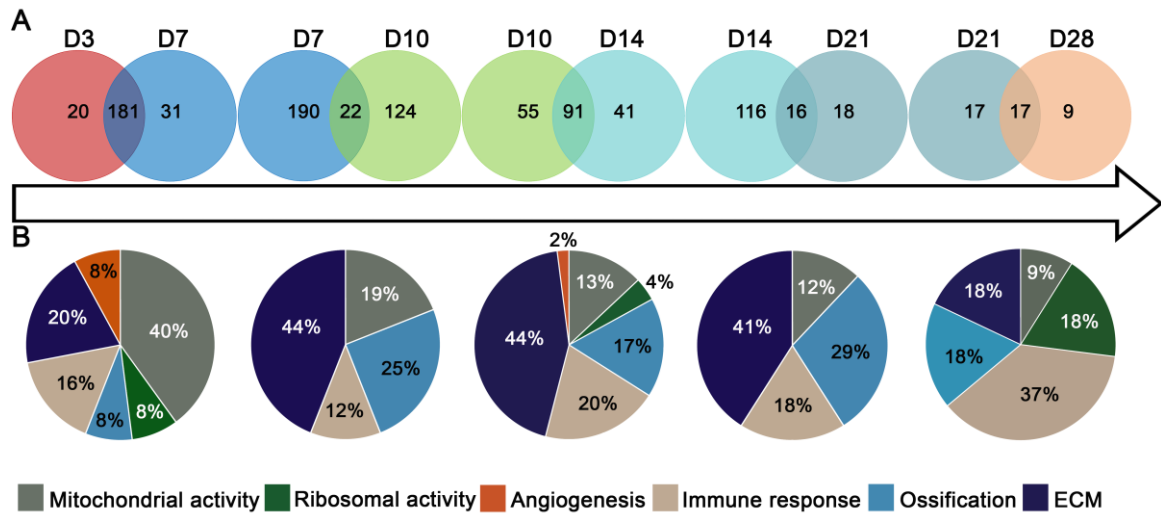


**Figure 6: Functional annotation of overlapping genes between consecutive time points showed higher percentage of mitochondrial and ECM genes.** DEG list between two consecutive time points were compared to understand differential regulation throughout the healing process. (A) Venn diagram depicts the number of overlapping genes between every two consecutive time points. D3 & D7 showed highest number of overlapping genes. Number of DEGs were higher at D3, D7, D10, and D14 when compared to D21 and D28. (B) Functional annotation showed higher percentage of mitochondrial genes at D3 and D7. Higher percentage of ECM genes were differentially expressed at D7, D10, D14, and D21.

34 and 26 genes were differentially expressed at D21 and D28, respectively. 17 genes overlapped between D21 and D28 (Figure 6A). Immune response genes showed higher percentage (37%) in D21 and D28 overlap (Figure 6B). ECM, ossification, and ribosomal genes were present in equal percentage (18%) between D21 & D28. 9% of mitochondrial genes were present in D21 & D28 overlap (Figure 6B).

The comparison of consecutive time points showed highest number of overlapping genes present between D3 and D7 when compared to other overlapping time points. Furthermore, functional annotation showed the higher percentage presence of mitochondrial genes between D3 and D7. Whereas higher percentage of ECM genes were present between D7 & D10, D10 & D14, and D14 & D21 (Figure 6B). The detailed understanding of differential gene expression across time points is required, which instigated use of clustering algorithm.

### ***4.3 Hierarchical clustering of genes based on expression pattern across time points generated ten distinct clusters***

Hierarchical clustering was performed to investigate the changes in expression pattern of genes across time points of healing. DEGs present in at least one time point were used for hierarchical clustering. Genes present in each cluster were visualized in a heatmap (Figure 7, left panel). The obtained set of genes (clusters) were then functionally annotated (Figure 7, right panel).

Hierarchical clustering resulted in ten distinct clusters. Genes of the first, fifth, sixth, and tenth cluster were downregulated at all time points (Figure 7, left panel). 66 genes were present in first cluster and 21 genes were present in fifth cluster. Genes present in first and fifth cluster are related to mitochondrial activity and cytoskeleton organization, respectively. 33 genes were present in sixth cluster and 4 genes were present in tenth cluster. Genes present in sixth cluster are related to angiogenesis, ECM, and bone mineralization (Figure 7, right panel). Whereas, genes present in tenth cluster are related to cell repair activity. Furthermore, genes of the second, third, fourth, and ninth cluster were upregulated only at D10 and D14 whereas downregulated at other time points. 150 genes were present in second cluster. Genes in second cluster are related to ribosomal proteins, ECM, and innate immunity (Figure 7, right panel). 5 genes and 13 genes were present in third and ninth cluster, respectively. Genes in the third and ninth cluster are related to mitochondrial activity. 58 genes were present in fourth cluster. Genes in fourth cluster are related to bone mineralization, ECM, and immune response (Figure 7, right panel). Genes in seventh cluster were upregulated only at D14 while downregulated at all other time points (Figure 7, left panel). 14 genes were present in seventh cluster. Genes in the seventh cluster are related to glycolysis and post-translational activity. Genes in eighth cluster were upregulated only at D14 and D21 whereas downregulated at other time points. 33 genes were present in eighth cluster. Genes in the eighth cluster are related to cell adhesion, transcription, and ossification (Figure 7, right panel).

Among 66 genes within first cluster, several important genes crucial for ECM, bone homeostasis, and ribosomal proteins were differentially expressed. Genes like 3-Oxoacid CoA-Transferase 1 (Oxct1) which is needed for ketone body catabolism and Ubiquitin B (Ubb) which is required for translational activity were present in first cluster.

Among 150 genes within second cluster, several important genes crucial for ribosomal activity, immune response, and ECM were differentially expressed. Ribosomal protein s6 (Rps6) and Ribosomal protein s3 (Rps3) required for protein synthesis and phosphorylation were present in second cluster.

Among 5 genes within third cluster, Adenosine triphosphate synthase subunit beta, mitochondrial (Atp5b) which encodes for ATP synthesis and transport was differentially expressed.

Among 58 genes within fourth cluster, several important genes crucial for bone mineralization, ECM, and immune response were differentially expressed. Genes like Integrin binding sialoprotein (Ibsp) and Matrix gla protein (Mgp) that are crucial for ossification were present in fourth cluster.

Among 21 genes within fifth cluster, several important genes crucial for cytoskeleton organization and ECM were differentially expressed. Genes like Myomesin 1 (Myom1) which is required for muscle contraction and Calpain small subunit 1 (Capns1) which is required for cell proliferation were present in fifth cluster.

Among 33 genes within sixth cluster, several important genes crucial for angiogenesis and bone mineralization were differentially expressed. Genes including blood vessel formation marker like Vascular endothelial growth factor alpha (Vegfa) and bone matrix mineralization marker like Secreted phosphoprotein 1 (Spp1) were present in sixth cluster.

Among 14 genes within seventh cluster, genes that encode for protein synthesis within mitochondrion like Mitochondrial Ribosomal Protein 153 (Mrpl53) and Cytochrome c oxidase assembly homolog 19 (Cox19) were differentially expressed.

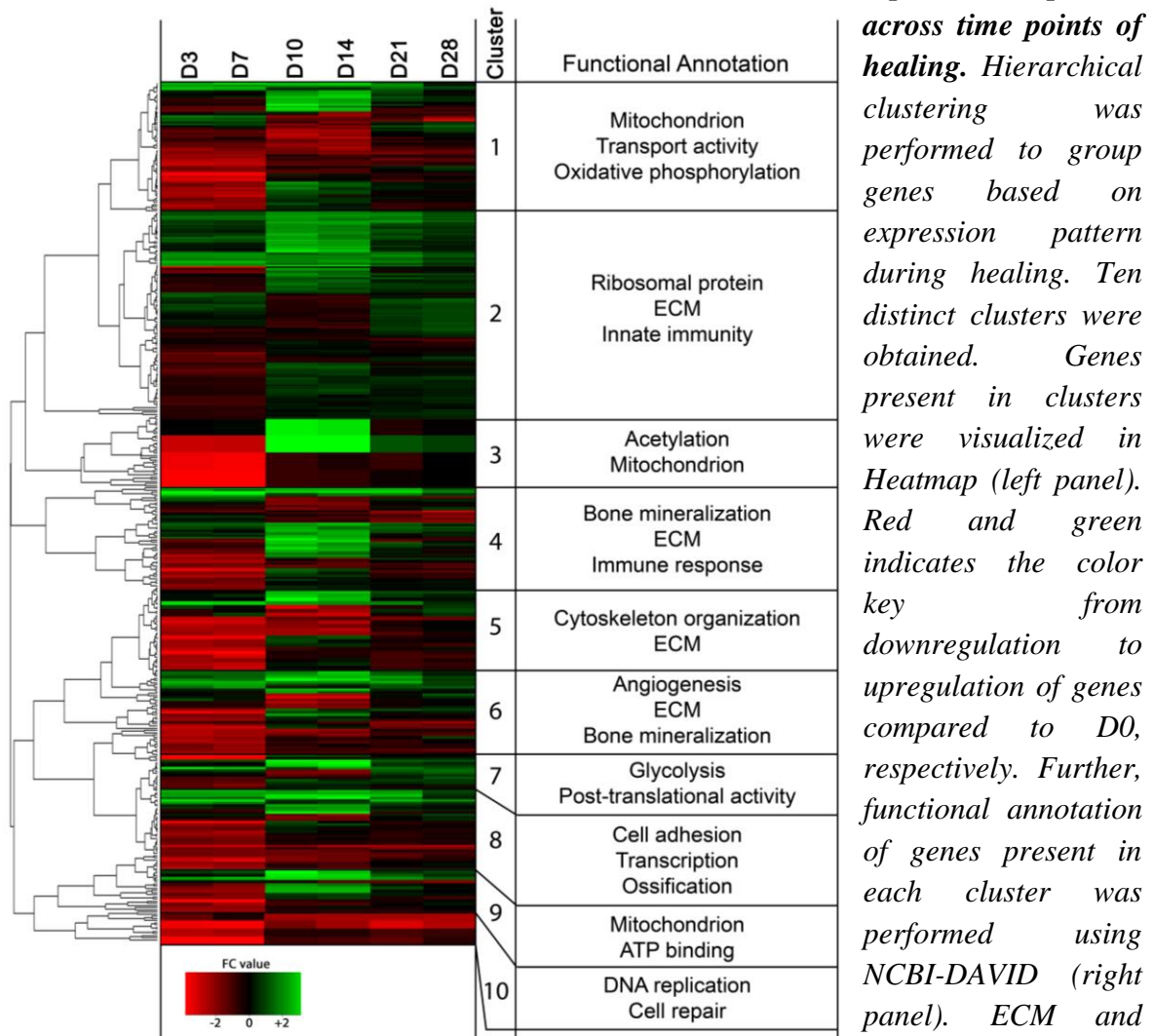
Among 33 genes within eighth cluster, several important genes crucial for transcription and ossification were differentially expressed. Genes like Ribosomal protein s2 (Rps2) and Matrix metalloproteinase 13 (Mmp13) that are required for protein translation and tissue remodeling, respectively were present in eighth cluster.

Among 13 genes within ninth cluster, genes like Cytochrome c1 (Cyc1) and Voltage dependent anion channel 1 (Vdac1) that encode for respiratory chain were differentially expressed.

Among 4 genes within tenth cluster, gene like Minichromosome maintenance complex component 7 (Mcm7) which encodes for DNA replication was differentially expressed.

The results showed higher number of downregulated genes at D3 and D7 when compared to other time points. Whereas, higher number of upregulated genes were present at D10 and D14 when compared to other time points. Furthermore, hierarchical clustering and functional annotation showed presence of mitochondrial and ECM related activity in more than two clusters (Figure 7, right panel). The global overview of differential gene expression across time points instigated further investigation of gene expression at each time point of study.

**Figure 7: Hierarchical clustering aligned genes into ten distinct clusters based on expression pattern across time points of healing.**



Hierarchical clustering was performed to group genes based on expression pattern during healing. Ten distinct clusters were obtained. Genes present in clusters were visualized in Heatmap (left panel). Red and green indicates the color key from downregulation to upregulation of genes compared to D0, respectively. Further, functional annotation of genes present in each cluster was performed using NCBI-DAVID (right panel). ECM and mitochondrial genes

were present in many clusters. ( $N = 5/\text{time point}$ , FC: fold-change).

#### ***4.4 D3 and D7 marked the active phase of differentially expressed angiogenesis genes***

Injury initiates inflammatory phase which is crucial for the progression of fracture healing. Simultaneously blood supply and revascularization are essential for a successful fracture healing. Differentially expressed genes involved in angiogenesis were analyzed to understand the underlying molecular mechanism of fracture healing.

In total 12 angiogenesis related genes were differentially expressed during course of healing, 7 genes were downregulated and 5 genes were upregulated (Table 2).

Among downregulated genes, there were angiogenic factors like Vascular endothelial growth factor A (Vegfa), Pleiotrophin (Ptn) and anti-angiogenic factor like Decorin (Dcn). Vegfa and Dcn were significantly downregulated at D3 and D7 only. Whereas, Ptn was significantly downregulated at D3, D7, D21, and D28. Endothelial cell migration and maintenance of oxidative stress is crucial during angiogenesis and fracture healing. Genes like Aquaporin 1 (Aqp1) which encodes for cell migration and Gpx1 which diminishes oxidative stress condition were significantly downregulated at D3 and D7. Furthermore, gene like Matrix metalloproteinase 2 (Mmp2) which degrades ECM to enhance blood vessel formation was significantly downregulated at D3 and D7. Mapk14 plays an important role in MAPK signaling and was significantly downregulated at D3 and D7.

Among upregulated genes, there were anti-angiogenic factor like Serpin family f member 1 (Serpinf1) and ECM anchorage protein like Matrix metalloproteinase 9 (Mmp9). Serpinf1 was significantly upregulated at D3 and D7. Whereas Mmp9 was significantly upregulated at D10, D14, and D21. Furthermore, genes like Transforming growth factor beta receptor 1 (Tgfbr1) and Transforming growth factor beta receptor 2 (Tgfbr2) that stimulate angiogenesis process were significantly upregulated at D14 and D10, respectively. Stress condition activates Secreted protein acidic and cysteine rich (Sparc) which is crucial for cell proliferation and development. Sparc was significantly upregulated at D10.

**Table 2: List of differentially expressed angiogenesis genes and their FC and P-value (white background: downregulated and grey background: upregulated)**

Gene	D3	D7	D10	D14	D21	D28
Vegfa	-2.313	-2.236				
	6.46E-05	1.91E-04				
Ptn	-2.374	-2.2878			-2.179	-2.292
	2.17E-05	4.64E-05			6.65E-05	1.34E-05
Dcn	-2.35442	-2.373				
	3.14E-04	3.10E-04				
Aqp1	-2.39845	-2.32452				
	5.61E-06	2.21E-05				
Gpx1	-2.95	-3.164				
	7.9E-06	8.9E-06				
Mmp2	-2.094	-2.262				
	1.07E-05	5.92E-05				
Mapk14	-2.713	-2.759				
	2.16E-05	1.43E-04				
Serpinf1	2.386	2.196				
	8.1E-07	2.65E-05				
Mmp9			2.3381	2.34614	2.19513	
			1.30E-05	1.26E-05	5.35E-06	
Tgfbr1				2.1474		
				3.79E-05		
Tgfbr2			2.042			
			7.46E-05			
Sparc			2.9793			
			1.85E-06			

The investigation of angiogenesis genes showed highest number of differentially expressed genes at D3 and D7 compared to other time points. Further understanding of angiogenesis during fracture healing requires histological evaluation of blood vessels.

#### ***4.5 Evaluation of ASMA activity during fracture healing showed higher positive signal at D7***

ASMA serve as a biological marker for blood vessel visualization. Therefore, analysis of vascularization around callus was performed using ASMA immunohistochemistry (Figure 8). ASMA positive area and blood vessels count were evaluated and then normalized to total callus area (Figure 8 B, D).

Descriptively, blood vessels were located within the fractured gap and endosteum region both at D7 and D10 (Figure 8A). While at D14, blood vessels were detected within the mineralized matrix present in periosteal region. Furthermore, blood vessels were located mainly near the cortices at D21. Blood vessels were detected within bone marrow and newly formed bone at D28 (Figure 8C).

Histomorphometry showed higher ASMA positive area at D7 when compared with other time points (Figure 8B). Furthermore, D21 showed lower ASMA positive area when compared with other time points. ASMA positive area showed variation at D10, D14, and D28 but no significant differences were observed (Figure 8B). Blood vessels count was higher at D7 when compared with other time points (Figure 8D). Furthermore, D21 showed lower blood vessels count compared with other time points. While, blood vessels count fluctuated between D10, D14, and D28 (Figure 8D). Blood vessels count was significantly higher at D7, D10, and D28 when compared with D21 ( $p = 0.017, 0.003, 0.022$ , respectively). The formation of blood vessels during initial phase provides the suitable environment required for fracture healing, thereby initiating the calcification of cartilage and replacement with new bone. Therefore, detailed understanding of fracture healing process requires the investigation of differentially expressed ossification genes.

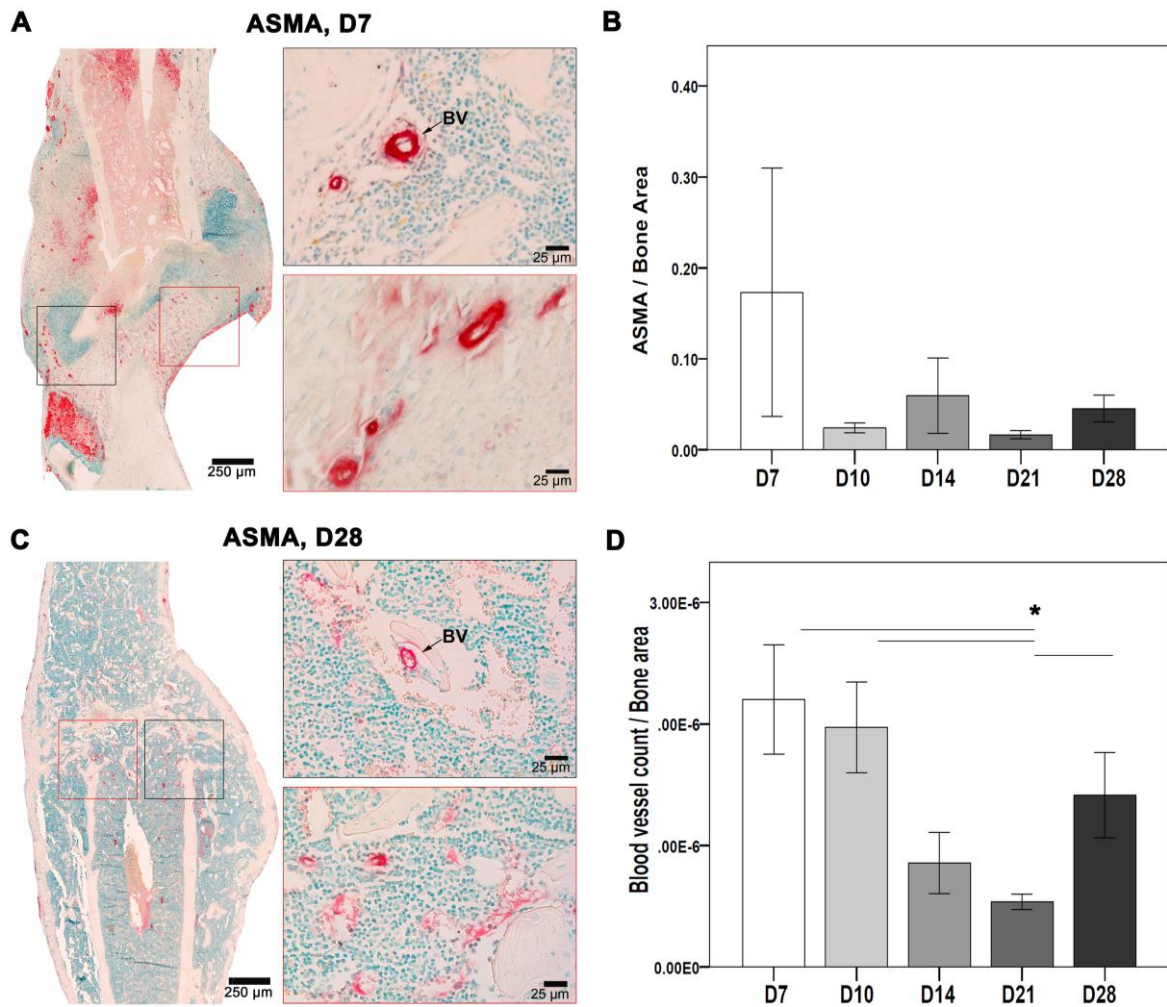


**Figure 8: Quantitative analysis of ASMA signal during fracture healing showed higher signal at D7.** ASMA immunohistochemistry was performed to analyze blood vessel formation during fracture healing. Histomorphometry was performed to evaluate ASMA positive area and blood vessels count. Methyl Green was used as counter-stain. (A) Positive stained regions were located near the fractured gap at D7. (B) D7 showed the higher ASMA area and D21 showed the lower ASMA area higher and lower ASMA area. (C) ASMA stained regions at D28 were seen near the newly formed bone. (D) Blood vessels count was higher at D7 and lower at D21 compared with other time points. D7, D10, and D28 showed significantly higher blood vessels count when compared with D21 ( $N = 4$  (D7),  $N = 6$  (D10),  $N = 3$  (D14),  $N = 5$  (D21, D28); Non-parametric distribution, Mann-Whitney U-test,  $* = p \leq 0.05$ , BV: blood vessels).

#### **4.6 D10 and D14 marked the active time points with differentially expressed ossification genes**

The restoration of blood supply at the fracture site provides different cellular signal required for new bone formation. Ossification is an important process which involves

resorption of primary soft cartilaginous callus, which later get replaced by hard bony callus. Therefore, differential expression of genes involved in ossification were examined to understand the underlying molecular mechanism of fracture healing.

In total 13 ossification related genes were differentially expressed, 2 genes were downregulated and 11 genes were upregulated (Table 3).

Among downregulated genes, there were genes like Ubb and Myocyte enhancer factor 2c (Mef2c) that encode chondrocytes hypertrophy. Ubb was significantly downregulated at D3 and D7, while Mef2c was significantly downregulated at D10 and D14.

Among upregulated genes, there were collagen family genes like Collagen type 1 alpha 1 (Col1a1), Collagen type 10 alpha 1 (Col10a1), and Collagen type 2 alpha 1 (Col2a1) that are important for bone mineralization. Col1a1 was significantly upregulated at D10, D14, and D21. Col10a1 was significantly upregulated only at D10. Col2a1 was significantly upregulated at D10 and D14. Furthermore, Mmp's family genes like Mmp9 and Mmp13 that play important role during bone formation and remodeling were also significantly expressed. Mmp9 was significantly upregulated at D10, D14, and D21. While, Mmp13 was significantly upregulated from D3 through D7, D10, D14 until D21. Additionally, a Tissue inhibitor of metalloproteinase 1 (Timp1) was significantly upregulated at D3, D7, and D21. Endochondral ossification related genes like Cathepsin k (Ctsk) and Specificity protein 7 (Sp7) were significantly expressed. Ctsk was significantly upregulated at D10, D14, and D21.

Sp7 was significantly upregulated at D3, D7, and D14. Further, Mgp which inhibits bone mineralization was significantly upregulated only at D10. Gene like Spp1 which stimulates bone formation and osteoclast anchorage was significantly upregulated at D10 and D14. Another important gene was Integrin binding sialoprotein (Ibsp) that binds to hydroxyapatite providing stiffness and strength to bone. Ibsp was significantly upregulated from D3 through D7, D10, D14 until D28.

**Table 3: List of differentially expressed ossification genes and their FC and P-value (white background: downregulated and grey background: upregulated)**

Gene	D3	D7	D10	D14	D21	D28
Ubb	-3.837	-3.823				
	5.82E-08	3.13E-06				

Mef2c			-2.582	-3.08		
			8.99E-05	1.67E-04		
Col1a1			3.073	2.745	2.038	
			7.99E-06	1.16E-05	3.86E-05	
Col10a1			3.1519			
			2.21E-07			
Col2a1			5.08	2.982		
			9.26E-08	8.81E-06		
Mmp9			2.3381	2.34614	2.19513	
			1.30E-05	1.26E-05	5.35E-06	
Mmp13	2.05	2.166	2.235	2.36	2.291	
	4.11E-06	3.73E-06	5.46E-05	3.83E-06	1.90E-06	
Timp1	2.2396	2.2505			2.2906	
	2.55E-05	1.02E-05			4.71E-06	
Ctsk			2.6148	2.54762	2.26895	
			3.75E-06	5.01E-06	2.20E-05	
Sp7	2.867	2.833		2.107		
	4.85E-07	9.27E-05		3.04E-06		
Mgp			2.119			
			1.62E-06			
Spp1			2.434	2.313		
			3.51E-04	5.41E-04		
Ibsp	3.345	3.379	2.821	3.008	2.956	
	9.05E-06	8.26E-05	3.40E-05	3.00E-04	2.51E-05	

High number of ossification genes were significantly upregulated at D10 and D14 when compared to other time points. No differentially expressed gene related to ossification were present at D28. Furthermore, the investigation of bone mineralization during fracture healing process is required.

#### ***4.7 Trichrome Masson Goldner depicted changes in bone mineralization with progression of fracture healing process***

Trichrome Masson Goldner stain differentiates mineralized bone matrix from non-mineralized bone matrix. Therefore, changes in bone mineralization were visualized using Trichrome Masson Goldner stain (Figure 9).

Descriptively, cartilaginous callus was formed around the fracture gap and chondrocytes were seen in the callus at D7 (Figure 9A). Furthermore, non-mineralized bone matrix portion was higher compared to mineralized bone matrix portion at D7 (Figure 9A). D10 showed an increase in the size of cartilaginous callus and mineralized bone matrix portion when compared with D7 (Figure 9 A, B). Proliferative chondrocytes in callus region and initiation of mineralization in periosteal region were seen at D10 (Figure 9B).

A smaller cartilaginous callus was seen at D14 when compared with D10 (Figure 9 B, C). Hypertrophic chondrocytes were seen within the callus at D14 (Figure 9C). Mineralized bone matrix portion increased at D14 when compared with D7 and D10 (Figure 9 A, B, C). Furthermore, non-mineralized bone matrix were seen in small patches within the callus region. D21 showed the mineralization of callus borders (Figure 9D). Furthermore, portion of cartilage was replaced by newly formed bone by D21. While, small patches of non-mineralized bone matrix were seen in the callus and endosteum region. The complete mineralized bone matrix was formed by D28 (Figure 9E). Nonetheless, bridging of cortices were seen.

Mineralized bone matrix provides structural rigidity and mechanical support to the bone. Further work is required to understand the differential expression of ECM genes during fracture healing.

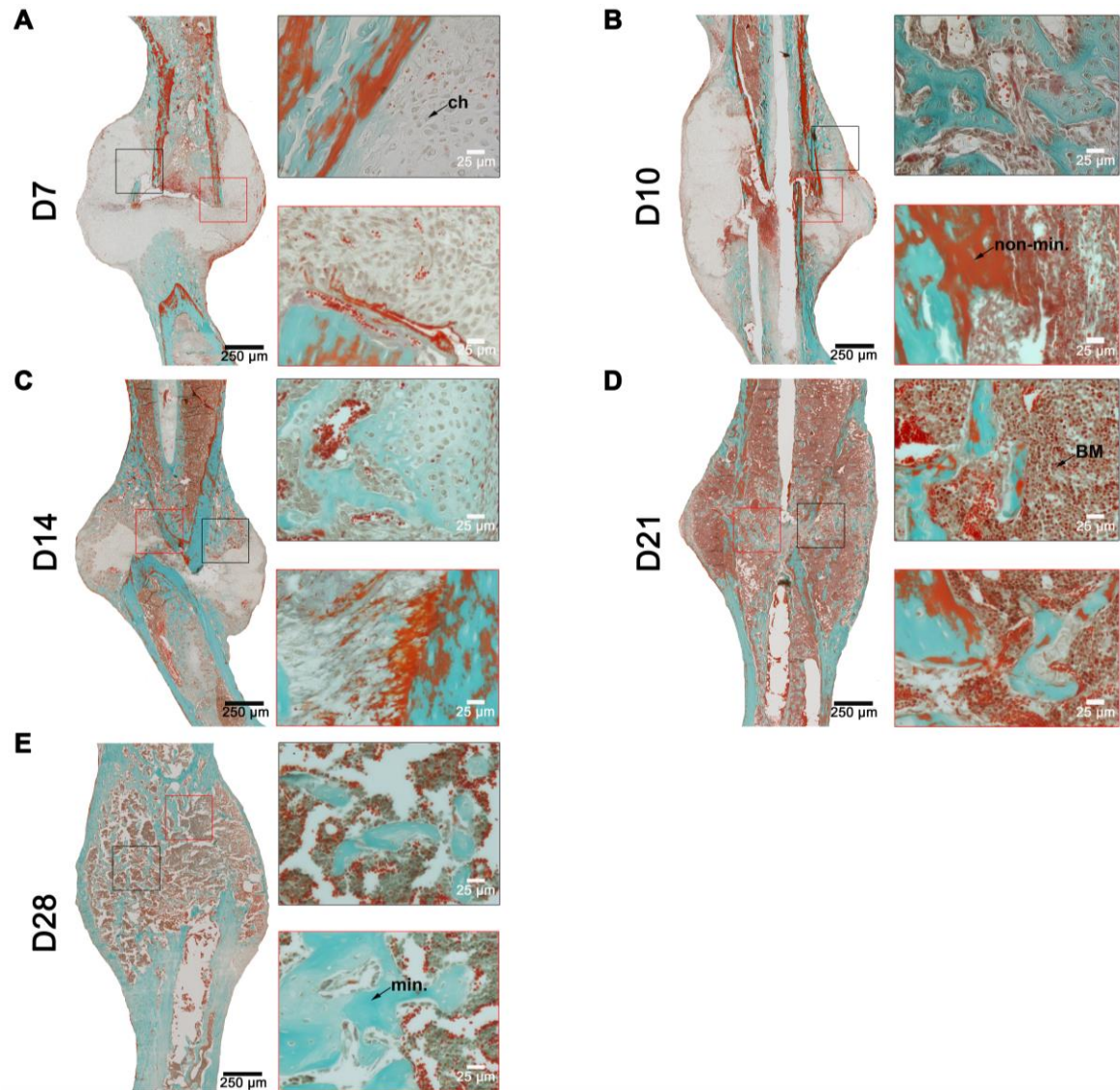


**Figure 9: Trichrome Masson Goldner stain provided an overview of mineralized and non-mineralized bone matrix around fractured callus.** Masson Goldner stain was performed to understand the progression of bone mineralization in fracture healing. (A) D7 showed higher portion of non-mineralized matrix compared with other time points, (B) D10 showed an initiation of bone mineralization in periosteal. (C) D14 showed an increase in mineralized bone matrix and less chondrocytes. (D) D21 showed the mineralization of cartilage in the cortices. (E) D28 showed the complete mineralization and bridging of fracture gap. (green: mineralized, red: non-mineralized, chondrocytes: grey, blood vessels: red, min: mineralized, non-min: non-mineralized, BM: bone marrow, ch: chondrocytes).

#### ***4.8 D10 marked the active time point related to differentially expressed ECM genes***

ECM provides a natural scaffold for bone mineralization and serve as a reservoir of growth factors and cytokines. Therefore, differentially expressed genes involved in ECM related activity were investigated to understand the regulatory role of ECM during fracture healing.

In total 29 ECM genes were differentially expressed, 6 genes were downregulated and 22 genes were upregulated (Table 4). Lysyl oxidase (Lox), which plays a role in post-translational modification of collagens was significantly downregulated at D3 while significantly upregulated at D10 and D14.

Among downregulated genes, there were ECM degradation markers like Mmp2 and ECM deposition factor like Osteoglycin (Ogn). Both Mmp2 and Ogn were significantly downregulated at D3 and D7. Proteoglycans like Dcn and Lumican (Lum) that are crucial for ECM structural integrity were also differentially expressed. Both Dcn and Lum were significantly downregulated at D3 and D7. One collagen family gene; Collagen type 12 alpha 1 (Col12a1) was significantly downregulated at D7. Another important gene for matrix mineralization is Ptn which contributes in interaction with mesenchymal stem cells. Ptn was significantly downregulated at D3, D7, D21, and D28.

Among upregulated genes, there were ECM markers like Mmp13 and Mmp9 that are crucial for cell differentiation and invasion. Mmp13 was significantly upregulated from D3 through D7, D10, D14 until D21. While, Mmp9 was significantly upregulated at D10, D14, and D21. Genes like Ibsp and Timp1 that regulate ECM deposition were also differentially expressed. Ibsp was significantly upregulated from D3 through D7, D10, D14 until D21. While, Timp1 was significantly upregulated at D3, D7, and D21. Furthermore, genes like Tgfbr1 and Tgfbr2 that are crucial for ECM production through TGF-beta signaling were upregulated. Tgfbr1 was significantly upregulated at D14 while Tgfbr2 was significantly upregulated at D10. Sh3 and Px domain containing protein 2b (Sh3pxd2b) and Epidermal growth factor containing fibulin ECM protein 2 (Efemp2) play an important role in cell matrix adhesion during connective tissue development. Both genes were significantly upregulated at D3 and D7. Mgp helps in ECM modeling and was only significantly upregulated at D10. While, gene like Tenascin c (Tnc) which helps in

ECM development was significantly upregulated at D10 and D14. Furthermore, ECM structural component like Aggrecan (Acan) and ECM degradation marker like Cartilage associated protein (Crtap) were significantly upregulated at D10. ECM protein like Spp1 was significantly upregulated at D10 and D14. Further, balanced bone formation and bone remodeling process relies on Wnt signaling and Carboxypeptidase Z (Cpz) is crucial for binding to Wnt. Cpz was significantly upregulated at D10 and D14. Many collagen family genes like Collagen type 24 alpha 1 (Col24a1), Collagen type 6 alpha 1 (Col6a1), Col1a1, Col1a2, Col10a1, Collagen type 9 alpha 2 (Col9a2), and Col2a1 were significantly upregulated. Col24a1 was significantly upregulated at D7 only while Col6a1 was significantly upregulated at D10 only. Col1a1 was significantly upregulated at D10, D14, and D21. Col1a2 was significantly upregulated from D3 through D7, D10 until D14. Furthermore, Col10a1 was significantly upregulated at D10. Col9a2 and Col2a1 were significantly upregulated at D10 and D14. Arrangement of collagen fibers provides the higher tensile strength to bone. Gene like Sparc which associates with collagen fiber assembly was significantly upregulated at D10.

Higher number of ECM genes were differentially expressed at D3, D7, D10, and D14 compared to D21. Collagens are one of the main component of bone matrix. Therefore, evaluation of changes in collagen fibers orientation and distribution with the progression of healing is required.

**Table 4: List of differentially expressed ECM genes and their FC and P-value (white background: downregulated and grey background: upregulated)**

Gene	D3	D7	D10	D14	D21	D28
Mmp2	-2.094	-2.262				
	1.07E-05	5.92E-05				
Ogn	-2.401	-2.078				
	3.72E-05	2.20E-03				
Den	-2.354	-2.373				
	3.14E-04	3.10E-04				
Lum	-3.642	-3.55				
	2.22E-05	1.7E-03				
Col12a1		-2.052				
		4.80E-04				
Ptn	-2.374	-2.287			-2.179	-2.292

	2.17E-05	4.64E-05			6.65E-05	1.34E-05
Mmp13	2.05	2.166	2.235	2.36	2.291	
	4.11E-06	3.73E-06	5.46E-05	3.83E-06	1.90E-06	
Mmp9			2.338	2.346	2.195	
			1.30E-05	1.26E-05	5.35E-06	
Ibsp	3.345	3.379	2.821	3.008	2.956	
	9.05E-06	8.26E-06	3.40E-05	3.00E-04	2.51E-05	
Timp1	2.239	2.25			2.29	
	2.55E-05	1.02E-05			4.71E-06	
Tgfb1				2.147		
				3.79E-05		
Tgfb2			2.042			
			7.46E-05			
Sh3pdx2b	2.1583	2.0547				
	3.02E-06	6.34E-06				
Efemp2	2.04	2.1007				
	2.70E-06	9.64E-06				
Mgp			2.119			
			1.62E-06			
Tnc			2.811	2.585		
			7.41E-08	1.67E-06		
Acan			3.268			
			1.54E-07			
Crtap			2.166			
			8.87E-10			
Spp1			2.434	2.313		
			3.51E-04	5.41E-04		
Cpz			2.404	2.096		
			3.27E-06	4.02E-05		
Col24a1		2.126				
		2.9E-03				
Col6a1			2.019			
			3.81E-06			
Col1a1			3.073	2.745	2.038	
			7.99E-06	1.16E-05	3.86E-05	
Col1a2	2.322	3.109	2.63	2.88		

	1.81E-04	1.23E-04	9.32E-05	5.28E-05		
Col10a1			3.151			
			2.21E-07			
Col9a2			2.903	2.148		
			1.36E-05	2.14E-04		
Col2a1			4.952	3.244		
			7.54E-08	1.39E-05		
Sparc			2.979			
			1.85E-06			
Lox	-2.023		2.164	2.345		
	9.3E-03		5.41E-05	4.11E-05		

#### ***4.9 Changes in collagen fibers arrangement with progression of healing***

Discrepancies in arrangement of collagen fibers reflects on ECM quality. Sirius red stain helps in type I, type II, and type III collagen visualization under polarized light. Therefore, Sirius red stain was carried out to explore the changes in collagen fibers with progression of healing (Figure 10). The current study focused on type I collagen and fibril orientation was quantified using CT-FIRE program (Figure 11).

Descriptively, type I collagen fibers were seen in the soft callus and around the cortices at D7. Further, type I collagen fragments were seen within fracture gap at D7. Type I collagen at D10 was seen in the periosteal region. Type I collagen distribution changed with the healing progression. Both regular and irregular orientation of collagen were seen at D14. However, well-aligned and longer collagen fibers were seen in both endosteum and periosteum region at D21 and D28.

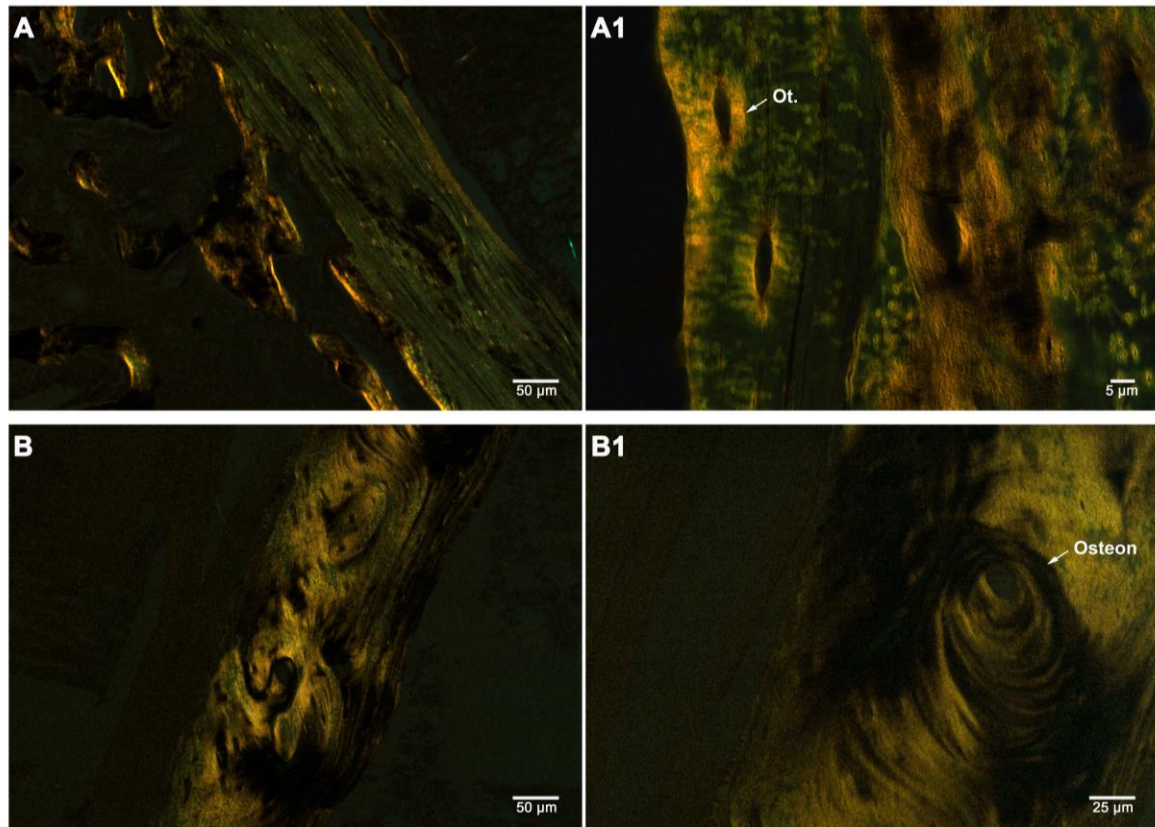


**Figure 10:** *Sirius red stain depicted the arrangement of type I collagen in the mineralized bone matrix. Polarized microscopy was carried out to determine the change and distribution of type I collagen fibers around fractured callus. (A, A1) Type I collagen ring like structure were seen around the osteocytes at all time points. (B, B1) Well-arranged collagen fibers seen in the bone matrix (Ot: osteocyte).*

The distinct type I collagen fibers were visible around newly formed bone at D28. Intriguingly, type I collagen ring like structure were seen around the osteocytes at all time points (Figure 10). Besides, the collagen fibers arrangement was seen in the bone matrix within the fractured callus region (Figure 10).

The quantitative segmentation of Sirius red stained monochrome images helped in identification of fiber properties embedded within bone matrix. The CT-FIRE standalone software calculates the distinct fiber properties (angle, length, width, and straightness) (Figure 11). The analysis showed significant differences between the fiber properties across time points (Figure 11C).

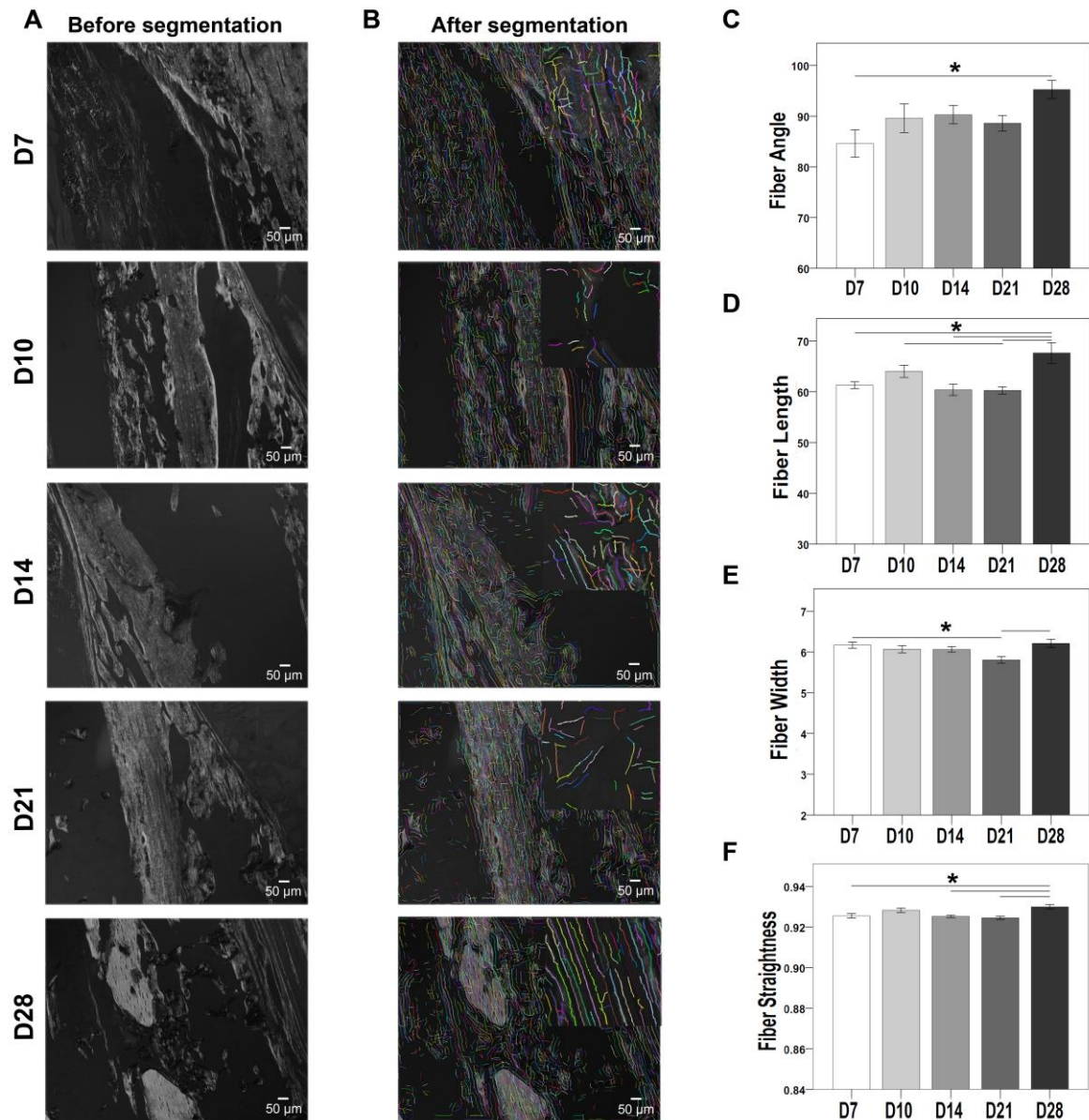


**Figure 11: Enhanced collagen fiber properties reflected on bone matrix quality at D28.** CT-FIRE tool was used to quantify the collagen fibers from Sirius red stained images. (A) Before segmentation, (B) After segmentation. The right upper side shows the enlarged collagen fibers (C-F) D28 showed higher fiber angle, length, width, and straightness when compared with D7, D10, D14, and D21. ( $N = 4$  (D7),  $N = 6$  (D10),  $N = 3$  (D14),  $N = 5$  (D21, D28); Nonparametric distribution, Mann-Whitney U-test,  $* = p \leq 0.05$ ).

Fiber angle points to the orientation of bone mineralization pattern. The fiber angle was significantly higher at D28 when compared with D7 ( $p = 0.013$ ).

Fiber length is an important parameter in the determination of biomechanical properties (Figure 11D). D28 showed significantly longer fibrils when compared with D7 ( $p = 0.005$ ), D10 ( $p = 0.014$ ), D14 ( $p = 0.007$ ), and D21 ( $p = 0.001$ ). Fiber width and

straightness governs the collagen networking and anisotropic nature, respectively. Fiber width was significantly higher at D28 when compared with D7 ( $p = 0.042$ ) and D21 ( $p = 0.015$ ) (Figure 11E). Fiber straightness showed no significant differences between time points (Figure 11F).

The presence of type I collagen structure around osteocytes encouraged the further investigation of osteocytes morphological structure.

#### ***4.10 Quantitative evaluation of osteocytes using silver nitrate stain showed lower count at D28***

Osteocyte is a crucial part of ECM, providing mechanical support to bone. Therefore, Silver Nitrate stain was used to investigate morphological changes in osteocytes during fracture healing (Figure 12). Osteocytes counts were normalized to total callus area.

Descriptively, all three types of osteocytes: empty lacunae, spherical, and spindle shaped were seen around fractured callus (Figure 12A). Osteocytes showed well-connected network at all time points.

Histomorphometry showed higher empty lacunae count at D7 when compared with other time points (Figure 12B). D28 showed lower empty lacunae count when compared with other time points. Whereas, D10, D14, and D21 showed variation in empty lacunae count without significant differences (Figure 12B). D28 showed significantly lower empty lacunae count when compared with D10 ( $p = 0.029$ ) and D21 ( $p = 0.029$ ).

Spherical shaped osteocytes count was higher at D7 when compared with other time points (Figure 12C). While, D28 showed lower spherical shaped osteocytes compared with other time points.

Spherical shaped osteocytes were not at all significant at D10, D14, and D21. D28 showed significantly lower spherical shaped osteocytes when compared with D7 ( $p = 0.045$ ), D10 ( $p = 0.001$ ), and D21 ( $p = 0.008$ ).

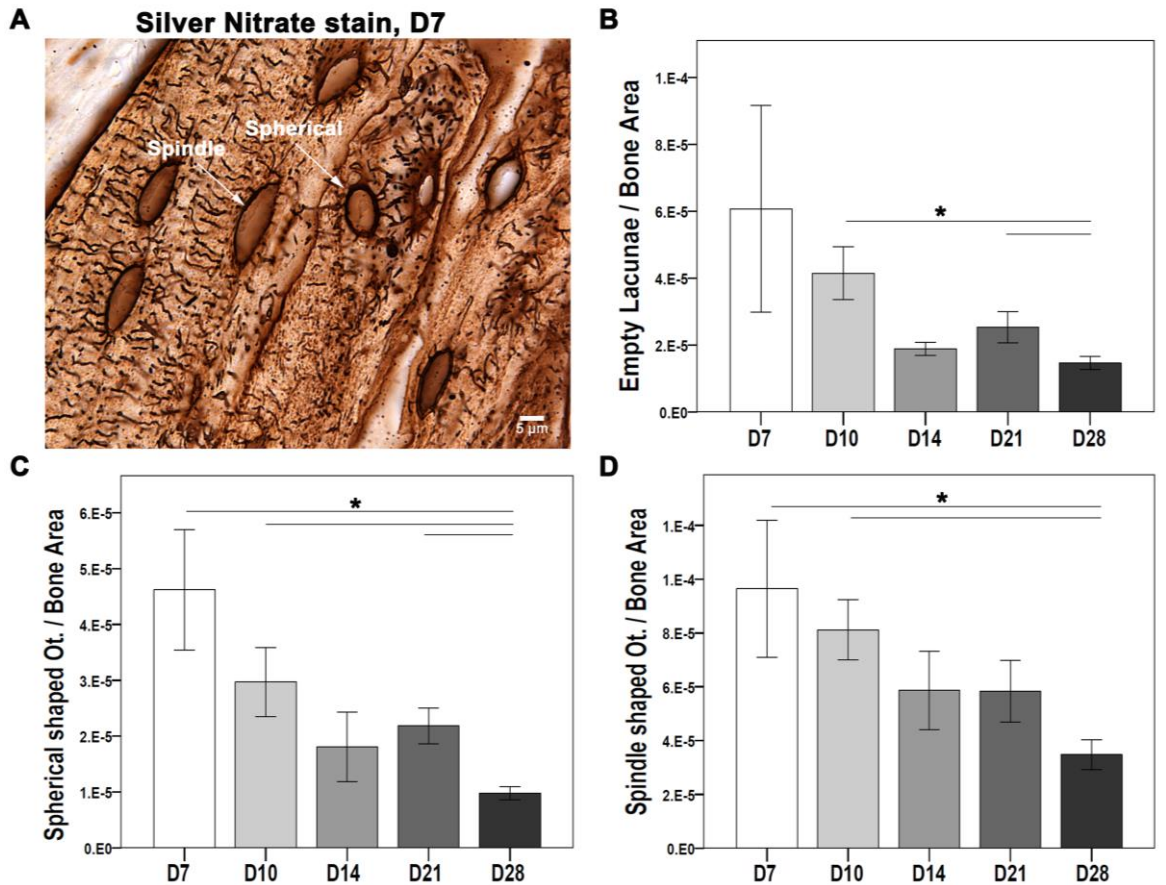


**Figure 12: Quantitative evaluation of osteocytes showed higher activity at D7 and lower activity at D28 during fracture healing.** Silver nitrate stain was used to visualize and quantify morphological changes in osteocytes. Empty lacunae, spherical, and spindle shaped osteocytes were higher at D7 when compared with other time points. (A) Osteocytes were present in abundance around the fractured callus at D7. (B) Empty lacunae were significantly lower at D28 when compared with D10 and D21. (C) Spherical shaped osteocytes were significantly lower at D28 when compared with D7, D10, and D21. (D) Spindle shaped osteocytes were significantly lower at D28 when compared with D7 and D10. (N = 4 (D7), N = 6 (D10), N = 3 (D14), N = 5 (D21, D28); Ot: osteocytes, Non-parametric distribution with Mann-Whitney U-test; \*  $\leq p = 0.05$ ).

Spindle shaped osteocytes count was higher at D7 compared with other time points (Figure 12D). However, D28 showed lower spindle shaped osteocytes count compared with other time points. D10, D14, and D21 showed slight variation in spindle shaped osteocytes count with no significant differences (Figure 12D). D28 showed significantly lower spindle shaped osteocytes when compared with D7 ( $p = 0.045$ ) and D10 ( $p = 0.002$ ).

Quantitative evaluation showed lower spindle shaped osteocytes with the progression of fracture healing. While, empty and spherical shaped osteocytes count declined from D7

until D14 followed by an increase at D21 and then again decline at D28. Further understanding of cellular changes within ECM during fracture healing process is required to understand the underlying molecular mechanism.

#### ***4.11 Evaluation of MEPE and ERK during fracture healing showed negative correlation across time points***

Osteocytes express MEPE which regulates bone mineralization important for fracture healing. ERK is an ECM marker required for cell adhesion and migration. Therefore, MEPE and ERK immunohistochemistry were performed to understand the cellular changes within ECM during fracture healing (Figure 13 A, C). Furthermore, MEPE stained and ERK stained areas were quantified and then normalized to the total callus area (Figure 13 B, D).

Descriptively, MEPE signal was seen in the fracture gap and in the periosteal region at D7. Furthermore, MEPE signal at D7 was also seen around bone marrow fat cells. MEPE signal was seen in proliferative chondrocytes and within bone marrow at D10. MEPE signal at D14 was seen within bone marrow and bone matrix (Figure 13A). MEPE signal at D21 was seen in osteocytes and within bone marrow. Furthermore, D28 showed MEPE signal within bone marrow surrounding fat cells. Histomorphometry showed higher MEPE stained area at D7 when compared with D10, D21, and D28 (Figure 13B). Furthermore, D10 showed higher MEPE stained area when compared with D21 and lower stained area when compared with D7, D14, and D28. MEPE stained area was higher at D14 when compared with other time points (Figure 13B). D21 showed lower MEPE stained area when compared with other time points. The positive stained area was higher at D28 compared with D10 and D21 (Figure 13B). MEPE stained area was significantly lower at D10 compared with D28 ( $p = 0.038$ ).

Descriptively, ERK signal was seen around the callus border, in chondrocytes and within monocytes at D7. ERK signal at D10 was seen near proliferative chondrocytes and within bone marrow. D14 showed small patches of ERK signal in hypertrophy chondrocytes and bone marrow. Furthermore, ERK signal was seen within bone matrix and around fat cells present within bone marrow at D21 (Figure 13C). ERK signal was seen in bone matrix, bone marrow, and in close proximity of newly formed bone at D28.

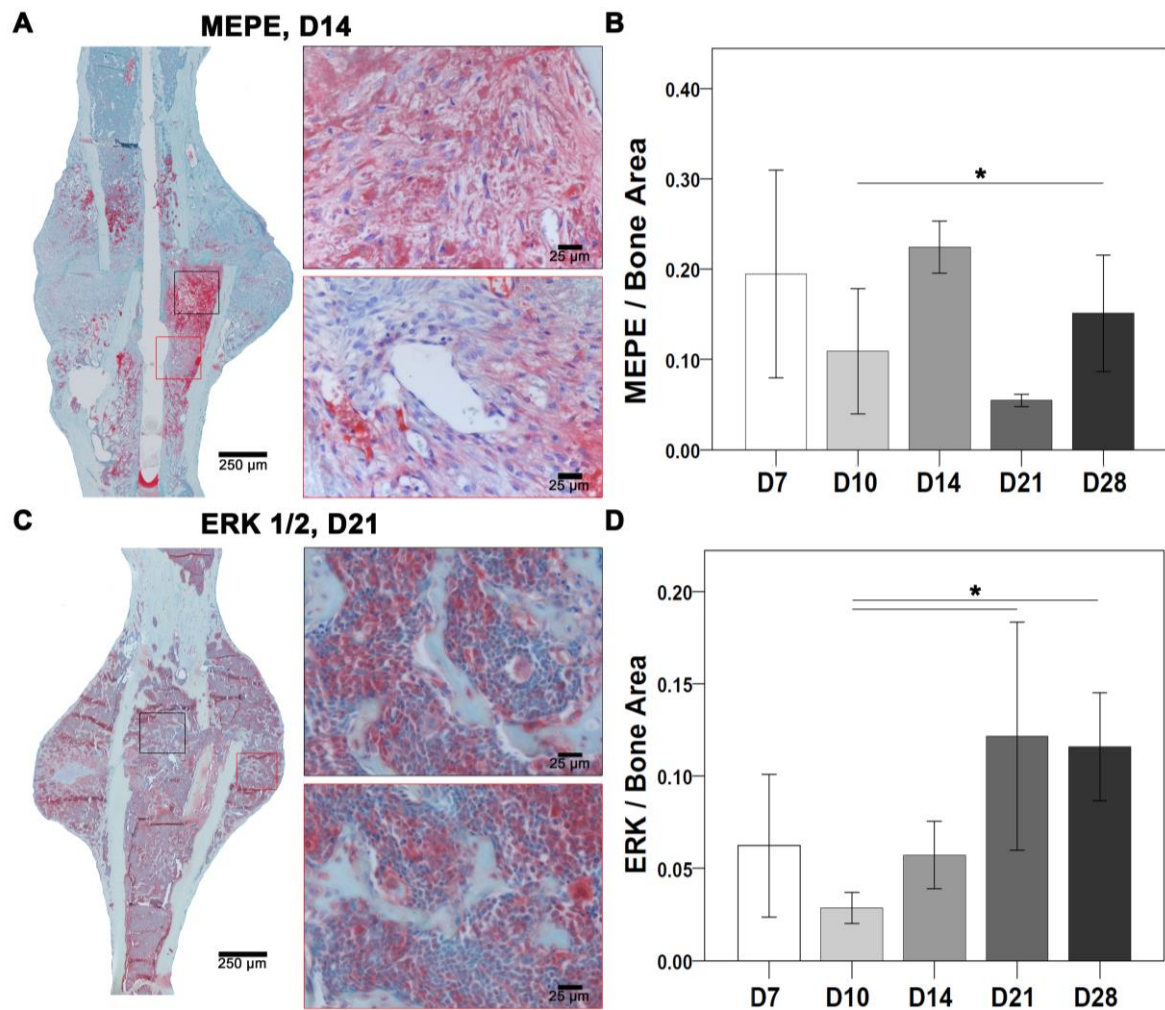


**Figure 13: Histological analysis of MEPE and ERK activity showed negative correlation across time points of healing.** To understand the regulatory role of ECM in fracture healing, MEPE and ERK immunostaining were performed. (A) D14 showed MEPE stained region around the callus and mineralized matrix. (B) MEPE stained area was higher at D14 compared with other time points. D10 showed significantly lower MEPE area when compared with D28. (C) D21 showed ERK stained regions within the whole callus region. (D) ERK stained area was higher at D21 compared with other time points. D10 showed significantly lower ERK area when compared with D21 and D28. ( $N = 4$  (D7),  $N = 6$  (D10),  $N = 3$  (D14),  $N = 5$  (D21, D28); Non-parametric distribution with Mann-Whitney U-test;  $* \leq p = 0.05$ ).

Histomorphometry showed higher ERK stained area at D7 when compared with D10 and D14 (Figure 13D). Furthermore, ERK stained area was lower at D10 when compared with other time points. D14 showed higher ERK stained area when compared with D10 (Figure 13D).

Interestingly, ERK stained area was higher at D21 when compared with other time points. D28 showed higher positive stained when compared with D7, D10, and D14 (Figure 13D).

Furthermore, ERK stained area was significantly lower at D10 when compared with D21 ( $p = 0.038$ ) and D28 ( $p = 0.009$ ).

Evaluation of MEPE and ERK signal intensity and localization during fracture healing process showed a well-balanced regulatory mechanism. Histomorphometry showed that ERK activity was lower in the region of higher MEPE activity and vice-versa. Furthermore bone mineralization and ECM regulation requires the continuous energy source during fracture healing. Therefore, further investigation of mitochondrial activity during fracture healing is required.

#### ***4.12 High number of differentially expressed genes related to mitochondrial activity were present only at D3 and D7***

Demand of energy increases for cellular metabolism at the time of injury. Mitochondrion serve as an energy source inside a cell. Therefore, differentially expressed genes involved in mitochondrial activity were investigated.

In total 39 mitochondrial genes were differentially expressed, 38 genes were downregulated and only 1 gene was upregulated (Table 5).

Among downregulated genes were; Gpx1, Peroxidase 2 (Prdx2), and Peroxidase 3 (Prdx3) that play role against oxidative stress condition. Gpx1, Prdx2, and Prdx3 were significantly downregulated at D3 and D7. Furthermore, gene like 3-Oxoacid CoA transferase 1 (Oxct1) which plays a central role in ketone body catabolism was significantly downregulated at D3 and D7. Energy production process requires transmembrane interaction and minerals transport. Genes like Solute carrier family 25 member 11 (Slc25a11) and Solute Carrier Family 25 member 20 (Slc25a20) plays an important role in minerals transport and exchange through mitochondrial membrane. Furthermore, Branched chain ketoacid dehydrogenase kinase (Bckdk) plays a crucial role in transmembrane interaction with lipid bilayers. Slc25a11, Slc25a20, and Bckdk were significantly downregulated at D3 and D7. Other important genes for mitochondrial transport and electron transport chain are Transmembrane proteome 14C (Tmem14c), Atp5b, ATP synthase H<sup>+</sup> transporting mitochondrial f1complex (Atp5f1), and Translocase of outer mitochondrial membrane 7 (Tomm7). Tmem14c, Atp5b, Atp5f1, and Tomm7 were significantly downregulated at D3 and D7. Another source of energy production are Krebs's cycle, respiratory chain, and TCA cycle within mitochondrion. Genes like Citrate

Synthase (Cs), Fumarate Hydratase 1 (Fh1), Succinyl CoA ligase (Suclg1), Ubiquinol-Cytochrome C Reductase Core Protein 2 (Uqcrc2), and Cyc1 are important for above mentioned energy producing signaling pathways. Cs, Fh1, Suclg1, Uqcrc2, Cyc1 were significantly downregulated at D3 and D7. Coenzyme Q9 (Coq9) which involves lipid biosynthesis for electron transport chain was significantly downregulated at D3 and D7. Another downregulated genes was Cytochrome P450 family 27 subfamily A member 1 (Cyp27a1) which plays a role in maintaining cholesterol homeostasis. Cyp27a1 was significantly downregulated at D3 and D7. Furthermore, there were erythropoiesis regulatory gene like Heat shock protein family a member 9 (Hspa9) and metal binding gene like Iron-Sulfur Cluster Assembly 1 (Isca1). Hspa9 and Isca1 were significantly downregulated at D3 and D7. Cold Shock domain containing protein E1 (Csde1) which acts as RNA binding protein during transcription and translation was significantly downregulated at D3 and D7. Further, glucose and fatty acid metabolism is important for bone homeostasis regulated by gene like Pyruvate Dehydrogenase Kinase 4 (Pdk4), which was significantly downregulated at D3 and D7. Another important gene is Electron transfer flavoprotein alpha subunit (EtfA) which is required for amino acid metabolism. EtfA was significantly downregulated at D3 and D7. Furthermore, Glutathione S transferase P1 (Gstp1) which links stress kinase and cell apoptotic pathway was significantly downregulated at D3 and D7. Another downregulated gene was Translocase of inner mitochondrial membrane 8 homolog B (Timm8b) which acts as chaperone for protein transport. Timm8b was significantly downregulated at D3 and D7. Genes like Vdac1 and Voltage Dependent Anion Channel 3 (Vdac3) that perform role in diffusion and binding of molecules were also downregulated. Vdac1 was significantly downregulated at D7 and Vdac3 was significantly downregulated at D3, D7, and D21. Furthermore, Carnitine O-palmitoyltransferase 1 (Cpt1b) which acts as a component for fatty acid beta oxidation was significantly downregulated at D10 and D14. Another downregulated genes were Cytochrome c oxidase subunit 8B (Cox8b), Cytochrome C oxidase subunit 7A1 (Cox7a1), and Cytochrome C oxidase subunit 6A2 (Cox6a2) that are involved in electron transport activity. Cox8b and Cox7a1 were significantly downregulated at D10 and D14. Cox6a2 was significantly downregulated at D10. Another important gene was Creatine kinase S-type (Ckmt2) which serves as energy transducer was significantly downregulated from D3 through D7, D10 until D14. Furthermore, carbohydrate metabolism gene like Succinate dehydrogenase cytochrome b560 subunit

(Sdhc) was significantly downregulated at D14. Lyr motif containing protein 5 (Lyrm5) which acts as electron transfer flavoprotein regulator was significantly downregulated at D14. Another important gene was Dual Specificity Phosphatase 26 (Dusp26) which acts as an inhibitor of Mapk1 and Mapk3. Dusp26 was significantly downregulated at D14. Heme biosynthesis gene like Solute carrier family 25 member 37 (Slc25a37) was significantly downregulated at D21 and D28. Among upregulated genes, there was molecule exchange factor like Solute carrier family 25 member 5 (Slc25a5), which was significantly upregulated at D10.

Highest number of differentially expressed genes related to mitochondrial activity were present at D3 and D7 compared with other time points. The results further showed the downregulation of genes involved in bone homeostasis and energy production. Further, histological evaluation of changes due to bone homeostasis during fracture healing is needed.

**Table 5: List of drastically downregulated mitochondrial genes and their FC and P-value (white background: downregulated and grey background: upregulated)**

Gene	D3	D7	D10	D14	D21	D28
Gpx 1	-2.95	-3.164				
	7.9E-06	8.9E-06				
Prdx2	-3.235	-3.29				
	1.80E-06	1.96E-06				
Prdx3	-2.429	-2.396				
	6.92E-07	6.30E-06				
Oxct1	-3.157	-3.299				
	2.92E-05	4.41E-05				
Slc25a11	-2.06872	-2.1049				
	2.56E-03	7.53E-05				
Slc25a20		-2.10498				
		2.86E-06				
Bckdk	-2.633	-2.198				
	1.03E-05	7.8E-04				
Tmem14c	-2.46345	-2.075				
	1.07E-05	1.5E-04				

Alp5b	-2.64177	-2.618				
	1.15 E-07	3.93E-07				
Alp5f1	-2.5096	-2.491				
	2.22E-06	5.78E-04				
Tomm7	-2.322	-2.221				
	1.25E-06	2.95E-06				
Cs	-2.588	-2.573				
	8.93E-05	5.75E-05				
Fh1	-2.907	-2.907				
	6.72E-06	2.90E-06				
Suelg1	-2.205	-2.16				
	1.87E-06	1.97E-05				
Uqerc2	-2.277	-2.278				
	7.33E-06	6.90E-06				
Cyc1	-3.796	-3.73				
	1.75E-06	3.08E-06				
Coq9	-3.328	-3.539				
	1.06E-05	2.28E-07				
Cyp27a1	-2.164	-2.303				
	5.91E-06	2.05E-06				
Hspa9	-2.499	-2.468				
	1.1E-03	2.1E-04				
Isca1	-2.204	-2.368				
	1.39E-06	3.89E-06				
Csde1	-3.414	-3.501				
	3.15E-05	1.19E-04				
Pdk4	-2.35	-2.255				
	2.17E-05	1.43E-03				
Etf1a	-3.692	-3.623				
	8.17E-05	1.36E-05				
Gstp1	-2.566	-2.7103				
	5.11E-05	1.76E-05				
Timm8b	-3.668	-3.866				
	2.37E-05	6.14E-06				
Vdac1		-2.549				
		3.77E-06				
Vda c3	-2.609	-2.732			-2.045	

	7.90E-04	9.26E-06			7.20E-03	
Cpt1b			-2.445	-2.156		
			1.03E-05	3.40E-07		
Cox8b			-2.514	-2.289		
			1.53E-06	3.19E-05		
Cox7a1			-2.516	-2.491		
			1.76E-07	1.83E-05		
Cox6a2			-2.436			
			1.86E-07			
Ckmt2	-3.476	-3.454	-2.395	-2.112		
	3.33E-07	7.87E-07	4.44E-07	7.73E-06		
Sdhc				-2.1253		
				6.59E-07		
Lym5				-2.1653		
				1.15E-05		
Dusp26				-2.0079		
				4.45E-04		
Slc25a37					-2.4586	-2.684
					1.42E-05	8.88E-06
Slc25a5			2.109133			
			3.81E-06			

#### ***4.13 Evaluation of GPX1 immunohistochemistry showed higher positive signal at D28***

GPX1 is a mitochondrial gene which acts against oxidative stress to maintain bone homeostasis. Therefore, GPX1 immunohistochemistry was performed to investigate the changes during fracture healing process (Figure 14). GPX1 positive area normalized to callus area were evaluated from Toluidine Blue counter-stained sections (Figure 14 A, B). Furthermore, application of Silver Nitrate as counter-stain helped in investigating GPX1 signal within osteocytes vicinity (Figure 14C).

Descriptively in Toluidine Blue counter-stained slide, GPX1 signal was seen in small patches within bone marrow and in callus region at D7. Furthermore, D10 showed GPX1 signal in proliferative chondrocytes, bone marrow, and bone lining cells. GPX1 signal at D14 was seen within bone marrow and bone matrix. Furthermore, D21 and D28 showed higher GPX1 signal within bone matrix and around fat cells present within bone marrow.

Furthermore, GPX1 signal at D28 was also seen near the newly formed bone (Figure 14A).

Histomorphometry showed lower GPX1 positive area at D7 when compared with other time points (Figure 14B). D10 showed higher GPX1 positive area when compared with D7 but lower GPX1 positive area when compared with D14, D21, and D28. GPX1 positive area was higher at D14 when compared with D7, D10, and D21 (Figure 14B). Furthermore, GPX1 area was higher at D21 when compared with D7 and D10. D28 showed higher GPX1 stained area when compared with other time points (Figure 14B). But no significant differences were observed.

Descriptively, Silver Nitrate counter-stained sections showed GPX1 signal within osteocytes and around blood vessels (Figure 14C). GPX1 signal was seen around blood vessels rather than osteocytes at D7. Further, GPX1 positive signal was seen around blood vessels and some patches within osteocytes vicinity at D10. Interestingly, D14 showed higher number of GPX1 signal within osteocytes vicinity than blood vessels (Figure 14C). GPX1 signal was seen in osteocytes vicinity and around blood vessels at D21. GPX1 signal was not seen within osteocytes at D28.

Evaluation of GPX1 signal during fracture healing showed higher signal with progression of fracture healing. Furthermore, D14 and D21 showed higher GPX1 signal within osteocytes compared with other time points. Further analysis is needed to investigate the effect of oxidative stress on protein synthesis activity.

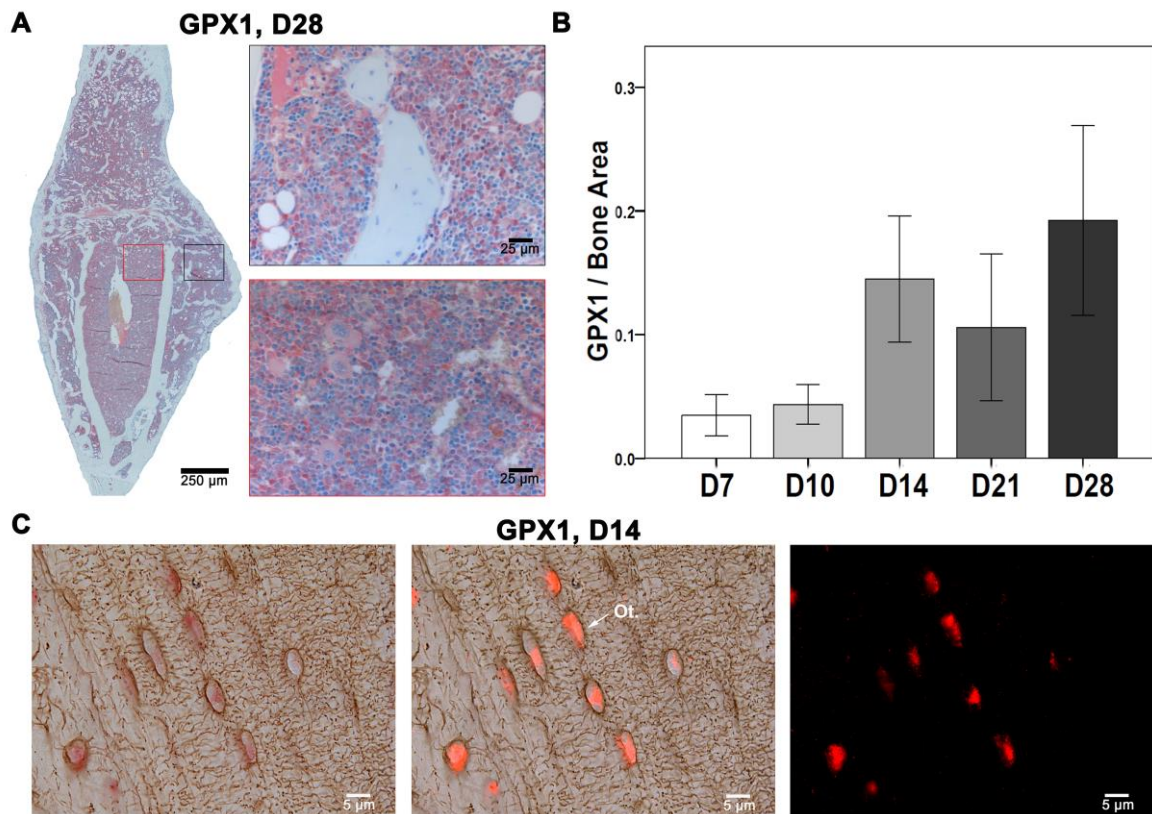


**Figure 14: Histological analysis of GPX1 activity during fracture healing showed active positive signal around blood vessels and osteocytes vicinity.** To understand the changes in anti-oxidant activity, GPX1 immunostaining were performed. Toluidine Blue and Silver Nitrate counter-stains were used to investigate overall and osteocyte-specific GPX1 positive signal, respectively. (A) D28 showed GPX1 stained region around the newly formed bone and bone marrow. (B) GPX1 stained area was higher at D28 compared with other time points. (C) Active osteocyte signals visualized via Silver Nitrate counter-stain within GPX1 positive areas. (N = 4 (D7), N = 6 (D10), N = 3 (D14), N = 5 (D21, D28), Ot: osteocytes).

#### **4.14 High number of differentially expressed genes related to ribosomal activity were present only at D3 and D7**

The ribosome plays a key role in protein synthesis which further relies on mitochondrion for energy production. Therefore, differentially expressed genes involved in ribosomal activity were investigated.

In total 15 ribosomal genes were differentially expressed, 13 genes were downregulated and 2 genes were upregulated (Table 6).

Among downregulated genes, there were cell differentiation and proliferation markers like Rps6, Ribosomal protein L24 (Rpl24), Ribosomal protein L27 (Rpl27), Ribosomal protein L31 (Rpl31), Rps2, and Ribosomal protein L36a like (Rpl36al). Interestingly, Rps6, Rpl24, Rpl27, Rpl31, Rps2, and Rpl36a1 were significantly downregulated at D3 and D7. Another important gene was Ubb which regulates cell cycle via proteasome complex crucial for cell survival. Ubb was significantly downregulated at D3 and D7. Furthermore, Mrpl53 which plays role in erythrocyte differentiation was significantly downregulated at D3 and D7. Another downregulated genes were ribosomal structural constituent like Mitochondrial ribosomal protein L33 (Mrpl33) and ribosomal biogenesis gene like Nucleophosmin 1 (Npm1). Mrpl33 was significantly downregulated at D3. While, Npm1 was significantly downregulated at D3 and D7. Gene like Methionyl aminopeptidase 1 (Metap1) which plays role in protein maturation was significantly downregulated at D7. Furthermore, E2F transcription factor 2 (E2f2) which controls cell cycle progression was significantly downregulated at D21 and D28. Another downregulated gene was Heterogeneous Nuclear Ribonucleoprotein H1 (Hnrnph1) which plays an important role in RNA splicing. Hnrnph1 was significantly downregulated at D3, D7, D21, and D28.

Among upregulated genes, there were Metallothionein 3 (Mt3) which encodes ion homeostasis and Protein disulfide isomerase family a member 3 (Pdia3) which encodes endoplasmic reticulum. Mt3 was significantly upregulated at D10, D14, and D21. While, Pdia3 was significantly upregulated at D10.

High number of ribosomal genes were significantly expressed at D3 and D7 when compared to other time points.

**Table 6: List of differentially expressed ribosomal genes and their FC and P-value (white background: downregulated and grey background: upregulated)**

Gene	D3	D7	D10	D14	D21	D28
Rps6	-3.925	-3.542				
	3.40E-05	7.50E-04				
Rpl24	-3.0135	-2.987				
	5.92E-05	3.45E-05				

Rpl27	-2.704	-2.7882				
	2.35E-07	5.13E-06				
Rpl31	-4.360	-3.889				
	5.82E-06	1.54E-05				
Rps2	-4.3006	-4.174				
	5.25E-05	1.72E-07				
Rpl36al	-2.352	-2.328				
	1.55E-06	2.62E-05				
Ubb	-3.837	-3.823				
	5.82E-08	3.13E-06				
Mrpl53	-2.1221	-2.8511				
	3.84E-06	1.10E-03				
Mrpl33	-2.035					
	1.41E-05					
Npm1	-2.5708	-2.758				
	1.12E-05	5.11E-05				
Metap1		-2.02905				
		1.13E-03				
E2f2					-2.040	-2.350
					9.61E-05	2.00E-03
Hnrnp1	-2.261	-2.319			-2.053	-2.003
	1.92E-06	1.49E-05			2.82E-06	1.20E-04
Mt3			2.1711	2.177	2.2716	
			2.90E-03	3.19E-03	2.54E-03	
Pdia3			2.083			
			3.82E-06			

The results showed the downregulation of genes involved in bone synthesis and cell cycle regulation. Furthermore, histological evaluation of changes during fracture healing due to cell cycle regulation is needed.

#### ***4.15 Evaluation of UBB immunohistochemistry showed higher positive signal at D7***

UBB is a conserved proteasome complex which regulates cell cycle and Nuclear factor Kappa-light-chain-enhancer of activated B cells (NF- $\kappa$ B) signaling. Therefore, UBB immunohistochemistry was performed to understand the changes during fracture healing process (Figure 15). UBB positive area normalized to callus area were evaluated from Toluidine Blue counter-stained sections (Figure 15 A, B). Furthermore, application of Silver Nitrate as counter-stain helped in investigating the UBB signal within osteocytes vicinity.

Descriptively in Toluidine Blue counter-stained sections, UBB signal was seen in chondrocytes, callus border, and bone marrow at D7 (Figure 15A). Further, UBB signal at D10 was seen in the proliferative chondrocytes and endosteum region. Interestingly, both D14 and D21 showed UBB signal within bone marrow and mineralized callus region. UBB signal was seen within bone marrow and in newly formed bone at D28.

Histomorphometry showed higher UBB stained area at D7 when compared with other time points (Figure 15B). D10 showed higher UBB stained area when compared with D14, D21, and D28. UBB stained area was higher at D14 when compared with D21 and D28 (Figure 15B). UBB stained area at D21 was lower when compared with other time points. Furthermore, UBB stained area was higher at D28 when compared with D21 (Figure 15B). UBB stained area was significantly higher at D7 when compared with D21 ( $p = 0.003$ ) and D28 ( $p = 0.006$ ). Furthermore, D10 showed significantly higher UBB stained area when compared with D21 ( $p = 0.040$ ). D14 showed significantly higher UBB stained area compared with D21 ( $p = 0.017$ ).

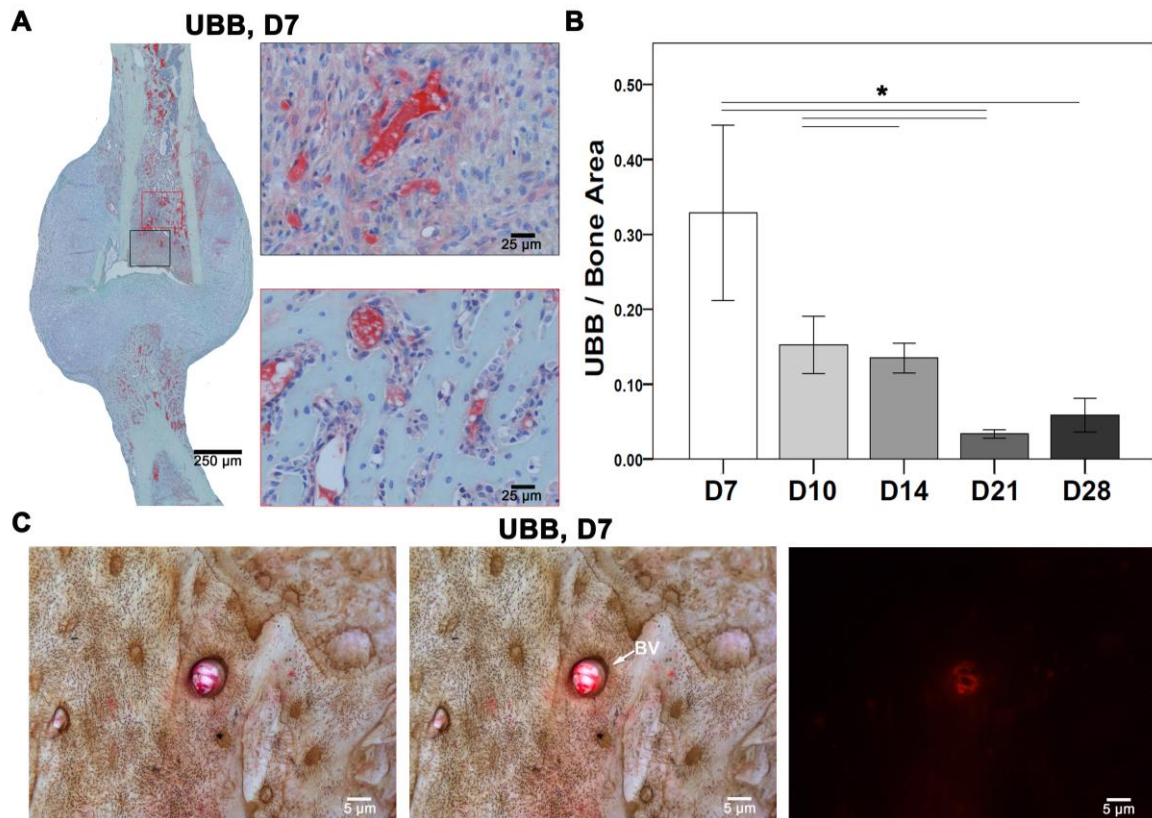


**Figure 15: Histological analysis of UBB activity during fracture healing showed active positive signal around blood vessels.** To understand the changes in ribosomal activity, UBB immunostaining was performed. Toluidine Blue and Silver Nitrate counter-stains were used to investigate overall and osteocyte-specific UBB positive signal, respectively. (A) D7 showed UBB stained region near to periosteal region and bone marrow. (B) UBB stained area was significantly higher at D7, D10, and D14 when compared with D21. Furthermore, D7 showed significantly higher UBB stained area compared with D28. (C) Positive signal of UBB visualized around blood vessels in the fractured callus via Silver Nitrate counter-stain. (BV: blood vessel; N = 4 (D7), N = 6 (D10), N = 3 (D14), N = 5 (D21, D28),  $* = p \leq 0.05$ , Non-parametric distribution: Mann Whitney U-test).

Descriptively, UBB counter-stained with Silver Nitrate showed positive signal around blood vessels than osteocytes (Figure 15C). UBB signal was prominent around blood vessels at D7. While, UBB signal at D10 was lower around blood vessels compared with D7. Furthermore, UBB signal at D14 around blood vessels increased compared to D10. While, D21 and D28 showed comparatively very less positive signal around blood vessels. No osteocytes positive signal was seen at any time point of healing.

Evaluation of UBB signal showed a wave like pattern with a decline from D7 to D14 and then an increase until D28. Ribosomal proteins plays important role in different signaling

like immune system and cell development. Further understanding of fracture healing relies on the examination of differentially expressed genes involved in immune system.

#### ***4.16 High number of differentially expressed genes related to immune response were present only at D10***

Fracture healing process initiates with pro-inflammatory reaction that triggers healing events. Immune system plays a key role in providing defense mechanism at the time of injury. Therefore, differentially expressed genes involved in immune response were investigated.

In total 15 immune response genes were differentially expressed, 5 genes were downregulated and 9 genes were upregulated (Table 7). Gene like beta 2 microglobulin (B2m) which is part of adaptive immune response was significantly downregulated at D3 and D7 while significantly upregulated at D10.

Among downregulated genes, there were innate immune response genes like S100 Calcium Binding Protein A8 (S100a8) which induces neutrophil chemotaxis was significantly downregulated at D3, D7 and Radical S-Adenosyl Methionine Domain Containing 2 (Rsad2) which prevents virus infection was significantly downregulated at D21 and D28. Another important gene was Interleukin 11 receptor subunit alpha 1 (Il11ra1) which helps in cell proliferation. Il11ra1 was significantly downregulated at D10. Synuclein alpha (Snca) which serves in membrane trafficking was significantly downregulated at D10, D21, and D28. Gene like Adenosine monophosphate deaminase 1 (Ampd1) which encodes for adaptive immune response, specifically T cells was significantly downregulated at D7, D10, and D14.

Among upregulated genes, there were innate immune response genes like Cathepsin G (Ctsg), Lipocalin 2 (Lcn2), and Peptidoglycan recognition protein 1 (Pglyrp1) that provide defense against pathogens. Ctsg, Lcn2, and Pglyrp1 were significantly upregulated at D10 and D14. Fc fragment of IgE Receptor 1g (Fcer1g) which performs collagen mediated platelet and neutrophil activation was significantly upregulated at D10 and D14. Another important gene is Interferon induced transmembrane protein 2 (Ifitm2) which inhibits virus entry to cytosol. Ifitm2 was significantly upregulated at D10. Another innate immune response gene is Ficolin B (Fcnb) which plays a role in lectin complement pathway activation to protect against micro-organisms. Fcnb was significantly upregulated at D10.

Furthermore, NF-kB signaling plays an important role in cytokine production and cell-survival. Gene like Secretory Leukocyte Peptidase Inhibitor (Slpi) which plays role in regulating NF-Kb signaling was significantly upregulated at D10. Natural killer cells and T cells express perforin (Prf) to target cell membranes. Prf1 was significantly upregulated only at D7. Gene like Placenta specific 8 (Plac8) encodes for adaptive immune response, specifically B cells. Plac8 was significantly upregulated at D10 and D14.

**Table 7: List of differentially expressed immune response genes and their FC and P-value (white background: downregulated and grey background: upregulated)**

Gene	D3	D7	D10	D14	D21	D28
S100a8	-4.5539	-4.54909				
	5.83E-06	5.16E-06				
Rsad2					-2.7446	-2.333
					1.45E-06	7.18E-06
Il1Ira1			-2.3639			
			3.09E-06			
Snca			-2.182		-3.173	-3.102
			7.69E-06		2.38E-06	1.46E-05
B2m	-3.156	-3.394	2.04			
	1.63E-04	4.56E-07	2.49E-05			
Ampd1			-2.3216	-2.5181		
			1.88E-05	3.83E-06		
Ctsg			2.769	2.342		
			2.01E-05	2.32E-05		
Lcn2			4.061	3.698		
			1.56E-06	2.76E-06		
Pglyrp1			2.73	2.361		
			3.78E-04	7.2E-04		
Fcer1g			2.316	2.598		
			9.37E-06	1.81E-06		
Ifitm2			2.008			
			3.87E-05			
Fcnb			2.521			
			1.13E-05			

Slpi			2.3009			
			1.16E-05			
Prf1		2.0429				
		1.35E-04				
Plac8			3.0235	2.3921		
			1.49E-04	9.89E-04		

Higher number of genes were differentially expressed at D10 and D14 when compared with other time points. Differentially expressed genes involved in immune response are involved in cell survival and metabolism related signaling pathways. Therefore, a better understanding of cross-talk between immune response and bone metabolism is required to unravel complexity of fracture healing.

## 5. DISCUSSION

Fracture healing involves well-coordinated molecular and cellular overlapping events with distinct histological characteristics [88]. The overlapping events of healing involve: 1) an early inflammatory response, 2) formation of soft callus, 3) hard callus formation, 4) bony bridging, and 5) bone remodeling [89]. However, 10 to 15% of fractures fail to reach bony consolidation resulting in a non-union or delayed healing [90]. Cellular deformities and genetic change leads to severe skeletal disorders like osteogenesis imperfecta [91] and neurofibromatosis type 1 [92].

This study investigates cellular and molecular changes during femoral fracture healing in a wild type male mice model. The research aims at understanding the differentially expressed genes in the fracture healing. Further, common genes in the overlapping healing events were also focus of this study. The current study focused on unraveling the role of six highly enriched biological processes: angiogenesis, ossification, ECM regulation, immune response, mitochondrial, and ribosomal activity in fracture healing. This understanding of overlapping healing events and enriched biological processes shall reflect on the translational potential to treat cases of delayed healing, non-union, and skeletal disorders.

Prior to detailed analysis, this study examined the validity of different FC cut-off criteria along with lower P-value to test the discrepancies in microarray data interpretation. The comparison of FC cut-off showed decline in gene numbers, whereas the highly enriched biological processes stayed at all cut-offs. Further, the comparison of DEG in every two consecutive time points provided an insight to the overlapping healing events. Hierarchical clustering based on expression profile across time points provided an overview of differential expression during fracture healing. This study showed presence of overlapping genes between enriched biological processes suggesting possible cross-talk during fracture healing. Quantitative evaluation of collagen fibril arrangement were carried out using CT-FIRE plugin in this study. The transition from woven bone to lamellar bone structure were evident during fracture healing. Further, type I collagen ring like structure was seen around osteocytes at all investigated time points. On the cellular level, MEPE and ERK evaluation showed a feedback mechanism with the progression of fracture healing. This study, described for the first time, -to my knowledge- differential expression of mitochondrial

and ribosomal genes in fracture healing. Further, immunostaining of mitochondrial protein GPX1 and ribosomal protein UBB were carried out to validate the differential expression. Microarray data analysis and histological analysis altogether provided a building block of successful fracture healing.

### **5.1 Fold change cut-off and data interpretation**

Microarray technology enables identification of biomarkers to diagnose diseases [93, 94]. FC and P-value cut-off criteria is usually applied to obtain DEGs in microarray data analysis. The choice of FC and P-value cut-off relies on the biological question. Many studies used FC cut-off of  $|0.5|$ ,  $|1|$ , or  $|2|$  and  $P\text{-value} \leq 0.05$  to obtain DEG in different fracture healing animal models [4, 5, 95, 96]. Dalman MR et al. 2012 reported the discrepancies in data interpretation with change in FC cut-off in zebrafish microarray data [97]. Therefore, this study tested whether changing FC cut-off results in misinterpretation of microarray data.

The obvious decline in number of DEG with increasing FC cut-off were seen in this study. This loss of genes with increasing cut-off reflected on gene ontology pattern (Figure 5). Nonetheless, the highly representative processes were present at all FC criteria's despite the decline in gene numbers. Genes involved in processes like angiogenesis, ossification, ECM regulation, and immune response with known role in fracture healing were detected at all FC cut-offs. Intriguingly, genes involved in processes like mitochondrial and ribosomal activity with undefined role in bone healing were also present at all cutoffs in similar or close ratios.

Angiogenesis is essential for bone regeneration and also used as a possible therapeutic approach to enhance bone regeneration [98]. This study showed the lower percentage of upregulated angiogenesis related genes when compared with ossification, ECM regulation, and immune response (Figure 5). The lower percentage of angiogenesis points to the crucial role of some genes over the others for successful healing.

Ossification and ECM regulation are interdependent processes essential for bone homeostasis [99]. This study showed the higher percentage of upregulated ossification and ECM genes with increasing FC cut-off (Figure 5 A, C, E). The increased percentage points to the presence of higher number of DEG with  $FC \geq |2|$  involved in ossification and/or ECM regulation in this study. Immune response were present in higher percentage at  $FC \geq$

1 and  $FC \geq 1.5$ , however at  $FC \geq 2$ , immune response were present in equal percentage as ossification and ECM in upregulated pattern (Figure 5C). This directs towards the equal need and importance of ossification, ECM, and immune response for successful fracture healing.

Ribosomal proteins are important for protein synthesis which serve for metabolic activities. This study showed lower percentage of ribosomal genes at all FC cut-off in both up- and down-regulated panels (Figure 5). The importance of ribosomal proteins in fracture healing is not known in fracture healing as per my knowledge. However, the percentage contribution of ribosomal genes at all FC cut-offs in this study points to an essential role to infer the underlying molecular mechanism.

Mitochondrial activity plays a fundamental role in energy production, cell signaling, apoptosis, and homeostasis [100]. However, little is known about the exact role of mitochondrial genes in fracture healing. In this study, the presence of mitochondrial activity in highest percentage among downregulated panel at all FC cut-offs reflects on its importance and need during fracture healing (Figure 5 B, D, F).

Collectively, this study showed the consistent presence of highly represented biological processes despite the change in FC cut-off and percentage distribution. This study reported the importance of FC cut-off comparison as pre-requisite for microarray data analysis to correctly investigate the underlying molecular mechanism. The comparison of FC cutoffs showed that the highly altered genes during fracture healing remained as well at higher cut-off. Therefore, detailed analysis were carried out using cut-off of  $FC = |2|$  and P-value  $\leq 0.01$ .

## ***5.2 Fracture healing: series of overlapping events***

Fracture healing process is divided into five overlapping events, each characterized by specific cellular and molecular activity [89]. However, a clear delineation of each healing event is missing because of experimental limitations. The approach to find the beginning and end of each healing event is to sacrifice animals at each consecutive time points from D0 until D28. However, such experimental design is impractical due to animal ethics and costs involved. This study compared DEG present between every two consecutive time points to identify overlapping genes crucial for fracture healing. Further, gene ontology of

overlapping genes provided an insight to the pattern of highly representative biological processes (Figure 6).

This study showed the highest percentage of mitochondrial genes in the overlap between D3 and D7 (Figure 6). Mitochondrial proteins carry out energy production which is more important at the time of injury. Leung KS et al. 1989 reported higher adenosine triphosphate (ATP) content within fractured callus of 12 week old rabbits during the early phase of healing [101]. This study suggests that the presence of mitochondrial genes during inflammatory phase is important for successful bone regeneration.

Highest percentage of ECM genes in the overlap between D7 & D10, D10 & D14, and D14 & D21 were seen in this study. This points to the central role of ECM during endochondral ossification and primary bone formation. Horton WA et al. 1988 showed that ECM serve as a scaffold during the transition from cartilage to bone in endochondral ossification phase in humans [102]. The continuous highest percentage of ECM genes in this study points to the regulatory role of ECM in transition from one to another healing event (Figure 6B).

Highest percentage of genes related to immune response were detected in the overlap between D21 and D28 (Figure 6). Immune response is very important against infection and inflammation, which can result in delayed healing. The highest percentage of immune response in this study during late phase of healing directs towards prevention of any inflammatory response. Raggatt LJ et al. 2010 reported the importance of innate and adaptive immune response in balanced bone remodeling process [103].

Taken together, comparison of DEG in consecutive time points helped in inferring overlapping genes important for fracture healing. Further, gene ontology provided an insight to crucial biological processes across overlapping time points. These results provided a better understanding to the overlapping healing events. To my knowledge, no previous study has evaluated the number and role of overlapping genes in the healing stages.

### ***5.3 Hierarchical clustering method***

Alignment of genes based on expression profile provides a global overview of upregulation and downregulation pattern. This study utilized hierarchical clustering

method which resulted in ten distinct clusters. Gene ontology of genes from each cluster provided a general picture of important biological process for bone healing (Figure 7).

Genes involved in same biological process like mitochondrial activity were aligned in more than one cluster (Figure 7). The presence of mitochondrial genes in different clusters directs to the varied expression profile during fracture healing. Similar alignment were seen with ECM genes, ossification, immune response, and ribosomal proteins in this study. Intriguingly, only angiogenesis genes were present in a single cluster, which directs toward similar expression profile across time points. Mitochondrial activity and ECM regulation were the highly enriched biological processes seen in this study.

Mitochondrial enzymes like *Oxct1* which plays a role in ketone body catabolism [104] were differentially expressed in this study. Other mitochondrial genes like *Gpx1* which acts against oxidative stress [105] were differentially expressed in this study.

ECM genes were present in four distinct clusters (Figure 7). Further, this study showed the presence of ECM, immune response / angiogenesis, and bone mineralization in the same cluster. This points to the cross-talk between biological processes and multi-functional role of genes during fracture healing. Genes like *Ibsp* and *Mgp*, that are part of ECM and important for bone mineralization [106] were present in this study. Further, *Mmp13* gene which plays a role in ECM organization, bone mineralization, and angiogenesis [107] was present in one cluster.

Taken together, hierarchical clustering followed by gene ontology connected temporal expression profile of DEG with highly enriched biological processes.

#### **5.4 Angiogenesis**

Blood supply is an essential need for normal fracture healing [108]. Hematoma formed at the site of injury serve as template for blood vessel development. Incomplete vascularization results in delayed healing or cases of non-union [98].

ASMA immunostaining used in this study helped in blood vessel visualization (Figure 8). Higher ASMA stained area and higher blood vessel count were seen at D7 in the fractured callus region (Figure 8). The higher blood vessel count points towards the increased cellular activity and mineral transport in early phase. Further, the blood vessels count were lower at D21 and higher at D28 suggesting potential involvement in bone remodeling

phase. McDonald SJ et al. 2012 reported that the higher gene expression of Asma at D7 post-fracture promote fracture healing via callus contraction in rat fractured callus [109]. Kinner B et al. 2002 reported that smooth muscle actin containing cells enables contractile motion required for bony bridging in murine model [110]. Saran U et al. 2014 showed that vascularization is prerequisite for ossification and new blood vessels provides the medium to osteoprogenitor cells for bone formation [111]. The transitional change in blood vessels count with fracture healing progression as seen in this study suggests a possible cross-talk between vascularization and bone formation process (Figure 8).

Growth factors and cytokines work together at molecular level to carry out successful angiogenesis. The compromised blood supply at the time of injury and oxygen deprivation results in hypoxic condition. Under the hypoxic condition, the anti-oxidant enzymes plays an important role to establish bone homeostasis and prevent oxidative damage. An anti-oxidant enzyme; Gpx1 was significantly downregulated only at D3 and D7 in this study. The differential expression of Gpx1 during inflammatory phase of healing points to its importance to overcome hypoxic situation. Lubos E et al. 2011 showed that Gpx1 reduces ROS (hydrogen peroxide) to water, by preventing cellular damage [32]. Intriguingly, previous reports also showed that ROS is essential for embryonic stem cell differentiation in a murine model [112]. Further, differentiation of embryonic stem cells results in endothelial cells that are crucial for vasculogenesis [113]. The downregulation of Gpx1 in this study directs towards increased ROS, which leads to stem cell differentiation into endothelial cells.

Hypoxic condition further induces the activation of pro-angiogenic factor like Vegfa, which is required for endothelial cell migration and proliferation [114]. Vegfa was significantly downregulated at D3 and D7 in this study. The differential expression of Vegfa during inflammatory phase suggests the possible role in promoting angiogenesis. However, Vegfa is also a key mediator of angiogenesis in cancer, where it influence the production of tumor vasculature for nutrients exchange [115]. Therefore, an excess of Vegfa expression can result in pathological condition. Hoeben A et al. 2004 showed that Vegfa induce angiogenesis via endothelial cell proliferation and migration [114]. The migration of endothelial precursor cells to form new blood vessels during embryonic development is regulated by the activity of angiogenic and anti-angiogenic factors [116]. The differential expression of Serpinf1, an anti-angiogenic factor, was detected at D3 and

D7 in this study. The downregulation of *Vegfa* and an upregulation of *Serpinf1* points to the regulatory interaction during angiogenesis. Venturi G et al. 2012 showed that *Serpinf1* is essential for the differentiation of osteoprogenitor cells required for fracture healing [117]. They also showed the antagonist potential of *Serpinf1* to *Vegfa* in regulating bone formation and resorption. The current study showed that successful fracture healing took place when *Vegfa* was downregulated and *Serpinf1* was upregulated. Intriguingly, Homan EP et al. 2011 reported the loss of *Serpinf1* in the pathology of osteogenesis imperfecta type VI [118]. The upregulation of *Serpinf1* during inflammatory phase in this study further suggests its therapeutic potential to treat angiogenesis related diseases and rare bone diseases.

The success of angiogenesis relies on ECM proteins as well besides angiogenic and anti-angiogenic factors [98]. MMP family proteins regulates *Vegfa* and degrade bone matrix, thereby promoting angiogenesis. *Mmp2* gene which is important for ECM degradation was downregulated at D3 and D7 in this study. The differential expression of *Mmp2* during inflammatory phase suggests that *Mmp2* degrade old bone matrix to make space for new blood vessel formation. Stetler-Stevenson WG. 1999 showed that *Mmp2* promote endothelial cell invasion by selectively degrading ECM to promote angiogenesis [119]. Other *Mmp* family gene; *Mmp9* was significantly upregulated in this study at D10, D14, and D21. *Mmp9* expression in this study points to the role in the overlapping of inflammatory and ossification phase. Colonot C et al. 2003 reported the generation of large cartilaginous callus and delayed vascularization in a knock-out mice model of *Mmp9*<sup>-/-</sup> [120].

Blood vessel integrity is crucial for the success of fracture healing. Transforming growth factors family proteins play an important role in establishment and maintenance of blood vessel integrity [121]. *Tgfbr1* and *Tgfbr2* were upregulated in this study at D14 and D10, respectively. This points to the importance of *Tgfbr1* and *Tgfbr2* in the overlapping region of angiogenesis and ossification. Larsson J et al. 2001 reported the early death of mice lacking *Tgfbr1* because of vascularization defect [122]. Further, weakened cell migration and differentiation properties in endothelial cells were seen in *Tgfbr1* deficient mice. Wu M et al. 2016 also showed defective vascularization due to lack of *Tgfbr2* in mice, that further resulted in rheumatoid arthritis [22]. Nonetheless, overproduction of either *Tgfbr1*

or *Tgfr2* can result in fibrosis related disorders [123, 124]. Therefore, a balanced gene expression of *Tgfr1* and *Tgfr2* is essential to prevent any complication during healing.

Taken together, differential expression analysis showed the interdependence of different growth factors, ECM proteins, and cytokines in successful blood vessel formation. The altered regulation in angiogenesis process can result in delayed healing. Further, the results showed an insight to the pathological condition that might occur due to lower or higher expression of genes. The cross talk between different proteins further suggests the overlapping transition from angiogenesis process to ossification phase.

## **5.5 Ossification**

Soft cartilaginous callus formed around the fracture gap serves as a route for cellular activity and ECM deposition, which is important in fracture healing [125]. Chondrocytes gather in the fractured callus and proliferate, thereby initiating bone matrix synthesis (Figure 9 A, B). Chondrocytes proliferate until all fibrous tissue is replaced by cartilage [126, 127]. Chondrocytes undergo hypertrophy to mineralize the cartilaginous matrix and once the mineralized matrix is formed, chondrocytes apoptosis takes place [128]. The mineralization of callus started from periosteal region by D10 post-fracture and mineralized bone matrix area increased at D14 (Figure 9 B, C). The hard callus formation progresses with mineralization of cortices at D21, by providing mechanical stability (Figure 9D). However, the hard callus formed is typically woven bone and not mechanically stable as normal bone [89]. Therefore, bone remodeling takes place to form regular lamellar bone by balanced osteoblasts and osteoclasts activity [70]. Bone remodeling phase resulted in complete mineralization of bone matrix with bony bridging by D28 (Figure 9E).

Well-coordinated molecular signals are required for ossification to result in bone mineralization and bony bridging. Cell differentiation and degradation of old bone matrix takes place to build new bone. Ubiquitin proteasome complex controls cell differentiation and degradation of intracellular proteins [129]. *Ubb*, which encodes ubiquitin was downregulated in this study at D3 and D7. *Ubb* differential expression during inflammatory phase suggests its role in degradation of proteins. Schundt C et al. 2015 reported the upregulation of *Ubb* in macrophage depleted mouse model which showed defective ossification [130]. Uyama M et al. 2012 also reported the negative *in-vitro*

correlation between Ubb expression and osteoblast formation [131]. This indicates that Ubb downregulation inversely affects the ossification and osteoblast activity.

Osteoblasts initiate matrix mineralization via different factors like Ibsp, Mmp9, Mmp13, and collagen family proteins. Ibsp and Mmp13 were significantly upregulated in this study at D3, D7, D10, D14, and D21. The continuous differential expression of Ibsp and Mmp13 directs to their importance in soft callus and hard callus formation. Malaval L et al. 2008 reported undermined bone growth and mineralization in Ibsp depleted mouse model [132]. Inada M et al. 2004 reported the delay in endochondral ossification and early vascularization in *Mmp13*-null mice [133]. Another member of Mmp family; Mmp9 was upregulated in this study at D10, D14, and D21. The presence of both Mmp13 and Mmp9 at D10, D14, and D21 points to a combined role in ossification. Ortega N et al. 2009 reported that Mmp9 is important for invasion of osteoclasts and endothelial cells into hypertrophic cartilage whereas Mmp13 is important for bone formation [99]. Rodenberg E et al. 2011 reported the onset of heterotopic ossification due to early expression of Mmp9 post-fracture in murine model [134]. This points to the fact that aberrant expression of Mmp9 can lead to ossification related pathologies.

Collagen family proteins are the richest protein in human body and type I collagen is the most generous form of collagen in ECM [135]. Collagen family proteins (Col10a1, Col1a1, and Col2a1) were significantly upregulated in this study. This reflects on the mineralized matrix formation.

Collectively, this study showed the differential expression of ossification related genes mainly during intermediate phases of healing. Further, the successful ossification relies on balanced collagenous as well as non-collagenous proteins expression. Any dysregulation in ossification gene expression can result in defective mineralization and therefore affect the bone quality.

## **5.6 Extracellular matrix**

ECM is a network of macromolecules that control cell proliferation, survival, differentiation, and mineralization [136]. ECM is one of the key player in maintenance of bone integrity [137]. The main fibrous component of ECM is collagen, which is essential for biomechanical competence and integrity [138]. This study utilized Sirius red stain to investigate the changes in collagen fiber arrangement with healing progression (Figure 10,

11). Type I collagen were irregularly arranged at D7 post-fracture and later arranged in well-organized sheets by D28. The formation of organized collagen at the late phase of healing points to the stability of newly formed bone. Bigham-Sadegh A et al. 2015 reported the randomly arranged collagen fibers during woven bone formation while organized and parallel sheet after lamellar bone formation [139]. Further, significant upregulated expression of Colla1 at D7, D10, D14 and Collagen type 1 alpha 2 (Colla2) at D3 until D14 were seen in this study. This reflects on the importance of collagens proteins in ECM organization. Gajko-Galicka A. 2002 showed that the reduction in type I and type II collagen results in osteogenesis imperfecta, characterized by bone fragility and structural deformities [140]. This indicates the prime importance of collagens in maintenance of structural integrity.

Quantitative evaluation of collagen fibrils orientation provides a further insight to ECM organization. This study implemented CT-FIRE plug-in for the first time on monochrome 10X images taken from polarized filter (Figure 4, 11). The above mentioned plug-in was adapted previously for quantitative evaluation of fibril structure obtained from TEM and fluorescence microscopy [83, 141]. Fiber angle points to the bone quality via fibril alignment. Higher Fiber angle was detected in this study at D28 (Figure 11C). The higher angle indicates the higher bone stiffness. Vincentelli R et al. 1971 reported the influence of mechanical factors on collagen fiber orientation [142]. They noticed lower angle of orientation in older people and higher angle of orientation in young people. This might be due to the organization of bone matrix and lower cellular activity in older patients. Fiber length affects the mechanical and structural properties of bone. The higher fiber length at D28 points to the mechanical stability of bone (Figure 11D). Hanley CJ et al. 2016 reported the accumulation of smaller fibers in patients with multiple tumor [143]. Daghma DES et al. 2017 also reported the higher frequency of small fibers in osteoporotic rat model [83]. This shows that deviation of fiber length can result in pathological conditions. Evaluation of fiber width helps in investigation of collagen fibers networking. Fiber width was higher in this study at D28 (Figure 11E). This might be because of compact and cross-linked structure formed after bone remodeling. Kim CL et al. 2016 reported the impact of fiber thickness on compact or rough nature of collagen fibers [144]. Fiber straightness marks the anisotropic or isotropic nature of fibers (Figure 11F). Collagen fibers showed anisotropic nature in this study at all time points. Further, differential gene expression of other collagenous proteins besides type I and type II were detected in this study. Non-

collagenous proteins like *Ibsp* and *Spp1* were also significantly upregulated in this study. The differential expression of collagenous and non-collagenous proteins reflects on bone mineralization.

### **5.6.1 Osteocytes and ECM markers**

Mechanical loading of bone further affects the morphology of osteocytes. The presence of type I collagen around the borders of osteocytes were seen in this study at all-time points of healing (Figure 10 A, A1). This adheres to previous report which showed that osteocytes align to the collagen to preserve ECM integrity [145]. This study showed the decline in osteocytes count (spindle, spherical, empty lacunae) with the progression of healing (Figure 12). This suggests the urgent need of osteocytes during early phase to support the ECM structure, the count then lowered once the mechanical stability reached. El Khassawna T et al. 2015 reported the increase in empty lacunae and irregular canaliculi network of osteocytes in osteoporotic rat model [146]. Lanyon LE. 1993 also showed the arrangement of osteocytes influence the bone modeling and remodeling [147].

Osteocytes inhibit osteoclastic bone resorption by producing signaling molecule like MEPE around high bone loading areas [148]. This study showed a wave like pattern in the activity of MEPE during fracture healing (Figure 13 A, B). This transitional change in MEPE suggests its possible role in bone homeostasis, by maintaining osteoblast and osteoclast activity. Jain A et al. 2004 reported the decrease in MEPE serum level with the increasing age of patients and maintenance of bone metabolism [149]. Osteoblast activation also relies on MAPK pathway. Yan YX et al. 2012 reported the proliferation of osteoblasts in *in-vitro* via activation of ERK in response to mechanical strain [150]. ERK immunostaining in this study showed lower activity during early phase of healing and higher at the late phase of healing (Figure 13D). The higher ERK activity correlates with the need of mineralization of new matrix to progress the healing. Lai CF et al. 2001 also showed the importance of Erk for cell differentiation and growth of human osteoblastic cells to complete bone mineralization [23]. Further, this study showed the feedback mechanism between MEPE and ERK during fracture healing (Figure 13). This reflects on well-maintained bone metabolism during the healing events. El Khassawna T et al. 2015 reported higher MEPE and ERK signal in osteoporotic animal model reflecting on imbalanced bone metabolism [146]. David V et al. 2009 reported the defect in growth and mineralization with altered bone-renal vascularization due to over-expression of MEPE in

a murine model [151]. Intriguingly, Chen Z et al. 2015 reported impaired chondrocyte differentiation due to deletion of Erk1 and Erk2 from a mouse model [152]. This suggests that a fine balance between MEPE and ERK is important to prevent ECM related pathologies.

The integrity of ECM further relies on the gene expression of specific markers important for fracture healing. In this study, upregulation of Acan, which is a part of ECM was detected at D10. This suggests that Acan plays an important role in ECM maintenance during bone mineralization. Watanabe H et al. 1998 reported that Acan binds to hydroxyapatite to prevent cartilage from compression under stress [153]. Lauing KL et al. 2014 showed that Acan is essential for chondrocytes organization and survival during embryonic limb development [154]. Therefore, loss of Acan can result in severe complexity like chondrodysplasias [155]. Roughley PJ et al. 2014 showed that degradation of Acan results in articular cartilage among osteoarthritis patients [156]. Further, several factors responsible for ECM organization like Mmp2, Mmp9, and Mmp13 were differentially expressed in this study. The presence of Mmp genes in this study directs to their importance in ECM organization and degradation. Mosig RA et al. 2007 reported the onset of arthritis and joint contraction in *Mmp2*<sup>-/-</sup> mouse model, that lead to decreased bone mineralization [157]. Neuhold LA et al. 2001 reported the induction of osteoarthritis in mice due to excessive Mmp13 activity [158]. This indicates towards the essential role of Mmp2 and Mmp13 in fracture healing as well as in the prevention of skeletal abnormalities.

Taken together, histological evaluation and differential gene expression involved in ECM showed a cross talk of different cell types and multifunctional genes in reaching bony bridging and mechanically stable bone. The results showed that loss of ECM genes can result in pathological conditions affecting the balanced cellular activity.

### ***5.7 Mitochondrial activity***

Mitochondrion is the powerhouse of cell. Energy production is required for cell proliferation and differentiation. Few studies reported changes in mitochondrial gene expression during fracture healing [159], while a detailed analysis is still required. This study for the first time -to my knowledge- describes the changes in mitochondrial genes during successful fracture healing.

Oxidative stress during injury produces ROS that comes from mitochondrion. Gpx1 is a mitochondrion origin antioxidant enzyme, which was significantly downregulated in this study at D3 and D7. Gpx1 reduces hydrogen peroxides to water radicals to prevent oxidative stress and preserve homeostasis [160]. Mlakar SJ et al. 2010 showed Gpx1 polymorphism associates with therapeutic potential to prevent oxidative damage in osteoporotic patients [161]. GPX1 immunostaining followed by histomorphometry showed a tendency of higher GPX1 positive area with the healing progression (Figure 14B). This points to the higher need of GPX1 in late phase of healing. Lean JM et al. 2005 showed increased bone loss and osteoclast formation in the presence of hydrogen peroxidase [162]. The higher GPX1 signal at late healing event indicates towards the need of anti-oxidant activity to preserve bone homeostasis. Further, increased signal of GPX1 in osteocytes vicinity as seen in this study suggests the cross talk between ECM and mitochondrion to maintain bone homeostasis (Figure 14C).

At the time of injury, the energy demand increases which reflects on highest number of DEGs during the early phase of healing. The downregulation of *Oxct1* which is an essential part for ketone body catabolism was detected in this study at D3 and D7. Fenselau A et al. 1975 reported lower level of ketone bodies in normal liver while higher in the malignant cells to grow fast [163]. Cotter DG et al. 2011 reported ketone body oxidation is required for postnatal survival in mice [164]. Further, they showed the induction of metabolic condition like diabetes in *Oxct1*<sup>-/-</sup> mice. This suggests that normal fracture healing and prevention of metabolic bone diseases needs ketone bodies for energy source.

Signal transduction and mineral transport is essential for cellular activity besides energy need. *Vdac3* which forms the clear channel to mediate metabolite flux through membranes were downregulated in this study at D3, D7, and D21. This might correlate with the cellular signaling during the fracture healing. Majumder S et al. 2013 showed that *Vdac3* negatively regulates ciliogenesis which is important for cell signaling and cell cycle [165]. Reina S et al. 2016 reported *Vdac3* as a potential marker to diagnose mitochondrial dysfunction and ROS signaling [166]. Downregulation of *Vdac3* in fracture healing as seen in this study prevent any disruption of centrosome and energy production.

*Slc25a5* which is a component of mitochondrial inner membrane was significantly upregulated in this study at D10. The upregulation points to *Slc25a5* role in inducing cell

proliferation. Klingenberg M. 1993 showed that Slc25a5 catalyzes the exchange of Adenosine diphosphate (ADP) and ATP between cytosol and mitochondrion [167]. This energy exchange via Slc25a5 points to the requirement for cell proliferation.

Taken together, this data showed the differences in cellular and molecular aspect of mitochondrial gene. Although the mitochondrial genes were downregulated during inflammatory phase, the success of bone healing still relies on mitochondrial genes. Further, differentially expressed mitochondrial genes showed a connection with systemic skeletal disease like osteoporosis and mitochondrial dysfunction.

### ***5.8 Ribosomal activity***

Ribosome regulates protein synthesis which is important for cellular growth, proliferation, differentiation, and apoptosis [37]. Any disruption in ribosome biogenesis can result in congenital skeletal differences [168]. The role of ribosomal genes in fracture healing is not well studied before. This study attempts to understand the changes in ribosomal gene expression in fracture healing.

Cell cycle control and transcriptional regulation is important for the progress of fracture healing. Downregulation of Ubb, which controls the degradation of proteins was seen in this study at D3 and D7. The downregulation of Ubb directs towards the increased cellular activity during the inflammatory phase. Hochstrasser M. 1995 showed that ubiquitin proteasome complex acts as a governing factor in the cell cycle progression [169]. Dennissen FJ et al. 2011 showed the association of mutation in Ubb with the onset of neurodegenerative diseases [170]. This points to the additional role of Ubb besides bone healing. Further, UBB immunostaining followed by histomorphometry showed higher UBB positive stain at D7, and then lowered with progression of healing (Figure 15B). This reflects on the need of cell differentiation at early stage of healing. Furthermore, several blood vessels showed UBB positive stain in this study (Figure 15C). This suggest potential role of UBB in vascularization as well. Previous studies also showed an increase in angiogenesis in aortic tissue from rats in presence of extracellular ubiquitin [171]. Therefore, Ubb is essential for protein degradation as well as for blood vessel formation.

Controlled expression of cell cycle regulators are important for cell division. The downregulation of E2f2 which controls cell cycle regulation was seen in this study at D21 and D28. This downregulation at late healing phase might point to the removal of extra

cells that are not required. Pagliarini V et al. 2015 reported the downregulation of E2f under stress induces apoptosis of cells to prevent metastasis [172]. Iglesias-Ara A et al. 2010 reported that E2f2 acts as one of the suppressor of hematopoietic progenitor expansion resulting in DNA damage [173]. Therefore, downregulation of E2f2 is essential for cell proliferation and differentiation.

Ribosomal proteins also plays an important role in preventing oxidative stress condition. The upregulation of Mt3 which is induced under hypoxic condition was detected in this study at D10, D14, and D21. The upregulation directs towards establishment of bone homeostasis. Hwang YP et al. 2008 showed that Mt3 controls the intracellular level of ROS in human neuroblastoma cell lines by regulating an antioxidant enzyme [174].

Collectively, this study showed the important role of ribosomal proteins in bone homeostasis and cellular growth. UBB at cellular level showed an overlapping role in angiogenesis and ribosomal activity. Further, the downregulation of ribosomal genes showed a potential role in preventing cellular damage.

## **5.9 Immune response**

Immune system is important to provide defense against invading pathogens. An emerging field of osteoimmunology focuses on understanding the interplay between immune system and skeletal system [175]. This study aimed at understanding the role of innate and adaptive immune system in fracture healing. Both upregulation and downregulation of genes involved in immune response were detected in this study during fracture healing.

Preventing infection from virus or microbes is important for the successful fracture healing. In this study, Snca was significantly downregulated at D10, D21, and D28. Snca is a conserved protein in central nervous system and its role in pathogenesis of Parkinson disease is well-known [176]. Calabrese G et al. 2016 reported using bioinformatics analysis that Snca regulates bone network homeostasis an ovariectomy induced bone loss [177]. Shameli A et al. 2016 reported the hindered development of B-lymphocytes and T-lymphocytes in Snca knock-out model [178]. The presence of Snca in this study points to the defense mechanism against pathogens and bone loss. Labrie V et al. 2017 recently reported the increased expression of Snca around virus infection in brain [179]. This suggests that upregulation of Snca takes place under the attack of pathogens. This study showed the differential expression of B2m which displays antimicrobial activity. B2m was

downregulated at D3 and D7 while upregulated at D10 in this study. Xie J et al. 2003 reported that B2m acts as a negative regulator of immune system and the raised serum level of B2M was seen among rheumatoid arthritis and multiple myeloma patients [180]. The early downregulation of B2m in this study points to increased immune response during early phase of healing when compared with intermediate or late healing phase.

Neutrophils are among the first immune cells recruited at the site of injury to prevent infection. This study showed the upregulation of Ctsg which is a protease complex. Wilgus TA et al. 2013 showed that neutrophils produces Ctsg to target ECM proteins, thereby degrading membrane proteins [181]. Bangalore N et al. 1990 reported the antimicrobial role of Ctsg besides degrading membrane proteins to prevent infection [182]. Zou F et al. 2017 reported that downregulation of Ctsg prevents the increased T cell activity, thereby affecting bone remodeling process [183]. This indicates the multiple role of Ctsg in fracture healing.

Taken together, this study helped in providing a slight insight into immune response in fracture healing. Further, differential expression of genes and their roles was useful to gain information about the cross-talk of bone and immune system.

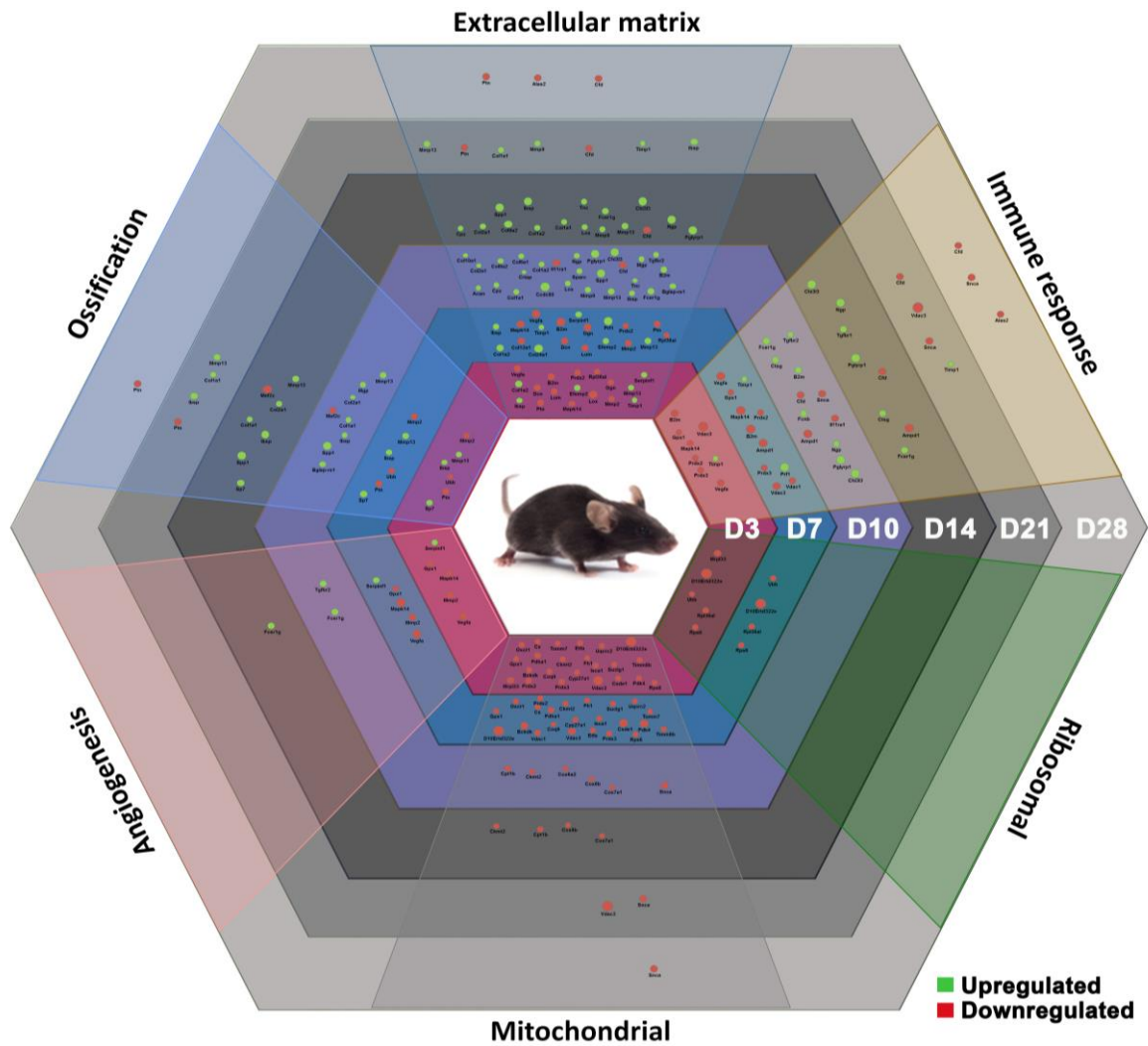


**Figure 16: Blueprint of differentially expressed genes involved in key biological processes during fracture healing.** To illustrate the complexity of fracture healing, DEG involved in the targeted processes were mapped across time points. Differential gene expression was visualized from D3 (pink) until D28 (grey). Angiogenesis genes were differentially expressed from D3 until D14. Ossification genes were differentially expressed at all time points. Higher ECM genes were present at D3 until D14 compared with D21 and D28. Higher immune response genes were downregulated at D3, D7, upregulated at D10, D14 and downregulated at D21, D28. Ribosomal and mitochondrial genes were highly downregulated at D3 and D7.

## 6. CONCLUSION

This study offers a new prospective about the overlapping healing events of fracture healing and the application of phase targeted approach for treating non-union or human skeletal disorders. The use of whole genome sequencing via microarray enabled the detailed investigation of differentially expressed genes across the time points of healing. This study presents the importance of FC cut-off comparison as a pre-requisite for differential analysis. The importance of angiogenesis, ossification, ECM regulation, and immune cells during fracture healing is well known. This study, however, showed the presence of overlapping genes among the key biological processes during healing. The cross-talk between different genes pointed to the overlapping transition through healing progression. This study showed the importance of differentially expressed genes like *Colla1*, *Mmp13*, *Ibsp*, *Serpinf1* in preventing skeletal abnormalities, delayed healing, or non-union cases.

The importance of ECM during fracture healing, systemic skeletal diseases, and therapeutics designing is well known. Here, the study showed the cross-talk between different cell types involved in signaling pathways and orientation of collagen fibers during fracture healing. The computation quantification of collagen fibers gained from Sirius red stain images reflects on bone healing. Further examination of ossification genes showed a balanced expression of collagenous and non-collagenous proteins.

This study for the first time presents the contribution of mitochondrial and ribosomal genes in the successful fracture healing. It explains the role of mitochondrial genes specifically during inflammatory phase to preserve bone homeostasis, by preventing the risk of osteoporosis. The combined differential gene expression and immunostaining used here revealed that mitochondrial genes play an essential part in fracture healing. Further, this study show the high potential of ribosomal genes in preventing cellular damage during fracture healing.

This work provided a blueprint of differentially expressed genes during successful healing (Figure 16). This study identified novel candidate markers for bone healing to develop phase-directed treatment.

## **7. IMPLICATIONS AND FUTURE DIRECTION**

This thesis using microarray data analysis and histology indicated the potential role of six main biological processes in the successful bone healing.

This study investigated the importance of angiogenesis, ossification, ECM, immune response, mitochondrial, and ribosomal activity but not the muscle cells in fracture healing. Muscles provide rich supply of oxygen and nutrients to the surrounding tissue. Some cases with delayed healing results from high energy trauma with extensive damage of soft tissue [184]. Therefore, investigation of bone and muscle interaction can provide further insight to the fracture healing mechanism.

This thesis showed a new therapeutic potential of phase targeted strategy for successful bone healing and for the treatment of diseases like osteoporosis and osteogenesis imperfecta. Nonetheless, the optimization of phase targeted markers is required to successfully improve the therapeutic outcome. Additional network analysis study between phase specific markers would unravel the complex underlying interactions.

The prediction of fragility fractures in osteoporotic patients depends on the identification of structural and genetic basis [185]. Another outlook to this study would be to understand the association between transcriptomic data and bone structural properties via genotype-phenotype correlation. The correlation will indeed provide a clearer picture of diagnostics potential.

# APPENDICES

## APPENDIX 1

### *Preparation of samples for paraffin embedding*

MATERIAL	
Ethanol (100%)	Methyl Ethyl Ketone denaturized solution; Herbeta Drug, Berlin, Germany
EDTA	Decalcifying solution; Herbeta Drug, Berlin, Germany
Paraffin	EM-400 Embedding Medium Paraffin; Leica Biosystems, Nussloch GmbH, Germany
Paraffin Dispenser	Leica EG1120, Leica Biosystems, Nussloch GmbH, Germany
PFA	4 % W/V Paraformaldehyde powder in DEPC treated water (pH = 9.1)

#### Samples dehydration machine procedure:

Step	Solution	Time (min.)	Repetition
1.	Ethanol (70%)	60	1x
2.	Ethanol (80%)	60	1x
3.	Ethanol (96%)	120	2x
4.	Ethanol (100%)	120	2x
5.	Ethanol (100%)	180	1x
6.	Xylol	60	2x
7.	Paraffin	120	2x

#### Protocol:

1. Fix the bone samples in 4% PFA solution for 48 hours.
2. Decalcify bones at 4 °C in 1:2 mixture of 4% PFA and EDTA for three weeks. Change solution twice in a week.
3. Place the bones in dehydration cassettes and rinse for 1 hour under running tap water.
4. Dehydrate the samples in machine as mentioned in the table above; all steps are carried out at RT.
5. Pre-heat the casting molds at 60 °C in incubator to prevent instant solidifying.
6. Place the samples in the mold holding gently using forceps.
7. Place the mold with samples on the hot plate and pour paraffin from the heated tank.
8. Remove the mold from hot plate carefully and place it on -5 °C cooling plate for 15 minutes.
9. Remove the embedded samples from the mold and store at RT.

## **APPENDIX 2**

### *Sirius Red Staining*

MATERIAL	
Sirius Red	Picro Sirius Red Stain Kit (ab150681, Abcam, Cambridge, MA, USA)
Acetic Acid	Acetic Acid Solution (ab150681, Abcam, Cambridge, MA, USA)

#### Protocol:

1. Deparaffinize sections via Xylene (2 x 10 minutes) and descending percentage of ethanol 100%, 96%, 70% for 2 minutes each.
2. Rehydrate in distilled water for 2 minutes.
3. Stain in Sirius red solution for 1 hour.
4. Rinse in acetic acid solution (2x).
5. Rinse in absolute ethanol.
6. Clear in absolute ethanol, two changes for 5 minutes each.
7. Cover slip the slides after mounting using Vitroclud.

## APPENDIX 3

### *Trichrome Masson Goldner Stain*

MATERIAL	
Weigert Hematoxylin solution A	Art. No. X906.1, Carl Roth GmbH and Co. KG, Karlsruhe, Germany
Weigert Hematoxylin solution B	Art. No. X907.1, Carl Roth GmbH and Co. KG, Karlsruhe, Germany
Goldner's staining I	Ponceau-Fuchsin solution (Art. No. 3469.1, Carl Roth GmbH and Co. KG, Karlsruhe, Germany)
Goldner's staining II	Phosphotungstic acid-Orange G solution (Art. No. 3470.1, Carl Roth GmbH and Co. KG, Karlsruhe, Germany)
Goldner's staining III	Light green SF yellowish solution (Art. No. 3473.1, Carl Roth GmbH and Co. KG, Karlsruhe, Germany)
Glacial Acetic acid	Acetic acid (glacial) 100% (1000631000, Merck KGaA, Darmstadt, Germany)

#### Protocol:

1. Deparaffinize sections via Xylene (2 x 5 minutes) and descending percentage of ethanol 100%, 96%, 70% for 5 minutes each.
2. Rinse in distilled water for 2 minutes.
3. Mix Hematoxylin solution A and solution B in 1:1 concentration.
4. Stain the sections with mixed solution for 3 minutes.
5. Rinse the sections in running tap water for 10 minutes.
6. Stain the sections with Goldner's staining solution I for 8 minutes.
7. Rinse the sections in 1% acetic acid solution for 30 seconds.
8. Stain the sections with Goldner's staining solution II for 5 minutes.
9. Rinse the sections in 1% acetic acid solution for 30 seconds.
10. Stain the sections with Goldner's staining solution III for 4 minutes.
11. Rinse the sections in 1% acetic acid solution for 3 minutes.
12. Dehydrate in ascending percentage of ethanol 70%, 96%, 100% for 5 minutes each.
13. Clear in Xylene, two changes for 5 minutes each.
14. Cover slip the slides after mounting using Vitroclud.

## **APPENDIX 4**

### ***Silver Nitrate Staining***

MATERIAL	
Formic acid	Formamide (EMD 1.09684.1000, Merck KGaA, Darmstadt, Germany)
Gelatin	Gelatin from bovine skin (G9391, Sigma-Aldrich Chemie GmbH, Munich, Germany)
Silver nitrate	Silver nitrate for analysis (ACS, ISO 131459, AppliChem GmbH, Darmstadt, Germany)
Solution A	Add 0.5g Gelatin in 24.75 ml double distilled water, mix well at room temperature. Add 250 µl Formic acid.
Solution B	50% silver nitrate prepared in double distilled water
Sodium thiosulfate	Sodium thiosulfate pentahydrate (10102-17-7, Merck KGaA, Darmstadt, Germany)

#### **Protocol:**

1. Deparaffinize sections via Xylene (2 x 5 minutes) and descending percentage of ethanol 100%, 96%, 70% for 5 minutes each.
2. Rehydrate the sections via double distilled water (2 x 5 minutes).
3. Mix solution A and B in 1:2 concentration.
4. Stain with the mixed solution for 73 minutes.
5. Rinse the sections in distilled water to stop the reaction.
6. Wash in distilled water for 5 minutes.
7. Place in 5% Sodium thiosulfate for 10 minutes.
8. Wash in distilled water for 5 minutes.
9. Dehydrate in ascending percentage of ethanol 70%, 96%, 100% for 5 minutes each.
10. Clear in Xylene, two changes for 5 minutes each.
11. Cover slip the slides after mounting using Vitroclud.

## APPENDIX 5

### *Immunohistochemical Staining*

MATERIAL	
TBS	TRIS PUFFERAN®, 4855.2, Carl Roth GmbH, Karlsruhe, Germany; Sodium chloride, 31434-1KG-R, Sigma Aldrich Chemie GmbH, Steinheim, Germany; Hydrochloric acid 25%, 1.00316.1011, Merck KGaA, Darmstadt, Germany
Triton	Triton® X-100, 1.08643.1000, Merck KGaA, Darmstadt, Germany
Citrate buffer	Citric acid monohydrate, 3958.2, Carl Roth GmbH, Karlsruhe, Germany; tri-Sodium citrate dihydrate, 1.06448.1000, Merck KGaA, Darmstadt, Germany
Blocking solution	BLOXALL™ Blocking solution, SP-6000, Vector Laboratories, Inc., Burlingame, CA, USA
ABC-AP kit	Alkaline phosphatase, AK 5200, Vectastain ABC kit, Vector Laboratories, Inc., Burlingame, CA, USA
ASMA (1:100)	Primary antibody, rabbit polyclonal, TA353561, Acris Antibodies GmbH, Herford, Germany
Osteocalcin (1:100)	Primary antibody, mouse monoclonal, MAB1419, R&D Systems, Inc., Minneapolis, MN, USA
MEPE (1:100)	Primary antibody, rabbit polyclonal, HPA038004, Sigma-Aldrich Chemie GmbH, Munich, Germany
ERK (1:100)	Primary antibody, rabbit monoclonal, ab32081, Abcam, Cambridge, MA, USA
Ubiquitin (1:150)	Primary antibody, rabbit polyclonal, ab7780, Abcam, Cambridge, MA, USA
Glutathione peroxidase 1 (1:325)	Primary antibody, rabbit monoclonal, ab22604, Abcam, Cambridge, MA, USA
AP-substrate kit	Vector® Red Alkaline phosphatase substrate, SK-5100, Vector Laboratories Inc., Burlingame, CA, USA
Methyl green	Methyl green, H-3402, Vector Laboratories Inc., Burlingame, CA, USA
Acetone	
Glacial acetic acid	Glacial Acetic Acid (EC Number 2005807, Merck, Darmstadt, Germany)
Formic acid	Formamide (EMD 1.09684.1000, Merck KGaA, Darmstadt, Germany)
Gelatin	Gelatin from bovine skin (G9391, Sigma-Aldrich Chemie GmbH, Munich, Germany)
Silver nitrate	Silver nitrate for analysis (ACS, ISO 131459, AppliChem GmbH, Darmstadt, Germany)
Solution A	Add 0.5g Gelatin in 24.75 ml double distilled water, mix well at room temperature. Add 250 µl Formic acid.
Solution B	50% silver nitrate prepared in double distilled water
Sodium thiosulfate	Sodium thiosulfate pentahydrate (10102-17-7, Merck KGaA, Darmstadt,

	Germany)
--	----------

General Protocol (for all IHC):

1. Deparaffinize sections via Xylene (2 x 5 minutes).
2. Wash in technical acetone for 10 minutes.
3. Mix technical acetone and washing buffer in 1:1 concentration. Wash the slides in the mixed solution for 10 minutes.
4. Rehydrate the slides in washing buffer (2 x 10 minutes).
5. Antigen retrieval using citrate buffer solution (pH = 6) for 1 hour at 60 °C.
6. Wash the slides in washing buffer at RT (2x).
7. Mark around the section using fat marker.
8. Inhibit endogenous peroxidase using blocking solution for 10 minutes at RT.
9. Wash the slides in washing buffer (2 x 5 minutes) at RT.
10. Add one drop of universal serum in 5 ml of TBS. Incubate the slides for 20 minutes at RT.
11. Incubate with primary antibody at 4°C overnight.
12. Wash in washing buffer (2 x 5 minutes).
13. Prepare secondary antibody by adding a drop of universal serum and a drop of biotinylated universal antibody in 2.5 ml of TBS. Incubate with secondary antibody for 30 minutes at RT.
14. Prepare ABC-AP complex 30 minutes before use. Add 25 µl Reagent A and 25 µl Reagent B in 2500 µl of TBS.
15. Rinse the slides in washing buffer (2 x 5 minutes).
16. Incubate in ABC-AP complex for 30 minutes at RT.
17. Rinse the slides in distilled water for 5 minutes.
18. Prepare AP substrate mix by adding all three reagents (2 drops each) in 5 ml of 150 Mm Tris-HCl buffer (pH = 8.3).
19. Incubate with AP substrate until a clear red color is detected.
20. Rinse in distilled water to stop the reaction (2 x 5 minutes).
21. Counter stain with methyl green for ASMA and Osteocalcin; toluidine blue for MEPE and ERK; silver nitrate for Ubiquitin and Gpx1.
22. Cover slip the slides after mounting using Vitroclud.

Protocol for use of Methyl Green as counter-stain:

1. Heat the hot plate at 60°C prior to stain.
2. Incubate the slides with methyl green for 5 minutes at 60°C.
3. Stop the reaction by washing the slides in distilled water.
4. Rinse the slides in distilled water for 1 minute.
5. Add 50 µl glacial acetic acid in 100 ml acetone. Dip the slides 5-10 times in the mixed solution.

6. Dip the slides in 96% and 100% ethanol (5 times each).
7. Dry the slides inside the incubator for 30 minutes at 60°C.
8. Cover slip the slides after mounting using Vitroclud.

Protocol for use of Toluidine Blue as counter-stain:

1. Prepare toluidine blue solution in 1:1 concentration.
2. Rinse the slides in toluidine blue solution for 35 seconds at RT.
3. Stop the reaction by washing in distilled water.
4. Dehydrate in 100% ethanol for 5 minutes.
5. Clear in Xylene (2 x 5 minutes).
6. Cover slip the slides after mounting using Vitroclud.

Protocol for use of Silver Nitrate as counter-stain:

1. Mix solution A and B in 1:2 concentration. Stain the slides using mixed solution for 35 minutes at RT.
2. Stop the reaction by washing the slides in double distilled water
3. Rinse the slides in double distilled water (3x).
4. Prepare 5% sodium thiosulfate solution. Incubate the slides with sodium thiosulfate for 2 minutes at RT.
5. Rinse in distilled water for 5 minutes.
6. Dehydrate by rinsing in 70% ethanol for 2 minutes and 100% ethanol for 10 minutes.
7. Dry the slides inside the incubator for 30 minutes at 60°C.
8. Cover slip the slides after mounting using Vitroclud.

## **APPENDIX 6**

### ***Histomorphometry using ImageJ (version 1.51)***

#### **Pre-requisites for software:**

1. Java version 8
2. Trainable Weka Segmentation plugin (v 3.2.13)
3. Minimum of 4 gb RAM.

#### **Protocol (also depicted as step-wise screenshots):**

1. Import Image onto ImageJ (Drag and drop/ File → Open).
2. Go to Image → Stacks → Tools → Montage to Stack. Select one stack that represents all segment of a histological stain.
3. Go to Plugins → Segmentation → Trainable Weka Segmentation. This will open a window with different options.
4. The default number of classes are two, but it can be increased up to an arbitrary number based on the analysis using “Create new class” option present on the left panel. The name of first two classes can be changed by going to “Settings” option. Define the classes on the basis of colors visualized in a specific stain. The points can be defined for each class using polygon tool or line.
5. After defining 10-15 points for each class, go to “Train Classifier”. It will take time according to the memory of computer and image size.
6. The log window will provide the information once segmentation is finished. Go to “Create result” to verify the segmentation done by plugin.
7. If the segmentation done is comparable to the initial image, go to “save classifier” and “save data” options to save time for the analysis of images from the same histological stain.
8. All other images from the same stain can be analyzed by uploading classifier and data file using “Load Classifier” and “Load Data” option present on Trainable Weka Segmentation window.
9. After segmentation, go to Analyze → Measure to obtain the percentage of area covered by each defined class in a picture.
10. Go to Analyze → Set Scale. The pixel size depends upon the microscope and magnification used for capturing the picture. The area percentage can be converted into ASBMR defined scale (mm or  $\mu\text{m}$ ) by multiplying the scale of image with the percentage obtained from the previous step.
11. The obtained results can be statistically tested later.

## APPENDIX 7

### *RNA isolation and Quality Control*

MATERIAL	
RNase free water	Ambion® Nuclease-Free Water, Thermo Scientific GmbH, Karlsruhe, Germany
Trizol Reagent	TRIzol™ Reagent, Invitrogen, Thermo Scientific GmbH, Karlsruhe, Germany
Isopropyl alcohol	127682001, Carl Roth GmbH, Karlsruhe, Germany

#### Protocol for RNA isolation:

1. Avoid any kind of contamination. Work on clean bench.
2. Pulverize flash frozen calluses using pestle and mortar under continuous cooling with liquid nitrogen.
3. Transfer the material to a 2 ml sterile Eppendorf tube.
4. Add 1 ml of TRIzol Reagent for each 200 mg of tissue.
5. Homogenize the samples in 15 seconds interval while kept in ice using a homogenizer (T10, Ultra Turrax, IKA-Werke GmbH & Co. KG, Staufen, Germany).
6. Add 0.2 ml chloroform per 1 ml of TRIzol Reagent. Securely close the sample tubes and vortex vigorously for 15 seconds.
7. Incubate the homogenized sample for 15 minutes at RT to allow complete dissociation of nucleoprotein complexes.
8. Centrifuge the samples to remove cell debris at no more than 12,000 x g for 15 minutes at 2-8°C.
9. After centrifugation, the mixture separates into three distinct phases: phenol-chloroform phase as lower red, an interphase, and a colorless upper aqueous phase. RNA remains exclusively in the aqueous phase. Carefully transfer the upper aqueous phase into fresh tube without disturbing the interphase. Then, measure the volume of the aqueous phase.
10. Add 200 µl of chloroform and 1 ml of TRIzol and repeat step 8-9.
11. Add 500 µl isopropyl alcohol per 1 ml of TRIzol Reagent used for the initial homogenization to precipitate RNA from the aqueous phase. Incubate samples for 10 minutes at RT.
12. Centrifuge at not more than 12,000 x g for 10 minutes at 2-4°C. The RNA precipitate, often invisible after centrifugation, forms a gel-like pellet on the side and bottom of the tube.
13. Carefully remove the supernatant completely. Wash the RNA pellet once with 75% ethanol, adding at least 1ml of 75% ethanol per 1 ml of TRIzol Reagent used for the initial homogenization. Vortex the tube and then centrifuge at no more than 7,500 x g for 5 minutes at 2-8°C. Repeat the washing procedure once. Remove the leftover ethanol completely.
14. Dry the RNA pellet by air-drying/vacuum-drying for 5-10 minutes. It is crucial not to let the RNA pellet dry completely as it will greatly affect RNA solubility. Partially dissolved RNA samples generally have an  $A_{260}/A_{280}$  ratio < 1.6. Dissolve RNA in RNase free water using pipette.
15. Use picodrop spectrophotometer to determine the sample concentration and purity. Use picodrop pipette tips and a 10 µl Gilson pipette to take 2 µl of sample to measure OD at 260nm and 280nm. The  $A_{260}/A_{280}$  ratio should be above 1.7, for microarray analysis RNA integrity in bio-analyzer should be above RIN.

16. Usually total RNA isolated using TRIzol method needs to be further cleaned using DNase I (Invitrogen Life Technologies) protocol.

## **APPENDIX 8**

### ***Quality assessment of Beadchip array using R***

Pre-requisite for the analysis: Install R from <https://cran.r-project.org> (v 3.0.3)

Protocol to change the working directory in R:

1. Open R console.
2. Go to File → Change dir... → “provide the path to the folder raw data is saved”.

The code below shows the protocol for quantile normalization for the Illumina beadchip array:

```
source ("https://bioconductor.org/biocLite.R")
biocLite (c ("illuminaio", "beadarray", "limma", "illuminaMousev2.db")) # install the required packages
library (illuminaio) # library command load the installed packages
library (beadarray)
library (limma)
library (illuminaMousev2.db)
Idatfiles <- dir (pattern = "idat") # Illumina's raw data is saved in idat file format, this command will
read and store all idat files present in the current directory under "Idatfiles"
# Annotation for Illumina beadchip array can be downloaded from NCBI-GEO or from Illumina web
site. The file with annotation usually have extension at ".txt" or ".bgx". Unzip the downloaded file and
save it in the current directory
Bgxfile <- dir (pattern = "bgx") # the command will read the bgx file and store it under "Bgxfile" for
further analysis.
X <- read.idat (Idatfiles, Bgxfile) # the command reads the information stored in "Idatfiles" and
"Bgxfile" and store it in X variable
Sig_value <- detectionPvalues (X) # this command detects the p-value within probes
Y <- propexpr (X) # this command estimates the proportion of expressed probes in array data
Z <- neqc (X) # this command performs background correction, log transformation and quantile
normalization for Illumina expressed data
# Save the outputs in txt file using following commands
write.table (Sig_value, file = "p_values.txt", sep = '\t', row.names = F)
write.table (Y, file = "proportion.txt", sep = '\t', row.names = F)
write.table (Z, file = "normalized_data.txt", sep = '\t', row.names = F)
```

## APPENDIX 9

### *Hierarchical clustering of DEG using R*

Pre-requisite for the analysis: Install R from <https://cran.r-project.org> (version 3.0.3)

Protocol to change the working directory in R:

1. Open R console.
2. Go to File → Change dir... → “provide the path to the folder in which gene list is saved”.

The code below shows the protocol to perform hierarchical clustering based on expression pattern:

```
install.packages(c("pvclust", "biclust", "modeltools", "som", "flexclust", "cluster", "scatterplot3d",
"plots", "e1071", "kernlab")) # install the required packages from the Comprehensive R archive
network
source("http://www.bioconductor.org/biocLite.R") # install required packages from Bioconductor
biocLite(c("genepattern", "ellipse", "ctc"))
List <- read.delim("genelist.txt", header=T, sep="\t") # read the gene list saved in txt file
rownames(List) <- List[,1];
List <- as.matrix(List[,-1]) # transform gene list into matrix object
dim(List) # this command can be used to re-check the dimensions of final sample matrix
#Hierarchical Clustering
library(gplots);
myheatcol <- redgreen(75) # import color scheme for heatmap visualization
List_scale <- t(scale(t(List))) # centers and scales the sample data
hr <- hclust(as.dist(1-cor(t(mydatascale)), method="pearson")), method="complete") # Cluster rows by
Pearson correlation.
Heatmap(List, Rowv=as.dendrogram(hr), Colv=NA, col=myheatcol, scale="row") #complete heatmap
with gene list
png("Heatmap.png", # create PNG for the heat map
width = 20*300, # 5 x 300 pixels
height = 60*300,
res = 600, # 300 pixels per inch
pointsize = 12)
```

## APPENDIX 10

### *Functional annotation using NCBI-DAVID (version 6.7)*

Protocol (also depicted with screenshots):

1. Go to <https://david.ncifcrf.gov/>
2. Click on “Start Analysis”
3. Copy and paste/ Upload your gene list onto the left panel “Enter Gene List”.
4. Select the identifier category for the gene list IDs added before.
5. Specify the list type as “Gene list” to submit for analysis.
6. Select the species of interest to get gene annotation.
7. Click on “Functional annotation tools” option provided by DAVID.
8. Click on “Functional Annotation table” to obtain the information about different selected functional categories.
9. Click on “Download file” to save the annotation info.

DAVID Bioinformatics Resources 6.8  
Laboratory of Human Retrovirology and Immunoinformatics (LHRI)

Home Start Analysis **Shortcut to DAVID Tools** Technical Center Downloads & APIs Term of Service Why DAVID? About Us

\*\*\* Welcome to DAVID 6.8 \*\*\*  
\*\*\* If you are looking for DAVID 6.7, please visit our development site. \*\*\*

Recommending: A paper published in *Nature Protocols* describes step-by-step procedure to use DAVID!

### Welcome to DAVID 6.8

2003 - 2018

The Database for Annotation, Visualization and Integrated Discovery (DAVID) v6.8 comprises a full Knowledgebase update to the sixth version of our original web-accessible programs. DAVID now provides a comprehensive set of functional annotation tools for investigators to understand biological meaning behind large list of genes. For any given gene list, DAVID tools are able to:

- Identify enriched biological themes, particularly GO terms
- Discover enriched functional-related gene groups
- Cluster redundant annotation terms
- Visualize genes on BioCarta & KEGG pathway maps
- Display related many-genes-to-many-terms on 2-D view.
- Search for other functionally related genes not in the list
- List interacting proteins
- Explore gene names in batch
- Link gene-disease associations
- Highlight protein functional domains and motifs
- Redirect to related literatures
- Convert gene identifiers from one type to another.
- And more...

**What's Important in DAVID?**

- [Cite DAVID](#)
- [IDs of Affy Exon and Gene arrays supported](#)
- [Novel Classification Algorithms](#)
- [Pre-built Affymetrix and Illumina backgrounds](#)
- [User's customized gene background](#)
- [Enhanced calculating speed](#)

**Statistics of DAVID**

DAVID Citations (2003-2017)

Year	Citations
03	~100
04	~200
05	~300
06	~400
07	~500
08	~600
09	~700
10	~800
11	~900
12	~1000
13	~1100
14	~1200
15	~1300
16	~1400
17	~1500

- [> 33,000 Citations](#)
- [Average Daily Usage: ~2,700 gene lists/sublists from ~900 unique researchers.](#)

**Shortcut to DAVID Tools**

- Functional Annotation**  
Gene-annotation enrichment analysis, functional annotation clustering, BioCarta & KEGG pathway mapping, gene-disease association, homologue match, ID translation, literature match and more
- Gene Functional Classification**  
Provide a rapid means to reduce large lists of genes into functionally related groups of genes to help unravel the biological content captured by high throughput technologies. [More](#)
- Gene ID Conversion**  
Convert list of gene ID/accessions to others of your choice with the most comprehensive gene ID mapping repository. The ambiguous accessions in the list can also be determined semi-automatically. [More](#)
- Gene Name Batch Viewer**  
Display gene names for a given gene list; Search functionally related genes within your list or not in your list; Deep links to enriched detailed information. [More](#)

\*\*\* Welcome to DAVID 6.8 \*\*\*  
 \*\*\* If you are looking for DAVID 6.7, please visit our [development site](#). \*\*\*

## Analysis Wizard

[Tell us how you like the tool](#)  
[Contact us for questions](#)

← Step 1. Submit your gene list through left panel.

**Upload** | List | Background

**Upload Gene List**

[Demolist 1](#) [Demolist 2](#)  
[Upload Help](#)

Step 1: Enter Gene List

A: Paste a list

Gpx1  
Mgp  
Ubb  
Efemp2

Clear

Or

B: Choose From a File

Choose File | No file chosen

Multi-List File ?

Step 2: Select Identifier

OFFICIAL\_GENE\_SYMBOL ▾

Step 3: List type

Gene List   
 Background

Step 4: Submit List

Submit List

An example:

Copy/paste IDs to "box A" -> Select Identifier as "Affy\_ID" -> List Type as "Gene List" -> Click "Submit" button

```

1007_s_at
1053_at
117_at
121_at
1255_g_at
1294_at
1316_at
1320_at
1405_i_at
1431_at
1438_at
1487_at
1494_f_at
1598_g_at
          
```

\*\*\* Welcome to DAVID 6.8 \*\*\*  
 \*\*\* If you are looking for DAVID 6.7, please visit our [development site](#). \*\*\*

## Analysis Wizard

[Tell us how you like the tool](#)  
[Contact us for questions](#)

**Upload** | List | Background

**Gene List Manager**

Select to limit annotations by one or more species [Help](#)

microcebus murinus(5)  
 Microtus ochrogaster(5)  
 Minioplerus neohomensis(7)  
 Mus musculus(5)

Select Species

List Manager [Help](#)

List\_1

Select List to:

Use | Rename  
 Remove | Combine

Show Gene List

Step 1. Successfully submitted gene list

Current Gene List: List\_1  
 Current Background: Canis lupus familiaris

Step 2. Analyze above gene list with one of DAVID tools

Which DAVID tools to use?

- ⌕ Functional Annotation Tool
  - [Functional Annotation Clustering](#)
  - [Functional Annotation Chart](#)
  - [Functional Annotation Table](#)
- ⌕ Gene Functional Classification Tool
- ⌕ Gene ID Conversion Tool
- ⌕ Gene Name Batch Viewer

\*\*\* Welcome to DAVID 6.8 \*\*\*  
\*\*\* If you are looking for DAVID 6.7, please visit our [development site](#). \*\*\*

Upload List Background

### Gene List Manager

Select to limit annotations by one or more species [Help](#)

- Use All Species -
- Canis lupus familiaris(6)
- Acinonyx jubatus(5)
- Ailuropoda melanoleuca(5)

Select Species

### List Manager [Help](#)

- List\_1

Select List to:

- Use
- Rename
- Remove
- Combine
- Show Gene List

## Annotation Summary Results

[Help and Tool Manual](#)

Current Gene List: List\_1

5 DAVID IDs

Current Background: Canis lupus familiaris

Check Defaults

Clear All

- Functional\_Categories (2 selected)
- Gene\_Ontology (3 selected)
- General\_Annotations (0 selected)
- Literature (0 selected)
- Main\_Accessions (0 selected)
- Pathways (2 selected)
- Protein\_Domains (3 selected)
- Protein\_Interactions (0 selected)
- Tissue\_Expression (0 selected)

\*\*\*Red annotation categories denote DAVID defined defaults\*\*\*

### Combined View for Selected Annotation

- Functional Annotation Clustering
- Functional Annotation Chart
- Functional Annotation Table

## ABBREVIATIONS LIST

<b><u>Abbreviation</u></b>	<b><u>Term</u></b>
[%]	Percentage
°C	Degree Celsius
Acan	Aggrecan
ADP	Adenosine diphosphate
Ampd1	Adenosine monophosphate deaminase 1
ANOVA	Analysis of variance
Aqp1	Aquaporin 1
ASMA	Alpha smooth muscle actin
ATP	Adenosine triphosphate
Atp5b	Adenosine triphosphate synthase subunit beta mitochondrial
Atp5f1	ATP synthase H <sup>+</sup> transporting mitochondrial f1 complex
B2m	Beta 2 microglobulin
Bckdk	Branched chain ketoacid dehydrogenase kinase
BMP	Bone morphogenetic protein
BMU	Basic multicellular unit
BSP	Bone sialoprotein
Capns1	Calpain small subunit 1
Ckmt2	Creatine kinase mitochondrial type 2
Col10a1	Collagen type 10 alpha 1
Col12a1	Collagen type 12 alpha 1
Col1a1	Collagen type 1 alpha 1
Col24a1	Collagen type 24 alpha 1
Col2a1	Collagen type 2 alpha 1
Col6a1	Collagen type 6 alpha 1
Col9a2	Collagen type 9 alpha 2
Coq9	Coenzyme q9
Cox19	Cytochrome c oxidase assembly homolog 19
Cox6a2	Cytochrome c oxidase subunit 6a2
Cox7a1	Cytochrome c oxidase subunit 7a1
Cox8b	Cytochrome c oxidase subunit 8b
Cpt1b	Carnitine o-palmitoyltransferase 1
Cpz	Carboxypeptidase z
Crtap	Cartilage associated protein
Cs	Citrate synthase
Csde1	Cold shock domain containing protein e1
Ctsg	Cathepsin g
Ctsk	Cathepsin k
Cycl	Cytochrome c1
Cyp27a1	Cytochrome p450 family 27 subfamily a member 1
D	Day

DAVID	Database for Annotation, Visualization and Integrated
Discovery	
Dcn	Decorin
DEG	Differentially expressed genes
DMP1	Dentin matrix protein 1
DNA	Deoxyribonucleic acid
Dusp26	Dual specificity phosphatase 26
E2f2	E2f transcription factor 2
ECM	Extracellular matrix
Efemp2	Epidermal growth factor containing fibulin ECM protein 2
ERK	Extracellular signal-regulated kinase
Etfa	Electron transfer flavoprotein alpha subunit
FC	Fold change
Fcer1g	Fc fragment of IgE receptor 1g
Fcnb	Ficolin b
Fh1	Fumarate hydratase 1
GPX1	Glutathione peroxidase 1
Gstp1	Glutathione s transferase p1
Hnrnp1	Heterogeneous nuclear ribonucleoprotein h1
Hspa9	Heat shock protein family a member 9
IBM	International business machines
Ibsp	Integrin binding sialoprotein
Ifitm2	Interferon induced transmembrane protein 2
IHC	Immunohistochemistry
IL-1	Interleukin 1
Il11ra1	Interleukin 11 receptor subunit alpha 1
IL-6	Interleukin 6
KEGG	Kyoto Encyclopedia of Genes and Genomes
Lcn2	Lipocalin 2
Lox	Lysyl oxidase
Lum	Lumican
Lyrn5	Lyr motif containing protein 5
MAPK	Mitogen activated protein kinase
Mapk14	Mitogen activated protein kinase 14
MATLAB	Matrix laboratory
Mcm7	Minichromosome maintenance complex component 7
M-CSF	Macrophage colony stimulating factor
Mef2c	Myocyte enhancer factor 2c
MEPE	Matrix extracellular phosphoglycoprotein
Metap1	Methionyl aminopeptidase 1
mg	Milligram
Mgp	Matrix gla protein
mm	Millimeter

Mmp13	Matrix metalloproteinase 13
Mmp2	Matrix metalloproteinase 2
Mmp9	Matrix metalloproteinase 9
MMPs	Matrix metalloproteinase
Mrpl33	Mitochondrial ribosomal protein l33
Mrpl53	Mitochondrial ribosomal protein l53
Mt3	Metallothionein 3
Myom1	Myomesin 1
NF-kB cells	Nuclear factor kappa-light-chain-enhancer of activated B cells
nm	Nanometer
Npm1	Nucleophosmin 1
OCN	Osteocalcin
Ogn	Osteoglycin
ONC	Osteonectin
OPG	Osteoprotegerin
OPN	Osteopontin
Oxct1	3-oxoacid CoA-transferase 1
Pdia3	Protein disulfide isomerase family a member 3
Pdk4	Pyruvate dehydrogenase kinase 4
PFA	Paraformaldehyde
Pglyrp1	Peptidoglycan recognition protein 1
Plac8	Placenta specific 8
Prdx2	Peroxidase 2
Prdx3	Peroxidase 3
Prf	Perforin
Ptn	Pleiotrophin
RANKL	Receptor activator of nuclear factor kappa B ligand
ROS	Reactive oxygen species
Rpl24	Ribosomal protein l24
Rpl27	Ribosomal protein l27
Rpl31	Ribosomal protein l31
Rpl36al	Ribosomal protein l36a like
Rps2	Ribosomal protein s2
Rps3	Ribosomal protein s3
Rps6	Ribosomal protein s6
rRNA	Ribosomal ribonucleic acid
Rsad2	Radical s-adenosyl methionine domain containing 2
RT	Room temperature
Runx2	Runt related transcription factor 2
S100a8	S100 calcium binding protein a8
Sdhc	Succinate dehydrogenase cytochrome b560 subunit
SEM	Standard error of mean

Serpinf1	Serpin family f member 1
Sh3pxd2b	Sh3 and Px domain containing protein 2b
Slc25a11	Solute carrier family 25 member 11
Slc25a20	Solute carrier family 25 member 20
Slc25a37	Solute carrier family 25 member 37
Slc25a5	Solute carrier family 25 member 5
Slpi	Secretory leukocyte peptidase inhibitor
Snca	Synuclein alpha
SOST	Sclerostin
Sp7	Specificity protein 7
Sparc	Secreted protein acidic and cysteine rich
Spp1	Secreted phosphoprotein 1
SPSS	Statistical package for the social sciences
Suclg1	Succinyl CoA ligase 1
TCA	Tricarboxylic acid
Tgf	Transforming growth factor
Tgfb1	Transforming growth factor beta receptor 1
Tgfb2	Transforming growth factor beta receptor 2
TGF- $\beta$	Transforming growth factor beta
Timm8b	Translocase of inner mitochondrial membrane 8 homolog b
Timp1	Tissue inhibitor of metalloproteinase 1
Tmem14c	Transmembrane proteome 14c
Tnc	Tenascin c
TNF	Tumor necrosis factor
Tomm7	Translocase of outer mitochondrial membrane 7
UBB	Ubiquitin B
Uqcrc2	Ubiquinol-cytochrome c reductase core protein 2
Vdac1	Voltage dependent anion channel 1
Vdac3	Voltage dependent anion channel 3
Vegfa	Vascular endothelial growth factor alpha

## **ACKNOWLEDGMENTS**

I would like to express my sincere gratitude to Dr. Thaqif El Khassawna and Prof. Christian Heiß for giving me the opportunity, continuous support, immense knowledge, and motivation to achieve this dream. I could not have imagined having a better advisor and mentor for my Ph.D. study.

My sincere thanks also goes to Dr. Katharina Schmidt-Bleek and Prof. Georg Duda, the collaborators from Julius Wolff Institute for Biomechanics and Musculoskeletal Regeneration, Berlin for their precious support and guidance to conduct this research.

Besides my advisors, I would like to thank Dr. Natali Bauer and other committee members for their insightful comments and encouragement, which incited me to widen my research from various perspectives.

I am thankful to Prof. Dr. Katrin Sussane Lips for her constant support at Justus-Liebig-University. I would like to extend my heartfelt gratitude to all of my fellow lab members especially: Mrs. Annette Stengel, Dr. Diaa Eldin S Daghma, Ms. Stefanie Kern, Dr. Fathi Hassan, Ms. Sabine Stoetzel, Dr. Seemun Ray, and Mrs. Ida Oberst for their support, stimulating discussions, and technical help. Further, thanks goes to the medical doctoral students from my team for their invaluable support.

A very special gratitude goes out to the German Research Foundation (DFG) for providing with the funding to carry out the work.

Last but not least, I am grateful to my family and friends, who have provided me through moral and emotional support in my life. My eternal thanks to my Mom and Dad who taught me to dream big and work hard towards a goal. I owe it all to you. Many Thanks! I am utterly thankful to my elder brother for being supportive in my decisions.

Thanks for all your encouragement!

## **THESIS DECLARATION**

I hereby declare that I have completed this dissertation single-handedly without the unauthorized help of a second party and only with the assistance acknowledged therein.

I have appropriately acknowledged and referenced all text passages that are derived literally from or are based on the content of published or unpublished work of others, and all information that relates to verbal communications.

I have abided by the principles of good scientific conduct laid down in the charter of the Justus Liebig University of Giessen in carrying out the investigations described in the dissertation.

Deeksha Malhan

Giessen

## REFERENCES

1. Giannoudis Pv Fau - Jones, E., T.A. Jones E Fau - Einhorn, and T.A. Einhorn, *Fracture healing and bone repair*. (1879-0267 (Electronic)).
2. Einhorn, T.A., *The cell and molecular biology of fracture healing*. (0009-921X (Print)).
3. Nakazawa, T., N. Nakajima A Fau - Seki, A. Seki N Fau - Okawa, M. Okawa A Fau - Kato, H. Kato M Fau - Moriya, N. Moriya H Fau - Amizuka, T.A. Amizuka N Fau - Einhorn, M. Einhorn Ta Fau - Yamazaki, and M. Yamazaki, *Gene expression of periostin in the early stage of fracture healing detected by cDNA microarray analysis*. (0736-0266 (Print)).
4. Khan, S.N., K.E. Solaris J Fau - Ramsey, X. Ramsey Ke Fau - Yang, M.P.G. Yang X Fau - Bostrom, D. Bostrom Mp Fau - Stephan, A. Stephan D Fau - Daluiski, and A. Daluiski, *Identification of novel gene expression in healing fracture callus tissue by DNA microarray*. (1556-3316 (Print)).
5. Bais, M., P. McLean J Fau - Sebastiani, M. Sebastiani P Fau - Young, N. Young M Fau - Wigner, T. Wigner N Fau - Smith, D.N. Smith T Fau - Kotton, T.A. Kotton Dn Fau - Einhorn, L.C. Einhorn Ta Fau - Gerstenfeld, and L.C. Gerstenfeld, *Transcriptional analysis of fracture healing and the induction of embryonic stem cell-related genes*. (1932-6203 (Electronic)).
6. Morgan, E.F., G.L. Barnes, and T.A. Einhorn, *Chapter 1 - The Bone Organ System: Form and Function A2 - Marcus, Robert*, in *Osteoporosis (Fourth Edition)*, D. Feldman, et al., Editors. 2013, Academic Press: San Diego. p. 3-20.
7. Weiner, S. and W. Traub, *Bone structure: from angstroms to microns*. (0892-6638 (Print)).
8. Rho, J.Y., P. Kuhn-Spearing L Fau - Zioupos, and P. Zioupos, *Mechanical properties and the hierarchical structure of bone*. (1350-4533 (Print)).
9. Walzer Sm Fau - Cetin, E., R. Cetin E Fau - Grubl-Barabas, I. Grubl-Barabas R Fau - Sulzbacher, B. Sulzbacher I Fau - Rueger, W. Rueger B Fau - Girsch, S. Girsch W Fau - Toegel, R. Toegel S Fau - Windhager, M.B. Windhager R Fau - Fischer, and M.B. Fischer, *Vascularization of primary and secondary ossification centres in the human growth plate*. (1471-213X (Electronic)).
10. Colnot, C., *Skeletal cell fate decisions within periosteum and bone marrow during bone regeneration*. (1523-4681 (Electronic)).
11. Luk Sc Fau - Nopajaroonsri, C., G.T. Nopajaroonsri C Fau - Simon, and G.T. Simon, *The ultrastructure of endosteum: a topographic study in young adult rabbits*. (0022-5320 (Print)).
12. Schonherr, E. and H.J. Hausser, *Extracellular matrix and cytokines: a functional unit*. (1044-6672 (Print)).
13. Le, B.A.-O., V. Nurcombe, S.M. Cool, C.A. van Blitterswijk, J. de Boer, and V.A.-O. LaPointe, *The Components of Bone and What They Can Teach Us about Regeneration*. *LID - E14 [pii] LID - 10.3390/ma11010014 [doi]*. (1996-1944 (Print)).
14. Wang, Y., M. Azais T Fau - Robin, A. Robin M Fau - Vallee, C. Vallee A Fau - Catania, P. Catania C Fau - Legriél, G. Legriél P Fau - Pehau-Arnaudet, F. Pehau-Arnaudet G Fau - Babonneau, M.-M. Babonneau F Fau - Giraud-Guille, N. Giraud-Guille Mm Fau - Nassif, and N. Nassif, *The predominant role of collagen in the nucleation, growth, structure and orientation of bone apatite*. (1476-1122 (Print)).
15. Rodan, G.A., *Bone homeostasis*. (0027-8424 (Print)).
16. Long, F., *Building strong bones: molecular regulation of the osteoblast lineage*. (1471-0080 (Electronic)).
17. Vaananen, H.K. and T. Laitala-Leinonen, *Osteoclast lineage and function*. (1096-0384 (Electronic)).
18. Russell, L.A., *Osteoporosis and osteomalacia*. (1558-3163 (Electronic)).

19. Hauge, E.M., E.F. Qvesel D Fau - Eriksen, L. Eriksen Ef Fau - Mosekilde, F. Mosekilde L Fau - Melsen, and F. Melsen, *Cancellous bone remodeling occurs in specialized compartments lined by cells expressing osteoblastic markers*. (0884-0431 (Print)).
20. Andersen, T.L., K.E. Sondergaard Te Fau - Skorzynska, F. Skorzynska Ke Fau - Dagnaes-Hansen, T.L. Dagnaes-Hansen F Fau - Plesner, E.M. Plesner Tl Fau - Hauge, T. Hauge Em Fau - Plesner, J.-M. Plesner T Fau - Delaisse, and J.M. Delaisse, *A physical mechanism for coupling bone resorption and formation in adult human bone*. (1525-2191 (Electronic)).
21. Caetano-Lopes, J., J.E. Canhao H Fau - Fonseca, and J.E. Fonseca, *Osteoblasts and bone formation*. (0303-464X (Print)).
22. Chen, G., Y.-P. Deng C Fau - Li, and Y.P. Li, *TGF-beta and BMP signaling in osteoblast differentiation and bone formation*. (1449-2288 (Electronic)).
23. Lai, C.F., A. Chaudhary L Fau - Fausto, L.R. Fausto A Fau - Halstead, D.S. Halstead Lr Fau - Ory, L.V. Ory Ds Fau - Avioli, S.L. Avioli Lv Fau - Cheng, and S.L. Cheng, *Erk is essential for growth, differentiation, integrin expression, and cell function in human osteoblastic cells*. (0021-9258 (Print)).
24. Siegel, P.M. and J. Massague, *Cytostatic and apoptotic actions of TGF-beta in homeostasis and cancer*. (1474-175X (Print)).
25. Miyazono, K., T. Maeda S Fau - Imamura, and T. Imamura, *BMP receptor signaling: transcriptional targets, regulation of signals, and signaling cross-talk*. (1359-6101 (Print)).
26. Papachroni, K.K., K.A. Karatzas Dn Fau - Papavassiliou, E.K. Papavassiliou Ka Fau - Basdra, A.G. Basdra Ek Fau - Papavassiliou, and A.G. Papavassiliou, *Mechanotransduction in osteoblast regulation and bone disease*. (1471-4914 (Print)).
27. Kim, E.K. and E.J. Choi, *Pathological roles of MAPK signaling pathways in human diseases*. (0006-3002 (Print)).
28. Westendorf, J.J., T.M. Kahler Ra Fau - Schroeder, and T.M. Schroeder, *Wnt signaling in osteoblasts and bone diseases*. (0378-1119 (Print)).
29. Kelly, D.P. and R.C. Scarpulla, *Transcriptional regulatory circuits controlling mitochondrial biogenesis and function*. (0890-9369 (Print)).
30. An, J.H., B.Y. Yang Jy Fau - Ahn, S.W. Ahn By Fau - Cho, J.Y. Cho Sw Fau - Jung, H.Y. Jung Jy Fau - Cho, Y.M. Cho Hy Fau - Cho, S.W. Cho Ym Fau - Kim, K.S. Kim Sw Fau - Park, S.Y. Park Ks Fau - Kim, H.K. Kim Sy Fau - Lee, C.S. Lee Hk Fau - Shin, and C.S. Shin, *Enhanced mitochondrial biogenesis contributes to Wnt induced osteoblastic differentiation of C3H10T1/2 cells*. (1873-2763 (Electronic)).
31. Ryter, S.W., A. Kim Hp Fau - Hoetzel, J.W. Hoetzel A Fau - Park, K. Park Jw Fau - Nakahira, X. Nakahira K Fau - Wang, A.M.K. Wang X Fau - Choi, and A.M. Choi, *Mechanisms of cell death in oxidative stress*. (1523-0864 (Print)).
32. Handy, D.E., Y. Lubos E Fau - Yang, J.D. Yang Y Fau - Galbraith, N. Galbraith Jd Fau - Kelly, Y.-Y. Kelly N Fau - Zhang, J.A. Zhang Yy Fau - Leopold, J. Leopold Ja Fau - Loscalzo, and J. Loscalzo, *Glutathione peroxidase-1 regulates mitochondrial function to modulate redox-dependent cellular responses*. (0021-9258 (Print)).
33. Jorgensen, P., J.R. Rupes I Fau - Sharom, L. Sharom Jr Fau - Schneper, J.R. Schneper L Fau - Broach, M. Broach Jr Fau - Tyers, and M. Tyers, *A dynamic transcriptional network communicates growth potential to ribosome synthesis and critical cell size*. (0890-9369 (Print)).
34. Stavreva, D.A., M. Kawasaki M Fau - Dundr, K. Dundr M Fau - Koberna, W.G. Koberna K Fau - Muller, T. Muller Wg Fau - Tsujimura-Takahashi, W. Tsujimura-Takahashi T Fau - Komatsu, T. Komatsu W Fau - Hayano, T. Hayano T Fau - Isobe, I. Isobe T Fau - Raska, T. Raska I Fau - Misteli, N. Misteli T Fau - Takahashi, J.G. Takahashi N Fau - McNally, and J.G. McNally, *Potential roles for ubiquitin and the proteasome during ribosome biogenesis*. (0270-7306 (Print)).

35. Komori, T., *Regulation of osteoblast differentiation by Runx2*. (0065-2598 (Print)).
36. Ali, S.A., C.S. Zaidi Sk Fau - Dacwag, N. Dacwag Cs Fau - Salma, D.W. Salma N Fau - Young, A.R. Young Dw Fau - Shakoori, M.A. Shakoori Ar Fau - Montecino, J.B. Montecino Ma Fau - Lian, A.J. Lian Jb Fau - van Wijnen, A.N. van Wijnen Aj Fau - Imbalzano, G.S. Imbalzano An Fau - Stein, J.L. Stein Gs Fau - Stein, and J.L. Stein, *Phenotypic transcription factors epigenetically mediate cell growth control*. (1091-6490 (Electronic)).
37. Neben, C.L., F.D. Lay, X. Mao, C.T. Tuzon, and A.E. Merrill, *Ribosome biogenesis is dynamically regulated during osteoblast differentiation*. (1879-0038 (Electronic)).
38. Shu, L., B.F. Zhang H Fau - Boyce, L. Boyce Bf Fau - Xing, and L. Xing, *Ubiquitin E3 ligase Wwp1 negatively regulates osteoblast function by inhibiting osteoblast differentiation and migration*. (1523-4681 (Electronic)).
39. Franz-Odenaal, T.A., P.E. Hall Bk Fau - Witten, and P.E. Witten, *Buried alive: how osteoblasts become osteocytes*. (1058-8388 (Print)).
40. Rochefort, G.Y., C.L. Pallu S Fau - Benhamou, and C.L. Benhamou, *Osteocyte: the unrecognized side of bone tissue*. (1433-2965 (Electronic)).
41. Bonewald, L.F., *The amazing osteocyte*. (1523-4681 (Electronic)).
42. Neve, A., F.P. Corrado A Fau - Cantatore, and F.P. Cantatore, *Osteocytes: central conductors of bone biology in normal and pathological conditions*. (1748-1716 (Electronic)).
43. Delgado-Calle, J., G.D. Bellido T Fau - Roodman, and G.D. Roodman, *Role of osteocytes in multiple myeloma bone disease*. (1751-4266 (Electronic)).
44. MacDougall, M., T.T. Simmons D Fau - Gu, J. Gu Tt Fau - Dong, and J. Dong, *MEPE/OF45, a new dentin/bone matrix protein and candidate gene for dentin diseases mapping to chromosome 4q21*. (0300-8207 (Print)).
45. Teitelbaum, S.L., *Bone resorption by osteoclasts*. (0036-8075 (Print)).
46. Feng, X. and S.L. Teitelbaum, *Osteoclasts: New Insights*. (2095-4700 (Print)).
47. Wittkowske, C., G.C. Reilly, D. Lacroix, and C.M. Perrault, *In Vitro Bone Cell Models: Impact of Fluid Shear Stress on Bone Formation*. (2296-4185 (Print)).
48. Hofbauer, L.C., B.L. Gori F Fau - Riggs, D.L. Riggs Bl Fau - Lacey, C.R. Lacey Dl Fau - Dunstan, T.C. Dunstan Cr Fau - Spelsberg, S. Spelsberg Tc Fau - Khosla, and S. Khosla, *Stimulation of osteoprotegerin ligand and inhibition of osteoprotegerin production by glucocorticoids in human osteoblastic lineage cells: potential paracrine mechanisms of glucocorticoid-induced osteoporosis*. (0013-7227 (Print)).
49. Kong, Y.Y., I. Feige U Fau - Sarosi, B. Sarosi I Fau - Bolon, A. Bolon B Fau - Tafuri, S. Tafuri A Fau - Morony, C. Morony S Fau - Capparelli, J. Capparelli C Fau - Li, R. Li J Fau - Elliott, S. Elliott R Fau - McCabe, T. McCabe S Fau - Wong, G. Wong T Fau - Campagnuolo, E. Campagnuolo G Fau - Moran, E.R. Moran E Fau - Bogoch, G. Bogoch Er Fau - Van, L.T. Van G Fau - Nguyen, P.S. Nguyen Lt Fau - Ohashi, D.L. Ohashi Ps Fau - Lacey, E. Lacey Dl Fau - Fish, W.J. Fish E Fau - Boyle, J.M. Boyle Wj Fau - Penninger, and J.M. Penninger, *Activated T cells regulate bone loss and joint destruction in adjuvant arthritis through osteoprotegerin ligand*. (0028-0836 (Print)).
50. Simonet, W.S., C.R. Lacey Dl Fau - Dunstan, M. Dunstan Cr Fau - Kelley, M.S. Kelley M Fau - Chang, R. Chang Ms Fau - Luthy, H.Q. Luthy R Fau - Nguyen, S. Nguyen Hq Fau - Wooden, L. Wooden S Fau - Bennett, T. Bennett L Fau - Boone, G. Boone T Fau - Shimamoto, M. Shimamoto G Fau - DeRose, R. DeRose M Fau - Elliott, A. Elliott R Fau - Colombero, H.L. Colombero A Fau - Tan, G. Tan Hl Fau - Trail, J. Trail G Fau - Sullivan, E. Sullivan J Fau - Davy, N. Davy E Fau - Bucay, L. Bucay N Fau - Renshaw-Gegg, T.M. Renshaw-Gegg L Fau - Hughes, D. Hughes Tm Fau - Hill, W. Hill D Fau - Pattison, P. Pattison W Fau - Campbell, S. Campbell P Fau - Sander, G. Sander S Fau - Van, J. Van G Fau - Tarpley, P. Tarpley J Fau -

- Derby, R. Derby P Fau - Lee, W.J. Lee R Fau - Boyle, and W.J. Boyle, *Osteoprotegerin: a novel secreted protein involved in the regulation of bone density*. (0092-8674 (Print)).
51. Miller, S.C., B.M. de Saint-Georges L Fau - Bowman, W.S. Bowman Bm Fau - Jee, and W.S. Jee, *Bone lining cells: structure and function*. (0891-7035 (Print)).
  52. Everts, V., W. Delaisse Jm Fau - Korper, D.C. Korper W Fau - Jansen, W. Jansen Dc Fau - Tigchelaar-Gutter, P. Tigchelaar-Gutter W Fau - Saftig, W. Saftig P Fau - Beertsen, and W. Beertsen, *The bone lining cell: its role in cleaning Howship's lacunae and initiating bone formation*. (0884-0431 (Print)).
  53. Komatsu, D.E. and S.J. Warden, *The control of fracture healing and its therapeutic targeting: improving upon nature*. (1097-4644 (Electronic)).
  54. Gerstenfeld, L.C., G.L. Cullinane Dm Fau - Barnes, D.T. Barnes Gl Fau - Graves, T.A. Graves Dt Fau - Einhorn, and T.A. Einhorn, *Fracture healing as a post-natal developmental process: molecular, spatial, and temporal aspects of its regulation*. (0730-2312 (Print)).
  55. Kolar, P., H. Schmidt-Bleek K Fau - Schell, T. Schell H Fau - Gaber, D. Gaber T Fau - Toben, G. Toben D Fau - Schmidmaier, C. Schmidmaier G Fau - Perka, F. Perka C Fau - Buttgerit, G.N. Buttgerit F Fau - Duda, and G.N. Duda, *The early fracture hematoma and its potential role in fracture healing*. (1937-3376 (Electronic)).
  56. Schell, H., G.N. Duda, A. Peters, S. Tsitsilonis, K.A.A.-O.h.o.o. Johnson, and K. Schmidt-Bleek, *The haematoma and its role in bone healing*. (2197-1153 (Print)).
  57. Andrew, J.G., A.J. Andrew Sm Fau - Freemont, D.R. Freemont Aj Fau - Marsh, and D.R. Marsh, *Inflammatory cells in normal human fracture healing*. (0001-6470 (Print)).
  58. Kon, T., T. Cho Tj Fau - Aizawa, M. Aizawa T Fau - Yamazaki, N. Yamazaki M Fau - Nooh, D. Nooh N Fau - Graves, L.C. Graves D Fau - Gerstenfeld, T.A. Gerstenfeld Lc Fau - Einhorn, and T.A. Einhorn, *Expression of osteoprotegerin, receptor activator of NF-kappaB ligand (osteoprotegerin ligand) and related proinflammatory cytokines during fracture healing*. (0884-0431 (Print)).
  59. Sandboe, F.D., A. Medin W Fau - Anseth, and A. Anseth, *Back to front AC IOL implantation combined with penetrating keratoplasty*. (0001-639X (Print)).
  60. Schmidt-Bleek, K., J. Schell H Fau - Lienau, N. Lienau J Fau - Schulz, P. Schulz N Fau - Hoff, M. Hoff P Fau - Pfaff, G. Pfaff M Fau - Schmidt, C. Schmidt G Fau - Martin, C. Martin C Fau - Perka, F. Perka C Fau - Buttgerit, H.-D. Buttgerit F Fau - Volk, G. Volk Hd Fau - Duda, and G. Duda, *Initial immune reaction and angiogenesis in bone healing*. (1932-7005 (Electronic)).
  61. Claes, L., A. Recknagel S Fau - Ignatius, and A. Ignatius, *Fracture healing under healthy and inflammatory conditions*. (1759-4804 (Electronic)).
  62. Dimitriou, R., P.V. Tsiridis E Fau - Giannoudis, and P.V. Giannoudis, *Current concepts of molecular aspects of bone healing*. (0020-1383 (Print)).
  63. Gerstenfeld, L.C., E.A. Alkhiary Ym Fau - Krall, F.H. Krall Ea Fau - Nicholls, S.N. Nicholls Fh Fau - Stapleton, J.L. Stapleton Sn Fau - Fitch, M. Fitch Jl Fau - Bauer, R. Bauer M Fau - Kayal, D.T. Kayal R Fau - Graves, K.J. Graves Dt Fau - Jepsen, T.A. Jepsen Kj Fau - Einhorn, and T.A. Einhorn, *Three-dimensional reconstruction of fracture callus morphogenesis*. (0022-1554 (Print)).
  64. Marsell, R. and T.A. Einhorn, *The biology of fracture healing*. (1879-0267 (Electronic)).
  65. Wang, C., Y. Abu-Amer, R.J. O'Keefe, and J. Shen, *Loss of Dnmt3b in Chondrocytes Leads to Delayed Endochondral Ossification and Fracture Repair*. (1523-4681 (Electronic)).
  66. Staines, K.A., I.M. Pollard As Fau - McGonnell, C. McGonnell Im Fau - Farquharson, A.A. Farquharson C Fau - Pitsillides, and A.A. Pitsillides, *Cartilage to bone transitions in health and disease*. (1479-6805 (Electronic)).
  67. Thompson, Z., D. Miclau T Fau - Hu, J.A. Hu D Fau - Helms, and J.A. Helms, *A model for intramembranous ossification during fracture healing*. (0736-0266 (Print)).

68. Kaplan, F.S. and E.M. Shore, *Progressive osseous heteroplasia*. (0884-0431 (Print)).
69. Marion, M.J., M.D. Gannon Fh Fau - Fallon, M.T. Fallon Md Fau - Mennuti, R.F. Mennuti Mt Fau - Lodato, F.S. Lodato Rf Fau - Kaplan, and F.S. Kaplan, *Skeletal dysplasia in perinatal lethal osteogenesis imperfecta. A complex disorder of endochondral and intramembranous ossification*. (0009-921X (Print)).
70. Eriksen, E.F., *Cellular mechanisms of bone remodeling*. (1573-2606 (Electronic)).
71. Hadjidakis, D.J. and Androulakis, Il, *Bone remodeling*. (0077-8923 (Print)).
72. El Khassawna, T., F. Merboth, D. Malhan, W. Bocker, D.E.S. Daghma, S. Stoetzel, S. Kern, F. Hassan, D. Rosenbaum, J. Langenstein, N. Bauer, A. Schlagenhauf, A. Rosen-Wolff, F. Schulze, M. Rupp, D. Hose, A. Secklinger, A. Ignatius, H.J. Wilke, K.S. Lips, and C. Heiss, *Osteocyte Regulation of Receptor Activator of NF-kappaB Ligand/Osteoprotegerin in a Sheep Model of Osteoporosis*. (1525-2191 (Electronic)).
73. Einhorn, T.A. and L.C. Gerstenfeld, *Fracture healing: mechanisms and interventions*. (1759-4804 (Electronic)).
74. Bonnarens F Fau - Einhorn, T.A. and T.A. Einhorn, *Production of a standard closed fracture in laboratory animal bone*. (0736-0266 (Print)).
75. Junqueira Lc Fau - Cossermelli, W., R. Cossermelli W Fau - Brentani, and R. Brentani, *Differential staining of collagens type I, II and III by Sirius Red and polarization microscopy*. (0004-0681 (Print)).
76. Goldner, J., *A modification of the masson trichrome technique for routine laboratory purposes*. (0002-9440 (Print)).
77. Bergers, G. and S. Song, *The role of pericytes in blood-vessel formation and maintenance*. (1522-8517 (Print)).
78. Staines, K.A., C.E. Mackenzie Nc Fau - Clarkin, L. Clarkin Ce Fau - Zelenchuk, P.S. Zelenchuk L Fau - Rowe, V.E. Rowe Ps Fau - MacRae, C. MacRae Ve Fau - Farquharson, and C. Farquharson, *MEPE is a novel regulator of growth plate cartilage mineralization*. (1873-2763 (Electronic)).
79. Ho, E., C.-C. Karimi Galougahi K Fau - Liu, R. Liu Cc Fau - Bhindi, G.A. Bhindi R Fau - Figtree, and G.A. Figtree, *Biological markers of oxidative stress: Applications to cardiovascular research and practice*. (2213-2317 (Electronic)).
80. Komine, M., Y. Matsuyama T Fau - Nojima, S. Nojima Y Fau - Minoda, M. Minoda S Fau - Furue, T. Furue M Fau - Tsuchida, S. Tsuchida T Fau - Sakai, Y. Sakai S Fau - Ishibashi, and Y. Ishibashi, *Systemic lupus erythematosus with hereditary deficiency of the fourth component of complement*. (0011-9059 (Print)).
81. Arganda-Carreras, I., V. Kaynig, C. Rueden, K.W. Eliceiri, J. Schindelin, A. Cardona, and H. Sebastian Seung, *Trainable Weka Segmentation: a machine learning tool for microscopy pixel classification*. (1367-4811 (Electronic)).
82. Daghma, D.E.S., D. Malhan, P. Simon, S. Stotzel, S. Kern, F. Hassan, K.S. Lips, C. Heiss, and T.A.-O.h.o.o. El Khassawna, *Computational segmentation of collagen fibers in bone matrix indicates bone quality in ovariectomized rat spine*. (1435-5604 (Electronic)).
83. Bredfeldt, J.S., Y. Liu, C.A. Pehlke, M.W. Conklin, J.M. Szulczewski, D.R. Inman, P.J. Keely, R.D. Nowak, T.R. Mackie, and K.W. Eliceiri, *Computational segmentation of collagen fibers from second-harmonic generation images of breast cancer*. (1560-2281 (Electronic)).
84. Smith, M.L., K.A. Baggerly, H. Bengtsson, M.E. Ritchie, and K.D. Hansen, *illuminaio: An open source IDAT parsing tool for Illumina microarrays*. (2046-1402 (Print)).
85. Dunning, M.J., M.E. Smith Ml Fau - Ritchie, S. Ritchie Me Fau - Tavare, and S. Tavare, *beadarray: R classes and methods for Illumina bead-based data*. (1367-4811 (Electronic)).
86. Ritchie, M.E., B. Phipson, D. Wu, Y. Hu, C.W. Law, W. Shi, and G.K. Smyth, *limma powers differential expression analyses for RNA-sequencing and microarray studies*. (1362-4962 (Electronic)).

87. Huang da, W., R.A. Sherman Bt Fau - Lempicki, and R.A. Lempicki, *Systematic and integrative analysis of large gene lists using DAVID bioinformatics resources*. (1750-2799 (Electronic)).
88. Gomez-Barrena, E., P. Rosset, D. Lozano, J. Stanovici, C. Ermthaller, and F. Gerbhard, *Bone fracture healing: cell therapy in delayed unions and nonunions*. (1873-2763 (Electronic)).
89. Schindeler, A., P. McDonald Mm Fau - Bokko, D.G. Bokko P Fau - Little, and D.G. Little, *Bone remodeling during fracture repair: The cellular picture*. (1084-9521 (Print)).
90. Marsell, R. and T.A. Einhorn, *Emerging bone healing therapies*. (1531-2291 (Electronic)).
91. Van Dijk, F.S. and D.O. Sillence, *Osteogenesis imperfecta: clinical diagnosis, nomenclature and severity assessment*. (1552-4833 (Electronic)).
92. Cimino, P.J. and D.H. Gutmann, *Neurofibromatosis type 1*. (0072-9752 (Print)).
93. Wang, Q., *Identification of biomarkers for metastatic osteosarcoma based on DNA microarray data*. (0028-2685 (Print)).
94. Morse, D.L., Y. Hostetter G Fau - Balagurunathan, R.J. Balagurunathan Y Fau - Gillies, H. Gillies Rj Fau - Han, and H. Han, *Identification of pancreatic cancer-specific cell-surface markers for development of targeting ligands*. (1940-6029 (Electronic)).
95. Zhong, D., *Identification of Differentially Expressed Gene after Femoral Fracture via Microarray Profiling*. (2314-436X (Print)).
96. Wang, K., G.S. Vishwanath P Fau - Eichler, M.O. Eichler Gs Fau - Al-Sebaei, C.M. Al-Sebaei Mo Fau - Edgar, T.A. Edgar Cm Fau - Einhorn, T.F. Einhorn Ta Fau - Smith, L.C. Smith Tf Fau - Gerstenfeld, and L.C. Gerstenfeld, *Analysis of fracture healing by large-scale transcriptional profile identified temporal relationships between metalloproteinase and ADAMTS mRNA expression*. (0945-053X (Print)).
97. Dalman, M.R., G. Deeter A Fau - Nimishakavi, Z.-H. Nimishakavi G Fau - Duan, and Z.H. Duan, *Fold change and p-value cutoffs significantly alter microarray interpretations*. (1471-2105 (Electronic)).
98. Hankenson, K.D., C. Dishowitz M Fau - Gray, M. Gray C Fau - Schenker, and M. Schenker, *Angiogenesis in bone regeneration*. (1879-0267 (Electronic)).
99. Ortega, N., Z. Behonick Dj Fau - Werb, and Z. Werb, *Matrix remodeling during endochondral ossification*. (0962-8924 (Print)).
100. Dyall, S.D., P.J. Brown Mt Fau - Johnson, and P.J. Johnson, *Ancient invasions: from endosymbionts to organelles*. (1095-9203 (Electronic)).
101. Leung, K.S., T.S. Sher Ah Fau - Lam, P.C. Lam Ts Fau - Leung, and P.C. Leung, *Energy metabolism in fracture healing. Measurement of adenosine triphosphate in callus to monitor progress*. (0301-620X (Print)).
102. Horton, W.A. and M.M. Machado, *Extracellular matrix alterations during endochondral ossification in humans*. (0736-0266 (Print)).
103. Raggatt, L.J. and N.C. Partridge, *Cellular and molecular mechanisms of bone remodeling*. (1083-351X (Electronic)).
104. Newman, J.C. and E. Verdin, *Ketone bodies as signaling metabolites*. (1879-3061 (Electronic)).
105. Endler, M.A.-O., S. Saltvedt, M. Eweida, and H. Akerud, *Oxidative stress and inflammation in retained placenta: a pilot study of protein and gene expression of GPX1 and NFKappaB*. (1471-2393 (Electronic)).
106. Sommer, B., W. Bickel M Fau - Hofstetter, A. Hofstetter W Fau - Wetterwald, and A. Wetterwald, *Expression of matrix proteins during the development of mineralized tissues*. (8756-3282 (Print)).
107. Yamagiwa, H., T. Tokunaga K Fau - Hayami, H. Hayami T Fau - Hatano, M. Hatano H Fau - Uchida, N. Uchida M Fau - Endo, H.E. Endo N Fau - Takahashi, and H.E. Takahashi,

- Expression of metalloproteinase-13 (Collagenase-3) is induced during fracture healing in mice.* (8756-3282 (Print)).
108. Dickson, K., E. Katzman S Fau - Delgado, D. Delgado E Fau - Contreras, and D. Contreras, *Delayed unions and nonunions of open tibial fractures. Correlation with arteriography results.* (0009-921X (Print)).
  109. McDonald, S.J., A.C. Dooley Pc Fau - McDonald, J.A. McDonald Ac Fau - Schuijers, A.R. Schuijers Ja Fau - Ward, B.L. Ward Ar Fau - Grills, and B.L. Grills, *Transient expression of myofibroblast-like cells in rat rib fracture callus.* (1745-3682 (Electronic)).
  110. Kinner, B., T.A. Gerstenfeld Lc Fau - Einhorn, M. Einhorn Ta Fau - Spector, and M. Spector, *Expression of smooth muscle actin in connective tissue cells participating in fracture healing in a murine model.* (8756-3282 (Print)).
  111. Saran, U., S. Gemini Piperni, and S. Chatterjee, *Role of angiogenesis in bone repair.* (1096-0384 (Electronic)).
  112. Wang, Q.Y., Z.S. Liu, J. Wang, H.X. Wang, A. Li, Y. Yang, X.Z. Wang, Y.Q. Zhao, Q.Y. Han, H. Cai, B. Liang, N. Song, W.H. Li, and T. Li, *Glutathione peroxidase-1 is required for self-renewal of murine embryonic stem cells.* (1090-2104 (Electronic)).
  113. Descamps, B. and C. Emanuelli, *Vascular differentiation from embryonic stem cells: novel technologies and therapeutic promises.* (1879-3649 (Electronic)).
  114. Hoeben, A., M.S. Landuyt B Fau - Highley, H. Highley Ms Fau - Wildiers, A.T. Wildiers H Fau - Van Oosterom, E.A. Van Oosterom At Fau - De Bruijn, and E.A. De Bruijn, *Vascular endothelial growth factor and angiogenesis.* (0031-6997 (Print)).
  115. Carmeliet, P., *VEGF as a key mediator of angiogenesis in cancer.* (0030-2414 (Print)).
  116. Kwiatkowski, S., T. Munjaal Rp Fau - Lee, P.Y. Lee T Fau - Lwigale, and P.Y. Lwigale, *Expression of pro- and anti-angiogenic factors during the formation of the periocular vasculature and development of the avian cornea.* (1097-0177 (Electronic)).
  117. Venturi, G., E. Gandini A Fau - Monti, L. Monti E Fau - Dalle Carbonare, M. Dalle Carbonare L Fau - Corradi, M. Corradi M Fau - Vincenzi, M.T. Vincenzi M Fau - Valenti, M. Valenti Mt Fau - Valli, E. Valli M Fau - Pelilli, A. Pelilli E Fau - Boner, M. Boner A Fau - Mottes, F. Mottes M Fau - Antoniazzi, and F. Antoniazzi, *Lack of expression of SERPINF1, the gene coding for pigment epithelium-derived factor, causes progressively deforming osteogenesis imperfecta with normal type I collagen.* (1523-4681 (Electronic)).
  118. Homan, E.P., I. Rauch F Fau - Grafe, C. Grafe I Fau - Lietman, J.A. Lietman C Fau - Doll, B. Doll Ja Fau - Dawson, T. Dawson B Fau - Bertin, D. Bertin T Fau - Napierala, R. Napierala D Fau - Morello, R. Morello R Fau - Gibbs, L. Gibbs R Fau - White, R. White L Fau - Miki, D.H. Miki R Fau - Cohn, S. Cohn Dh Fau - Crawford, R. Crawford S Fau - Travers, F.H. Travers R Fau - Glorieux, B. Glorieux Fh Fau - Lee, and B. Lee, *Mutations in SERPINF1 cause osteogenesis imperfecta type VI.* (1523-4681 (Electronic)).
  119. Stetler-Stevenson, W.G., *Matrix metalloproteinases in angiogenesis: a moving target for therapeutic intervention.* (0021-9738 (Print)).
  120. Colnot, C., T. Thompson Z Fau - Miclau, Z. Miclau T Fau - Werb, J.A. Werb Z Fau - Helms, and J.A. Helms, *Altered fracture repair in the absence of MMP9.* (0950-1991 (Print)).
  121. Pepper, M.S., *Transforming growth factor-beta: vasculogenesis, angiogenesis, and vessel wall integrity.* (1359-6101 (Print)).
  122. Larsson, J., L.J. Goumans Mj Fau - Sjostrand, M.A. Sjostrand Lj Fau - van Rooijen, D. van Rooijen Ma Fau - Ward, P. Ward D Fau - Leveen, X. Leveen P Fau - Xu, P. Xu X Fau - ten Dijke, C.L. ten Dijke P Fau - Mummery, S. Mummery Cl Fau - Karlsson, and S. Karlsson, *Abnormal angiogenesis but intact hematopoietic potential in TGF-beta type I receptor-deficient mice.* (0261-4189 (Print)).
  123. Blobel, G.C., H.F. Schieman Wp Fau - Lodish, and H.F. Lodish, *Role of transforming growth factor beta in human disease.* (0028-4793 (Print)).

124. Lichtman, M.K., M. Otero-Vinas, and V. Falanga, *Transforming growth factor beta (TGF-beta) isoforms in wound healing and fibrosis*. (1524-475X (Electronic)).
125. Breur, G.J., C.E. VanEnkevort Ba Fau - Farnum, N.J. Farnum Ce Fau - Wilsman, and N.J. Wilsman, *Linear relationship between the volume of hypertrophic chondrocytes and the rate of longitudinal bone growth in growth plates*. (0736-0266 (Print)).
126. Scammell, B.E. and H.I. Roach, *A new role for the chondrocyte in fracture repair: endochondral ossification includes direct bone formation by former chondrocytes*. (0884-0431 (Print)).
127. McKibbin, B., *The biology of fracture healing in long bones*. (0301-620X (Print)).
128. Li, H., F. Zhang X Fau - Wang, R. Wang F Fau - Li, S. Li R Fau - Wang, and S. Wang, *[A study on proliferation of chondrocyte in callus during second fracture healing]*. (1672-173X (Print)).
129. Schwartz, A.L. and A. Ciechanover, *Targeting proteins for destruction by the ubiquitin system: implications for human pathobiology*. (0362-1642 (Print)).
130. Schlundt, C., T. El Khassawna, A. Serra, A. Dienelt, S. Wendler, H. Schell, N. van Rooijen, A. Radbruch, R. Lucius, S. Hartmann, G.N. Duda, and K. Schmidt-Bleek, *Macrophages in bone fracture healing: Their essential role in endochondral ossification*. (1873-2763 (Electronic)).
131. Uyama, M., M. Sato Mm Fau - Kawanami, M. Kawanami M Fau - Tamura, and M. Tamura, *Regulation of osteoblastic differentiation by the proteasome inhibitor bortezomib*. (1365-2443 (Electronic)).
132. Malaval, L., M. Wade-Gueye Nm Fau - Boudiffa, J. Boudiffa M Fau - Fei, R. Fei J Fau - Zirngibl, F. Zirngibl R Fau - Chen, N. Chen F Fau - Laroche, J.-P. Laroche N Fau - Roux, B. Roux Jp Fau - Burt-Pichat, F. Burt-Pichat B Fau - Duboeuf, G. Duboeuf F Fau - Boivin, P. Boivin G Fau - Jurdic, M.-H. Jurdic P Fau - Lafage-Proust, J. Lafage-Proust Mh Fau - Amedee, L. Amedee J Fau - Vico, J. Vico L Fau - Rossant, J.E. Rossant J Fau - Aubin, and J.E. Aubin, *Bone sialoprotein plays a functional role in bone formation and osteoclastogenesis*. (1540-9538 (Electronic)).
133. Inada, M., M.H. Wang Y Fau - Byrne, M.U. Byrne Mh Fau - Rahman, C. Rahman Mu Fau - Miyaura, C. Miyaura C Fau - Lopez-Otin, S.M. Lopez-Otin C Fau - Krane, and S.M. Krane, *Critical roles for collagenase-3 (Mmp13) in development of growth plate cartilage and in endochondral ossification*. (0027-8424 (Print)).
134. Rodenberg, E., Z.W. Azhdarinia A Fau - Lazard, M. Lazard Zw Fau - Hall, S.K. Hall M Fau - Kwon, N. Kwon Sk Fau - Wilganowski, E.A. Wilganowski N Fau - Salisbury, M. Salisbury Ea Fau - Merched-Sauvage, E.A. Merched-Sauvage M Fau - Olmsted-Davis, E.M. Olmsted-Davis Ea Fau - Sevick-Muraca, A.R. Sevick-Muraca Em Fau - Davis, and A.R. Davis, *Matrix metalloproteinase-9 is a diagnostic marker of heterotopic ossification in a murine model*. (1937-335X (Electronic)).
135. Miller Ej Fau - Gay, S. and S. Gay, *The collagens: an overview and update*. (0076-6879 (Print)).
136. Gentili, C. and R. Cancedda, *Cartilage and bone extracellular matrix*. (1873-4286 (Electronic)).
137. Carey, D.J., *Control of growth and differentiation of vascular cells by extracellular matrix proteins*. (0066-4278 (Print)).
138. Frantz, C., V.M. Stewart Km Fau - Weaver, and V.M. Weaver, *The extracellular matrix at a glance*. (1477-9137 (Electronic)).
139. Bigham-Sadegh, A. and A. Oryan, *Basic concepts regarding fracture healing and the current options and future directions in managing bone fractures*. (1742-481X (Electronic)).

140. Gajko-Galicka, A., *Mutations in type I collagen genes resulting in osteogenesis imperfecta in humans.* (0001-527X (Print)).
141. Martin, A.C., E.F. Kaschube M Fau - Wieschus, and E.F. Wieschus, *Pulsed contractions of an actin-myosin network drive apical constriction.* (1476-4687 (Electronic)).
142. Vincentelli R Fau - Evans, F.G. and F.G. Evans, *Relations among mechanical properties, collagen fibers, and calcification in adult human cortical bone.* (0021-9290 (Print)).
143. Hanley, C.J., F. Noble, M. Ward, M. Bullock, C. Drifka, M. Mellone, A. Manousopoulou, H.E. Johnston, A. Hayden, S. Thirdborough, Y. Liu, D.M. Smith, T. Mellows, W.J. Kao, S.D. Garbis, A. Mirnezami, T.J. Underwood, K.W. Eliceiri, and G.J. Thomas, *A subset of myofibroblastic cancer-associated fibroblasts regulate collagen fiber elongation, which is prognostic in multiple cancers.* (1949-2553 (Electronic)).
144. Kim, C.L. and D.E. Kim, *Self-healing Characteristics of Collagen Coatings with Respect to Surface Abrasion.* (2045-2322 (Electronic)).
145. van Oers, R.F., R.G. Wang H Fau - Bacabac, and R.G. Bacabac, *Osteocyte shape and mechanical loading.* (1544-2241 (Electronic)).
146. El Khassawna, T., W. Bocker, K. Brodsky, D. Weisweiler, P. Govindarajan, M. Kampschulte, U. Thormann, A. Henss, M. Rohnke, N. Bauer, R. Muller, A. Deutsch, A. Ignatius, L. Durselen, A. Langheinrich, K.S. Lips, R. Schnettler, and C. Heiss, *Impaired extracellular matrix structure resulting from malnutrition in ovariectomized mature rats.* (1432-119X (Electronic)).
147. Lanyon, L.E., *Osteocytes, strain detection, bone modeling and remodeling.* (0171-967X (Print)).
148. Kulkarni, R.N., V. Bakker Ad Fau - Everts, J. Everts V Fau - Klein-Nulend, and J. Klein-Nulend, *Inhibition of osteoclastogenesis by mechanically loaded osteocytes: involvement of MEPE.* (1432-0827 (Electronic)).
149. Jain, A., M.T. Fedarko Ns Fau - Collins, R. Collins Mt Fau - Gelman, M.A. Gelman R Fau - Ankrom, M. Ankrom Ma Fau - Tayback, L.W. Tayback M Fau - Fisher, and L.W. Fisher, *Serum levels of matrix extracellular phosphoglycoprotein (MEPE) in normal humans correlate with serum phosphorus, parathyroid hormone and bone mineral density.* (0021-972X (Print)).
150. Yan, Y.X., Y. Gong Yw Fau - Guo, Q. Guo Y Fau - Lv, C. Lv Q Fau - Guo, Y. Guo C Fau - Zhuang, Y. Zhuang Y Fau - Zhang, R. Zhang Y Fau - Li, X.-z. Li R Fau - Zhang, and X.Z. Zhang, *Mechanical strain regulates osteoblast proliferation through integrin-mediated ERK activation.* (1932-6203 (Electronic)).
151. David, V., A.-M. Martin A Fau - Hedge, P.S.N. Hedge Am Fau - Rowe, and P.S. Rowe, *Matrix extracellular phosphoglycoprotein (MEPE) is a new bone renal hormone and vascularization modulator.* (1945-7170 (Electronic)).
152. Chen, Z., G. Yue Sx Fau - Zhou, E.M. Zhou G Fau - Greenfield, S. Greenfield Em Fau - Murakami, and S. Murakami, *ERK1 and ERK2 regulate chondrocyte terminal differentiation during endochondral bone formation.* (1523-4681 (Electronic)).
153. Watanabe, H., K. Yamada Y Fau - Kimata, and K. Kimata, *Roles of aggrecan, a large chondroitin sulfate proteoglycan, in cartilage structure and function.* (0021-924X (Print)).
154. Lauing, K.L., M. Cortes, M.S. Domowicz, J.G. Henry, A.T. Baria, and N.B. Schwartz, *Aggrecan is required for growth plate cytoarchitecture and differentiation.* (1095-564X (Electronic)).
155. Schwartz, N.B. and M. Domowicz, *Chondrodysplasias due to proteoglycan defects.* (0959-6658 (Print)).
156. Roughley, P.J. and J.S. Mort, *The role of aggrecan in normal and osteoarthritic cartilage.* (2197-1153 (Print)).

157. Mosig, R.A., A. Dowling O Fau - DiFeo, M.C.M. DiFeo A Fau - Ramirez, I.C. Ramirez Mc Fau - Parker, E. Parker Ic Fau - Abe, J. Abe E Fau - Diouri, A.A. Diouri J Fau - Aqeel, J.D. Aqeel Aa Fau - Wylie, S.A. Wylie Jd Fau - Oblander, J. Oblander Sa Fau - Madri, P. Madri J Fau - Bianco, S.S. Bianco P Fau - Apte, M. Apte Ss Fau - Zaidi, S.B. Zaidi M Fau - Doty, R.J. Doty Sb Fau - Majeska, M.B. Majeska Rj Fau - Schaffler, J.A. Schaffler Mb Fau - Martignetti, and J.A. Martignetti, *Loss of MMP-2 disrupts skeletal and craniofacial development and results in decreased bone mineralization, joint erosion and defects in osteoblast and osteoclast growth.* (0964-6906 (Print)).
158. Neuhold, L.A., W. Killar L Fau - Zhao, M.L. Zhao W Fau - Sung, L. Sung Ml Fau - Warner, J. Warner L Fau - Kulik, J. Kulik J Fau - Turner, W. Turner J Fau - Wu, C. Wu W Fau - Billinghamurst, T. Billinghamurst C Fau - Meijers, A.R. Meijers T Fau - Poole, P. Poole Ar Fau - Babij, L.J. Babij P Fau - DeGennaro, and L.J. DeGennaro, *Postnatal expression in hyaline cartilage of constitutively active human collagenase-3 (MMP-13) induces osteoarthritis in mice.* (0021-9738 (Print)).
159. Meyer, M.H. and R.A. Meyer, Jr., *Altered expression of mitochondrial genes in response to fracture in old rats.* (1745-3674 (Print)).
160. Lubos, E., D.E. Loscalzo J Fau - Handy, and D.E. Handy, *Glutathione peroxidase-1 in health and disease: from molecular mechanisms to therapeutic opportunities.* (1557-7716 (Electronic)).
161. Mlakar, S.J., J. Osredkar J Fau - Prezelj, J. Prezelj J Fau - Marc, and J. Marc, *The antioxidant enzyme GPX1 gene polymorphisms are associated with low BMD and increased bone turnover markers.* (1875-8630 (Electronic)).
162. Lean, J.M., B. Jagger Cj Fau - Kirstein, K. Kirstein B Fau - Fuller, T.J. Fuller K Fau - Chambers, and T.J. Chambers, *Hydrogen peroxide is essential for estrogen-deficiency bone loss and osteoclast formation.* (0013-7227 (Print)).
163. Fenselau A Fau - Wallis, K., H.P. Wallis K Fau - Morris, and H.P. Morris, *Acetoacetate coenzyme A transferase activity in rat hepatomas.* (0008-5472 (Print)).
164. Cotter, D.G., A.E. d'Avignon Da Fau - Wentz, M.L. Wentz Ae Fau - Weber, P.A. Weber Ml Fau - Crawford, and P.A. Crawford, *Obligate role for ketone body oxidation in neonatal metabolic homeostasis.* (1083-351X (Electronic)).
165. Majumder, S. and H.A. Fisk, *VDAC3 and Mps1 negatively regulate ciliogenesis.* (1551-4005 (Electronic)).
166. Reina, S., F. Guarino, A. Magri, and V. De Pinto, *VDAC3 As a Potential Marker of Mitochondrial Status Is Involved in Cancer and Pathology.* (2234-943X (Print)).
167. Klingenberg, M., *Dialectics in carrier research: the ADP/ATP carrier and the uncoupling protein.* (0145-479X (Print)).
168. Trainor, P.A. and A.E. Merrill, *Ribosome biogenesis in skeletal development and the pathogenesis of skeletal disorders.* (0006-3002 (Print)).
169. Hochstrasser, M., *Ubiquitin, proteasomes, and the regulation of intracellular protein degradation.* (0955-0674 (Print)).
170. Dennissen, F.J., D.J.H.P. Kholod N Fau - Hermes, N. Hermes Dj Fau - Kemmerling, H.W.M. Kemmerling N Fau - Steinbusch, N.P. Steinbusch Hw Fau - Dantuma, F.W. Dantuma Np Fau - van Leeuwen, and F.W. van Leeuwen, *Mutant ubiquitin (UBB+1) associated with neurodegenerative disorders is hydrolyzed by ubiquitin C-terminal hydrolase L3 (UCH-L3).* (1873-3468 (Electronic)).
171. Steagall, R.J., S. Daniels Cr Fau - Dalal, W.L. Dalal S Fau - Joyner, M. Joyner Wl Fau - Singh, K. Singh M Fau - Singh, and K. Singh, *Extracellular ubiquitin increases expression of angiogenic molecules and stimulates angiogenesis in cardiac microvascular endothelial cells.* (1549-8719 (Electronic)).

172. Pagliarini, V., P. Giglio, P. Bernardoni, D. De Zio, G.M. Fimia, M. Piacentini, and M. Corazzari, *Downregulation of E2F1 during ER stress is required to induce apoptosis*. (1477-9137 (Electronic)).
173. Iglesias-Ara, A., J. Zenarruzabeitia O Fau - Fernandez-Rueda, E. Fernandez-Rueda J Fau - Sanchez-Tillo, S.J. Sanchez-Tillo E Fau - Field, A. Field Sj Fau - Celada, A.M. Celada A Fau - Zubiaga, and A.M. Zubiaga, *Accelerated DNA replication in E2F1- and E2F2-deficient macrophages leads to induction of the DNA damage response and p21(CIP1)-dependent senescence*. (1476-5594 (Electronic)).
174. Hwang, Y.P., E.H. Kim Hg Fau - Han, H.G. Han Eh Fau - Jeong, and H.G. Jeong, *Metallothionein-III protects against 6-hydroxydopamine-induced oxidative stress by increasing expression of heme oxygenase-1 in a PI3K and ERK/Nrf2-dependent manner*. (1096-0333 (Electronic)).
175. Lorenzo, J., Y. Horowitz M Fau - Choi, and Y. Choi, *Osteoimmunology: interactions of the bone and immune system*. (0163-769X (Print)).
176. Lavedan, C., *The synuclein family*. (1088-9051 (Print)).
177. Calabrese, G., L.D. Mesner, P.L. Foley, C.J. Rosen, and C.R. Farber, *Network Analysis Implicates Alpha-Synuclein (Snca) in the Regulation of Ovariectomy-Induced Bone Loss*. (2045-2322 (Electronic)).
178. Shameli, A., W. Xiao, Y. Zheng, S. Shyu, J. Sumodi, H.J. Meyerson, C.V. Harding, and R.W. Maitta, *A critical role for alpha-synuclein in development and function of T lymphocytes*. (1878-3279 (Electronic)).
179. Labrie, V. and P. Brundin, *Alpha-Synuclein to the Rescue: Immune Cell Recruitment by Alpha-Synuclein during Gastrointestinal Infection*. (1662-8128 (Electronic)).
180. Xie, J., M.E. Wang Y Fau - Freeman, 3rd, B. Freeman Me 3rd Fau - Barlogie, Q. Barlogie B Fau - Yi, and Q. Yi, *Beta 2-microglobulin as a negative regulator of the immune system: high concentrations of the protein inhibit in vitro generation of functional dendritic cells*. (0006-4971 (Print)).
181. Wilgus, T.A., S. Roy, and J.C. McDaniel, *Neutrophils and Wound Repair: Positive Actions and Negative Reactions*. (2162-1918 (Print)).
182. Bangalore, N., V.C. Travis J Fau - Onunka, J. Onunka Vc Fau - Pohl, W.M. Pohl J Fau - Shafer, and W.M. Shafer, *Identification of the primary antimicrobial domains in human neutrophil cathepsin G*. (0021-9258 (Print)).
183. Zou, F., X. Lai, J. Li, S. Lei, and L. Hu, *Downregulation of cathepsin G reduces the activation of CD4+ T cells in murine autoimmune diabetes*. (1943-8141 (Print)).
184. Davis, K.M., T.G. Griffin Ks Fau - Chu, J.C. Chu Tg Fau - Wenke, B.T. Wenke Jc Fau - Corona, T.O. Corona Bt Fau - McKinley, M.A. McKinley To Fau - Kacena, and M.A. Kacena, *Muscle-bone interactions during fracture healing*. (1108-7161 (Print)).
185. Gilsanz, V., *Phenotype and genotype of osteoporosis*. (1043-2760 (Print)).